

Some pages of this thesis may have been removed for copyright restrictions.

If you have discovered material in Aston Research Explorer which is unlawful e.g. breaches copyright, (either yours or that of a third party) or any other law, including but not limited to those relating to patent, trademark, confidentiality, data protection, obscenity, defamation, libel, then please read our [Takedown policy](#) and contact the service immediately (openaccess@aston.ac.uk)

THE DEVELOPMENT OF NOVEL PHOTONICS BASED TECHNIQUES FOR BIOMEDICINE

Ilya Eduardovich Rafailov

Doctor of Philosophy

ASTON UNIVERSITY

October 2017

©Ilya Eduardovich Rafailov, 2017

Ilya Eduardovich Rafailov asserts his moral right to be identified as the author of this thesis

This copy of the thesis has been supplied on condition that anyone who consults it is understood to recognise that its copyright rests with its author and that no quotation from the thesis and no information derived from it may be published without appropriate permission or acknowledgement.

The development of novel photonics based techniques for biomedicine

Ilya Eduardovich Rafailov

Doctor of Philosophy

2017

The advances in technology capable of measuring various optical properties within organic materials and tissues have paved way for potentially revolutionary methods of detecting and diagnosing diseases as well as generally monitoring health. Thus, this thesis provides a background on a number of key optical properties crucial in organic tissues and describes how such properties can currently be detected and observed.

The thesis looks at a diverse selection of conditions and health-monitoring challenges to determine the effectiveness of non- and minimally invasive diagnostics. Urinary bladder cancer and a computational Monte Carlo model are described in an effort to predict the effectiveness of such diagnostics tools as well as aid in the overall detection of cancer within the organ. Beginning from porcine bladder, the model is advanced to function with human biopsy samples.

Furthermore, the thesis covers cardiovascular disease (CVD), specifically pre-eclampsia. Tools used for human analysis are tested on animal CVD models and ultimately employed to display their effectiveness at monitoring diseased mice from an established murine model. The thesis also presents potential parameters vital for diagnostics purposes.

Using the established parameters of interest from the above work, the thesis describes measurement of physiological (photonics based diagnostics) and psychological (reaction time assessment) effects resulting from short-term light exposure. Due to the frequency at which non-natural light interacts with people on a day-to-day basis, the thesis provides a basis to further expand health-monitoring research.

Finally, potential methods for assessing ocular health in the form of contact lens induced discomfort is assessed through objective analysis by photonics based techniques. The thesis also establishes a validation for the proposed approach.

Ultimately, the work presented in the thesis describes how novel photonics based technologies can be effectively employed in a wide variety of biomedical diagnostics and monitoring applications, whether used alone or in conjunction with other forms of diagnostics.

Keywords: urinary bladder cancer, pre-eclampsia, reaction time task, contact lenses, non-invasive diagnostics.

Acknowledgements

The work described in this thesis culminates to one of the most challenging, yet rewarding undertakings I have ever done. It would not have been possible without the support of many individuals who, over the course of years, have acted as guides and friends. Their aid through the toughest moments and companionship in the happiest ones ensured that I saw this work through to the end.

Special thanks is extended to Dr Karina Litvinova, who acted as my guide and mentor throughout. Her advice and teaching was instrumental in the completion of this thesis. Thanks also go to Dr Sergei Sokolovski, Dr Andrey Dunaev, Dr Ksenia Fedorova, Dr Amit Yadav and Mr Viktor Dremine, all of who not only contributed to the work in this thesis, but also spent time giving me scientific and moral support.

Another special thanks to my long-time friend and colleague Scott Palmer, who made the early difficulties and troubles bearable, and often even enjoyable. Thank you also to Prof Lin Zhang who became my supervisor and believed in my ability to carry out the work required of me.

Thank you to my mother and father who have provided me immeasurable support, emotionally as well as scientifically. This thesis would not be possible without them. Finally, thanks to Laura Clemens, who has stood by me from the beginning, having faith in my ability to succeed and supporting me through my lowest points.

These people helped me develop in many ways, so to all of them another sincere thanks.

Contents

Aston University	2
Acknowledgements.....	3
List of figures.....	8
List of tables.....	14
Chapter 1 : Thesis aims.....	15
1.1 Core thesis aims	15
1.2 Chapter aims	15
1.2.1 Diagnostics of cancer.....	16
1.2.2 Monitoring and diagnostics for cardiovascular diseases and pre-eclampsia	16
1.2.3 Non-disease monitoring and medical application.....	16
Chapter 2 : Introduction to light interactions with biological objects	18
2.1 Introduction.....	18
2.2 Light interaction with biological objects	19
2.2.1 Fundamental properties of light interaction.....	19
2.2.2 Tissue complexity and layering	21
2.2.3: Complex light interactions.....	24
2.2.4 Autofluorescence	25
2.3 Diagnostic and clinical relevance	26
2.3.1 Autofluorophores	26
2.3.2 Clinically and diagnostically relevant biomarkers.....	28
2.4 Conclusion	30
References.....	31
Chapter 3 : Principles of biophotonics techniques.....	33
3.1 Laser Doppler flowmetry	33
3.2 Spectroscopy.....	35
3.2.1 Fluorescence spectroscopy	35
3.2.2 Raman spectroscopy	37
3.3 Tissue reflectance oximetry	37
3.4 Optical coherence tomography	38
3.5 Other techniques	39
3.6 Conclusions.....	40

References.....	41
Chapter 4 : MLNDS and the LAKK series devices.....	44
4.1 The LAKK-M	44
4.2 Fundamental methodology of the LAKK-M device.....	47
4.2.1 Basic measurement of microcirculatory parameters.....	47
4.2.2 Basic measurement of fluorescence.....	48
4.2.3 Finalising experiments with the LAKK-M.....	50
4.3 Conclusions.....	50
References.....	51
Chapter 5 : Application in cancers: urinary bladder cancer.....	52
5.1 Introduction into bladder cancer	52
5.2 Bladder cancer tumour background.....	53
5.2.1 Anatomy and tumour progression.....	53
5.2.2 Cancer tumour properties.....	54
5.3 A computational bladder model.....	55
5.3.1 Justification of developing a model	56
5.3.2 Model requirements for relevance to bladder cancer.....	57
5.4 Methods for computational model development	57
5.4.1 Proof of concept model.....	57
5.4.2 Advanced model	60
5.4.3 Human tumour tissue measurement.....	62
5.5 Computational model construction and utilisation results.....	62
5.5.1 Proof of concept model.....	63
5.5.2 Advanced model	65
5.5.3 Human tumour tissue measurement.....	68
5.6 Analysis and discussions	73
5.6.1 Literature analysis.....	73
5.6.2 Inverse adding-doubling method: transport coefficients of porcine urinary bladder	73
5.6.3 Model construction	74
5.6.4 Three dimensional models	75
5.6.5 Future prospects and conclusions	76
References.....	78
Chapter 6 : Application in cardiovascular disease.....	82

6.1 Viability of the LAKK-M in CVD diagnostics on mouse models	82
6.1.1 Optimal recording areas on mice: introduction and methodology	82
6.1.2 Optimal recording areas on mice: results and outcomes	82
6.1.3 Effectiveness in murine disease models: introduction and methodology	84
6.1.4 Effectiveness in murine disease models: results and outcomes	85
6.2 Application in Pre-eclampsia	88
6.2.1 Introduction to Pre-eclampsia	88
6.2.2 Methods and materials	89
6.2.3 Results	92
6.2.4 Discussion	96
6.2.5 Conclusion	97
References	99
Chapter 7 : Application in non-disease monitoring	100
7.1 Lighting effects on biological function	100
7.1.1 Introduction	100
7.1.2 Methods and materials	101
7.1.3 Results	106
7.1.4 Discussion	110
7.1.5 Conclusion	112
7.2 Objective analysis of anterior eye health	113
7.2.1 Introduction	113
7.2.2 Methods and materials	113
7.2.3 Results	117
7.2.4 Discussion	123
7.2.5 Conclusion	125
References	126
Thesis conclusions	127
Appendix 1a: Lighting effects on biological function information sheet	129
Appendix 1b: Lighting effects on biological function consent form	131
Appendix 2a: Objective analysis of anterior eye health information sheet	132
Appendix 2b: Objective analysis of anterior eye health consent form	134
Appendix 3: Publications	135
Journal publications	135

Conference proceedings.....	135
Other presented work.....	136

List of figures

- Figure 2.1 Simple diagram of basic light interactions with an isotropic medium. The reflected, scattered, absorbed and transmitted light paths are presented. Additionally an unlabelled point of refraction, where the light enters a medium of a different refractive index, is displayed at the interface between the two different mediums. 20
- Figure 2.2 Simple diagram depicting refraction of a beam of light as it crosses the interface between two mediums of differing refractive index (n_1 and n_2). The angle of incidence (θ_1) and angle of refraction (θ_2) are also shown. 21
- Figure 2.3 Simplified cross section diagram of skin, featuring the epidermis and dermis layers. The four main layers of epithelial cells are presented. Vascularisation is also displayed, as is a sweat gland. (Image purchased from Shutterstock)..... 22
- Figure 2.4 Basic 2D schematic of a eukaryotic cell. The image features various organelles floating in the cytoplasm..... 23
- Figure 2.5 Basic schematic of the bladder cell layering. 24
- Figure 2.6 A typical example of emission spectra for four different excitation wavelengths (Dunaev et al. 2015). UV (365 nm), blue (450 nm), green (532 nm) and red (635 nm) excitations are presented. Biomarkers excited by the stated wavelengths of light are labelled next to their emission peaks..... 28
- Figure 3.1 Simple schematic of an LDF probe used to calculate the haemodynamics of an organic system. 34
- Figure 3.2 Simple Jablonski diagram presenting an example of fluorescence as a result of radiative relaxation. The figure presents UV wavelength excitation followed by blue wavelength emission due to the loss of energy during transition between vibrational levels (depicted as the dotted line). NADH autofluorescence is a real world example of this series of events..... 36
- Figure 3.3 A rough graph presenting the absorption spectra of oxygenated (HbO₂) and deoxygenated (Hb) haemoglobin. Red and green arrows indicate the specific absorption wavelengths employed to detect the differing haemoglobin fractions. 38
- Figure 4.1 Simplified block schematic of the LAKK-M. The device incorporates LDF, TRO, pulse oximetry and fluorescence spectroscopy methodologies. The key internal components are presented. 45
- Figure 4.2 The LAKK-M device. 1 – Power switch. 2 – Switch to set device into LDF and TRO recording mode. 3 – Calibration button for LDF mode. 4 – Switch to set device into fluorescence spectroscopy mode. 5 – Excitation wavelength selection buttons. 6 – Filter for

fluorescence excitation. 7 – Calibration dock. 8 – Main fibre with probe. 9 – Pulse oximeter finger clamp. 10 – Externally housed filters.....	46
Figure 4.3 A) External appearance of the main LAKK-M optical fibre probe housing the multiple radiation sources and detector fibres. B) Schematic depiction of the internal arrangement of the multiple radiation sources and detection fibres. Sources and detectors are labelled.....	46
Figure 4.4 The LAKK-M filters. From left to right - filters for excitation wavelengths of UV (365 nm), green (532 nm), blue (450 nm) and red (635 nm).....	49
Figure 5.1 A simplified diagram depicting various cancer tumour stages in a male bladder. Level of severity increases from Ta in a clockwise direction.....	54
Figure 5.2 Total transmittance (Tt) and diffuse reflectance (Rd) spectra of 2mm thick samples obtained from porcine urinary bladder.	61
Figure 5.3 (a) Full 3D model view representing photon passage through simulated tissue layers. The green circles represent the source and detector. (b) Side view of the same 3D model. Source, detector and the tissue layers are labelled. The visible darker lines illustrate photons, which are travelling directly towards the visible flat surface.	64
Figure 5.4 Comparison of the modelled and experimentally measured fluorescence at a 365 nm excitation wavelength. NADH and Collagen presence are incorporated into the model.	65
Figure 5.5 Spectra created from (a) the absorption coefficients of porcine urinary bladder and (b) the reduced scattering coefficients of porcine urinary bladder. Experimental data from Staveren (1995) is portrayed on the spectra.....	66
Figure 5.6 Light penetration depth into urinary bladder tissue.....	66
Figure 5.7 (a) Side and full 3D view of model depicting simulated UV light (365nm) within tissue. (b) Side and full 3D view of model depicting simulated Blue light (450nm) within tissue. The source, detector and tissue layers are displayed and labelled. The coloured lines indicate the passage of individual photons through the simulated tissue. These colours within a block are indicative of light intensity. Simulated source light is exclusively UV or blue, but red-shifted paths through the simulated tissue represent photons with lower intensities.	67
Figure 5.8 Comparison of (1) experimental and (2) model based spectra, calculated using the Monte-Carlo method. Model simulates presence of (a) NADH + collagen or (b) FAD + collagen.....	68
Figure 5.9 Total transmittance (Tt) and diffuse reflectance (Rd) spectra of 0.5 mm thick samples from HR1: (a) intact tissue and (b) tumour tissue.....	68

Figure 5.10 Total transmittance (T_t) and diffuse reflectance (R_d) spectra of 0.5 mm thick samples from HR2: (a) intact tissue and (b) tumour tissue.....	69
Figure 5.11(a) And (c) portray spectra created from the absorption coefficients of HB1 intact and tumour samples respectively. (b) And (d) portray spectra created from the reduced scattering coefficients of HB1 intact and tumour samples respectively.	69
Figure 5.12 (a) And (c) portray spectra created from the absorption coefficients of HB2 intact and tumour samples respectively. (b) And (d) portray spectra created from the reduced scattering coefficients of HB2 intact and tumour samples respectively.	70
Figure 5.13 Comparison of measured fluorescence and simulated fluorescence for HB1 intact and tumour tissue samples. The curves are labelled, where MCM stands for Monte Carlo Model. Presented are curves for (a) UV excitation at 365 nm and (b) blue excitation at 450 nm.	71
Figure 5.14 Comparison of measured fluorescence and simulated fluorescence for HB2 intact and tumour tissue samples. The curves are labelled, where MCM stands for Monte Carlo Model. Presented are curves for (a) UV excitation at 365 nm and (b) blue excitation at 450 nm.	72
Figure 6.1 Outcomes of the LAKK-M microcirculatory parameter measurements on various areas of the mice. The perfusion (I_m), saturation (StO_2) and blood velocity (V_b) are presented in images (A), (B) and (C) respectively.	83
Figure 6.2 Comparison of the I_m values between HO1 WT and KO mice as well as CSE WT and KO mice on day 1 (A) and day 2 (B).....	85
Figure 6.3 Comparison of the StO_2 values between HO1 WT and KO mice as well as CSE WT and KO mice on day 1 (A) and day 2 (B).....	86
Figure 6.4 Comparison of the RR values between HO1 WT and KO mice as well as CSE WT and KO mice on day 1 (A) and day 2 (B). It should be noted that while not statistically significant, there is an observable tendency towards significance between the HO1 WT and KO mice observable on the second day.....	87
Figure 6.5 Visual explanation of the four groups used in this experiment.	90
Figure 6.6 Data recording from tail of unanaesthetised mouse of the No-Gas group.	90
Figure 6.7 Comparison of the I_m values in the Gas and No-Gas groups, at the Pre and five days Post injection of CMV control and Ad-sFlt-1.	92
Figure 6.8 Figure 6.8. Comparison of the StO_2 values in the Gas and No-Gas groups, at the Pre and five days Post injection of CMV control and Ad-sFlt-1.....	93

Figure 6.9 Comparison of the Sm values in the Gas and No-Gas groups, at the Pre and five days Post injection of CMV control and Ad-sFlt-1.	94
Figure 6.10 Comparison of the RR values in the Gas and No-Gas groups, at the Pre and five days Post injection of CMV control and Ad-sFlt-1.	95
Figure 6.11 Comparison of the MR values in the Gas and No-Gas groups, at the Pre and five days Post injection of CMV control and Ad-sFlt-1.	95
Figure 7.1 Colour-tuneable LED panel developed by M-Squared Lasers and OSRAM. Image displays some of the light wavelengths produced by the panel as well as the control electronics (enabled through ethernet connection).	101
Figure 7.2 Reproduction of the visual search task depicting the various possible paradigms. The blue triangle is the desired target shape in this example. A – The single-search with target fielding 4 shapes. B – The single-search with no target fielding 8 shapes. C – The conjunction-search with target fielding 16 shapes. D – The conjunction-search with no target fielding 32 shapes. Note that the number of shapes was not exclusive to the paradigms above; the presented images are examples.	103
Figure 7.3 Unprocessed photographs of the testing area illuminated by the three tested light settings. Standard room light was categorised as “normal”. Cold light was measured at 9800K. Warm light was measured at 1820K.	105
Figure 7.4 The average comparisons of the index of oxygen saturation to perfusion of microvascular blood flow (A) and redox ratio (B) between different light colour temperatures. Initial exposure by “cold” light.	106
Figure 7.5 The average comparison of the metabolic ratio between different light colour temperatures. Initial exposure by “cold” light.	107
Figure 7.6 Results of the visual search task. Initial room light followed by “cold” then “warm” lights. (A) and (B): Field containing distractors of same colour as target shape, no target present and target present respectively. (C) and (D): Field containing distractors of same as well as different colour, no target present and target present respectively.	108
Figure 7.7 The average comparisons of the index of oxygen saturation to perfusion of microvascular blood flow (A) and redox ratio (B) between different light colour temperatures. Initial exposure by “warm” light.	109
Figure 7.8 The average comparison of the metabolic ratio between different light colour temperatures. Initial exposure by “warm” light.	109
Figure 7.9 Results of the reaction time task. Initial room light followed by “warm” then “cold” lights. (A) and (B): Field containing distractors of same colour as target shape, no	

target present and target present respectively. (C) and (D): Field containing distractors of same as well as different colour, no target present and target present respectively.	110
Figure 7.10 Standard headrest for ophthalmological slit lamp use.....	114
Figure 7.11 Figures depict experimental setup in use. A) Measurement of microcirculatory parameters and the connection of the LAKK-M device to the headstand. B) Measurement of fluorescence. The room is visibly darker during fluorescence measurements. Both images have had participants face blurred for privacy.....	116
Figure 7.12 Bulbar redness obtained by subjective grading following Efron scale.	118
Figure 7.13 Limbal redness obtained by subjective grading following Efron scale.....	118
Figure 7.14 Measurement of FAD and comparison by comfort level change. Large drop in subjective comfort rating after lens use was accompanied by a significant difference in FAD (* represents $p < 0.05$).	119
Figure 7.15 Measurement of Im and comparison by comfort level change. Large drop in subjective comfort rating after lens use was accompanied by a significant difference in perfusion, however a similar difference was observed in the group with no subjective comfort change (* represents $p < 0.05$).	119
Figure 7.16 Measurement of RR and comparison by comfort level change. Small drop in subjective comfort rating after lens use was accompanied by a significant difference in RR (* represents $p < 0.05$).	120
Figure 7.17 Measurement of MR and comparison by comfort level change. Large drop and small drop in subjective comfort ratings after lens use were accompanied by significant difference in MR (* represents $p < 0.05$)......	120
Figure 7.18 Measurement of Im and comparison by assigned condition differences. As expected, individuals with improved perfusion in the eye display a significant difference pre and post lens wear (* represents $p < 0.05$)......	121
Figure 7.19 Measurement of StO ₂ and comparison by assigned condition differences. Significant difference pre and post lens wear was only observed in individuals with a deteriorated condition (* represents $p < 0.05$).	121
Figure 7.20 Measurement of Vb and comparison by assigned condition differences. Significant difference pre and post lens wear was only observed in individuals with a deteriorated condition (* represents $p < 0.05$).	122
Figure 7.21 Measurement of Sm and comparison by assigned condition differences. Significant difference pre and post lens wear was observed in individuals both with a deteriorated and an improved condition (* represents $p < 0.05$).	122

Figure 7.22 Measurement of MR and comparison by assigned condition differences. Significant difference pre and post lens wear was observed in individuals with an improved condition (* represents $p < 0.05$). A tendency towards an opposite difference was also noted in the deteriorated group. 123

List of tables

Table 2.1 Excitation and emission wavelengths of various autofluorophores	27
Table 4.1 Wavelengths of corresponding LAKK-M channels. All values in nm.....	47
Table 5.1 Model parameters	58
Table 5.2 Optical parameters of human bladder tissues	63
Table 5.3 Optical parameters of pig bladder tissues	63
Table 6.1 Averages of measured microcirculatory parameters	92
Table 6.2 Averages of measured metabolic parameters	93
Table 6.3 Averages of calculated parameters	94

Chapter 1 : Thesis aims

This thesis is designed to present work conducted on the interface between two fields. As such, chapters two, three and four concentrate on bringing to light the idea that photonics based analysis of organic tissue is an ever-increasing research area with a large application in the biomedical fields. While the first two chapters detail specific technologies and their existing profound effect in fields such as medicine and biomedical research, it is important to note that photonics technology is continuously advancing. The direction towards combining multiple technologies as presented in chapter four lies at the heart of this thesis. It is precisely this type of combined technology that forms the backbone for the work conducted by the author. This short chapter will look at the core aim of the thesis and outline the progress of work.

1.1 Core thesis aims

This thesis heavily relied upon the recent technological advances within the field of photonics-based diagnostics. The combination of multiple complimentary diagnostics methodologies into single, easy-to-use devices presented a host of validation and application problems, which had to be addressed before such technology could continue to make a significant impact on the world.

In light of this, the one overarching aim of this thesis was to investigate the application of such photonics based technology on various diseases and in a number of medical applications. This implies the testing of suitability of such technologies on specific conditions in order to determine whether useful diagnostics data can be obtained.

Throughout this work, a secondary goal critical to completion of the primary aim, was to establish viable methodological and analytical approaches in the event of successful implementation of the diagnostics technology. Together, these two goals exist to exploit the various available photonics based techniques and form an experimentally supported foundation for further research into biomedicine.

1.2 Chapter aims

Multiple areas of interest were chosen for investigation in this thesis. This was primarily done to determine the effectiveness of multifunctional, photonics based diagnostics technologies and approaches in a broad spectrum of medical conditions. Below are short descriptions of the aims for each individual studied condition.

1.2.1 Diagnostics of cancer

In light of the tremendous impact of cancer on the lives of millions of people worldwide, chapter five of this thesis exclusively focuses on developing advancements in non- and minimally invasive early diagnostics of bladder cancer. The thesis provides a justification for the design and development of a computational 3D bladder tissue model in order to simulate the optical properties of multi-layered bladder tissue during irradiation by light of varying wavelengths. The ultimate goal of this work is the use of this model for comparison of different photonic devices and their potential clinical worth. Furthermore, the chapter aims to present a method for simulating the effects of bladder cancer progression on the tissue's optical properties and provide a diagnostic benchmark, which can aid in tumour staging and grading criteria.

1.2.2 Monitoring and diagnostics for cardiovascular diseases and pre-eclampsia

Along with cancer, cardiovascular diseases (CVD's) are one of the most prevalent diseases in the world. Chapter six of this thesis aimed to establish a viable method of monitoring cardiovascular deficiencies in CVD mouse models. In addition to establishing a validation for employing the LAKK-M diagnostics device on rodent models, the chapter also outlines potentially vital methods of analysis for effective diagnosis of various CVDs.

Combining the available technology with established mouse models, the chapter aims to work as a foundation for potential future research ultimately targeting non-invasive diagnostics of pre-eclampsia.

1.2.3 Non-disease monitoring and medical application

Monitoring and check-ups are important not just for individuals suffering from diseases, but also for unaffected people wishing to stay healthy. In light of this, chapter seven describes two potential directions of research into health monitoring within healthy individuals. Specifically, the chapter concentrates on the effects of light on the cognitive functions of healthy individuals and potential monitoring of eye health and contact lens comfort.

1.2.3.1 Effects of light on microcirculatory and metabolic processes

As technology advances in the form of new mobile phones, televisions and other devices based on light emitting screens, it is more important than ever to understand how natural and non-natural light affects healthy individuals. This chapter section ultimately aims to provide an initial assessment of physiological and cognitive changes in response to short exposures of intense warm

and cold light. Secondly, the section is aimed to provide a basis for deeper analysis into the light effects on humans by employing highly sensitive devices for physiological property measurement.

1.2.3.2 Analysis of eye health

In addition to diagnostics potentials of photonics based technology, the thesis aimed to establish potential applications of said technology in a monitoring and predictive capacity. Due to the prevalence of contact lens use and the ease of access to individuals with and without contact lenses, work in this thesis was carried out on determining the ability of diagnostics devices in predicting discomfort and irritation from eye lens use.

Specifically, work was conducted to establish and outline safe and effective monitoring methodology for the condition of the human eye, with and without lenses acting as irritants. Secondly, this work was completed as a basis to expand further into more complex applications of photonics based, non-invasive diagnostics devices in ophthalmology.

Chapter 2 : Introduction to light interactions with biological objects

2.1 Introduction

Throughout history, humanity has been searching for ever-improving approaches to medicine. Beginning with ancient civilisations, light, and often specifically sunlight, was deemed to have curative properties. Cultures such as the ancient Egyptians sought to improve health in a process now labelled as “heliotherapy”. The idea of exposure to light and the sun being medically important lasted all the way to the end of the 19th and the beginning of the 20th centuries, when the dangers of too much sun exposure started becoming more evident. By this point, however, light-based therapy was beginning to take on a new, more focused form.

Niels Ryberg Finsen, a Faroese-Danish physician, obtained the Nobel Prize for Physiology or Medicine in 1903 by successfully demonstrating the effects of light therapy for the treatment of Lupus Vulgaris (Finsen 1902). Instead of simply sunlight, Finsen employed specifically designed equipment to deliver concentrated light to target tissue areas (Gøtzsche 2011). While Finsen believed that his work was successful due to the bactericidal effect of ultraviolet (UV) radiation, there was no substantial scientific evidence backing the theory. It is even suspected that the treatment was successful due to the possible action of activated singlet oxygen (Møller et al. 2005). Despite the questioned mechanisms of therapeutic action, this was one of the earliest examples of targeted light being employed clinically and effectively.

The advent of laser technology further expanded on the possible uses of light within medical fields. The potential benefits of directly employing lasers in clinical practice were described almost simultaneously with their invention in the early 1960's (Townes 1962; Zaret et al. 1961). Though potential surgical applications were imagined even as the first lasers were being developed, the first described medical use of the laser was for photocoagulation in ophthalmology (Rosenberg et al. 1995). Over the next two decades, lasers spread through various and diverse medical fields, enhancing and aiding surgery in dermatology, otolaryngology, gynaecology, general surgery, neurosurgery, gastroenterology and urology (Choy 1988). With further advancement, fields such as cardiology and dentistry were also employing laser technology. However, by the late 1970's the potential applications of lasers diversified beyond simple surgery. Dougherty et al. (1978) demonstrated one of the earliest successful applications of lasers for photodynamic therapy involving a light activated compound for therapeutic treatment of various malignant tumours.

The development of lasers and increased control over the beam (such as pulsation) opened the floodgates of laser application in nearly all fields of medicine. Therapeutic applications diversified into a number of possible options. Depending on source of laser and exposure to it, therapeutic effects on both animals and humans could be achieved through electromechanical

(photomechanical or photodisruptive) approaches, ablation, photothermal (coagulative and vaporizing) processes, photochemical (photodynamic) reactions and through biostimulation and wound healing (Peng et al. 2008).

Alongside the therapeutic functionality, light (specifically laser technology) has found application in diagnostics. However, this direction of advancement has been a lot slower. While techniques such as fluorescence microscopy were first employed for observation of biological objects by Otto Heimstaedt and Heinrich Lehmann in the period between 1911 – 1913 (Jameson 2014), this was not used as a diagnostics tool and did not employ laser technology. Not until the later 20th century did photonics technology advance to the point where diagnosis of biological objects was readily available. Together with the development of lasers, techniques such as effective Raman spectroscopy (Porto & Wood 1962) and laser Doppler flowmetry (Stern 1975) began to improve, thereby formally launching the field of photonics based diagnostics.

Thus, the rapid advancement of photonics based diagnostic techniques has only been a recent phenomenon, with the field still displaying much room to grow. The body of work continues to expand and remains a forefront of its field. As such, this thesis establishes itself on the currently available technology and attempts to advance the area of photonics based diagnostics techniques. However, before exploiting and perfecting available techniques for novel applications, it is important to understand the basic principles they rely on. As such, this chapter will concentrate on the basics of light interactions with various media, specifically organic tissues.

2.2 Light interaction with biological objects

In all cases of light and laser application for biomedical purposes, light has to interact with organic tissue. It is this interaction, which elicits specific responses from the organism being irradiated. Before understanding how light produces various effects on organic tissues, we must understand, at a basic level, how light interacts with simple isotropic systems. Only then can we observe how such interactions vary in complex organic systems.

2.2.1 Fundamental properties of light interaction

Upon contact with any object, light undergoes a number of events. These are reflection, scattering, refraction, absorption and transmission. The degree to which these events occur is dependent on the medium with which the light is interacting. Figure 2.1 is a simple diagram of these light interactions with an isotropic medium (Boas et al. 2011; Vo-Dinh 2010).

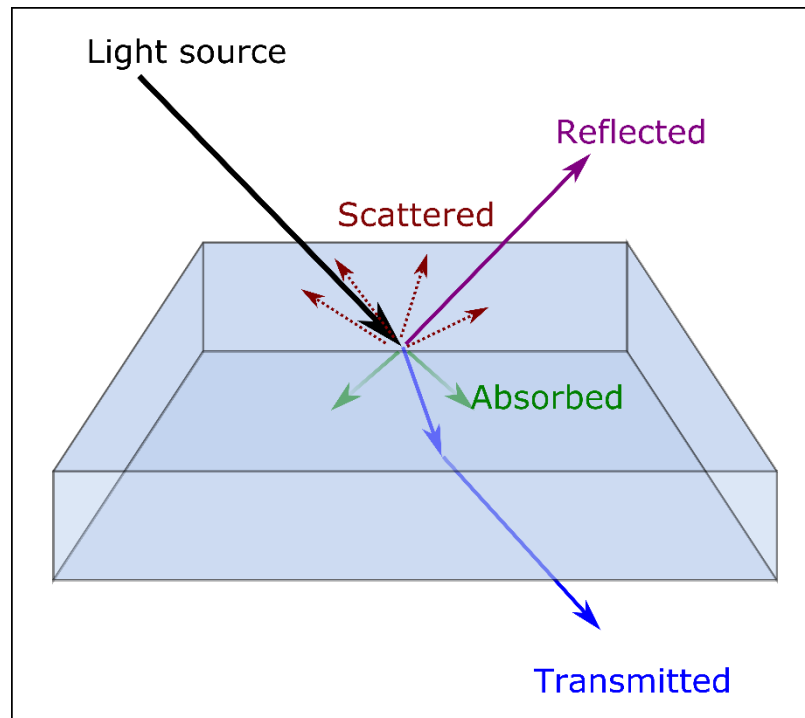


Figure 2.1 Simple diagram of basic light interactions with an isotropic medium. The reflected, scattered, absorbed and transmitted light paths are presented. Additionally an unlabelled point of refraction, where the light enters a medium of a different refractive index, is displayed at the interface between the two different mediums.

2.2.1.1 Reflection and refraction

To understand the events of reflection and refraction, it is important to understand that every material through which light can travel has a refractive index. The refractive index (n) describes the linear optical properties of homogeneous media. For such media it can be calculated by,

$$n = \frac{c}{v} \quad (2.1)$$

Where c is the speed of light in a vacuum ($2.998 \times 10^8 \text{ m s}^{-1}$) and v is the phase velocity of light in the medium.

Considering this, as light propagates through a medium with refractive index n_1 and encounters the boundary of a medium with a refractive index of n_2 , it will be redirected. Depending on the wavelength of the propagating light and the surface of the object it interacts with (smoothness, curvature, etc.), the light will either be reflected off the object (Figure 2.1) or will enter the object at an altered angle (Figure 2.2)(Boas et al. 2011; Vo-Dinh 2010).

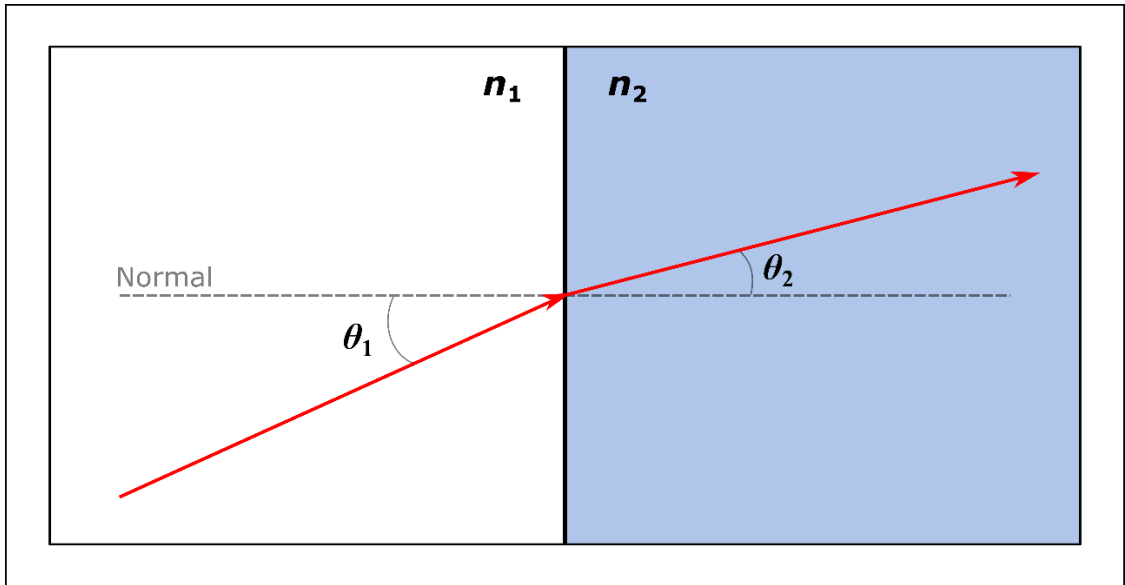


Figure 2.2 Simple diagram depicting refraction of a beam of light as it crosses the interface between two mediums of differing refractive index (n_1 and n_2). The angle of incidence (θ_1) and angle of refraction (θ_2) are also shown.

Snell's law, as proposed by Willebrord Snellius but also known about prior to the astronomer's lifetime (Wolf & Krotzsch 1995; Rashed 1990), can be used to calculate any of the values as long as the others are known. Below is the equation solving for the angle of refraction,

$$\sin \theta_2 = \frac{n_1}{n_2} \sin \theta_1 \quad (2.2)$$

2.2.1.2 Absorption and transmission

Upon entering the object, energy in the form of light can be absorbed. Absorption happens in a medium by atoms and molecules extracting the incoming light energy to be excited to a higher energy level. Depending on the atom or molecule, the regions of the spectrum where absorption tends to occur are collectively known as absorption bands.

Finally, light interacting with an isotropic medium that has not been reflected or absorbed will be transmitted through the object, once again being refracted upon exiting to a medium with a different refractive index (Figure 2.1) (Boas et al. 2011; Vo-Dinh 2010).

2.2.2 Tissue complexity and layering

Considering the above basic aspects of light interactions, it is also important to realise that organic tissue is far from an isotropic medium. While certain mediums such as glass will have few interactions with light passage due to their composition, organic tissue exhibits a much more complex structure. This huge complexity is derived from its heterogeneous state.

Figure 2.3 shows a simplified cross section of skin, comprised of cells forming tissues, which in turn form layers. Within each layer presented in the image below, further layers exist of similar types of cell. The epidermis, for example, is composed of predominantly keratinized, stratified squamous epithelium cells, which form four unique sublayers (with a fifth layer being present in skin on hands and feet). The dermis features two major layers rich in elastin and collagen fibres. Finally, the hypodermis layer (not present on the image below) connects the skin tissue with the underlying muscle and bone (OpenStax 2016).

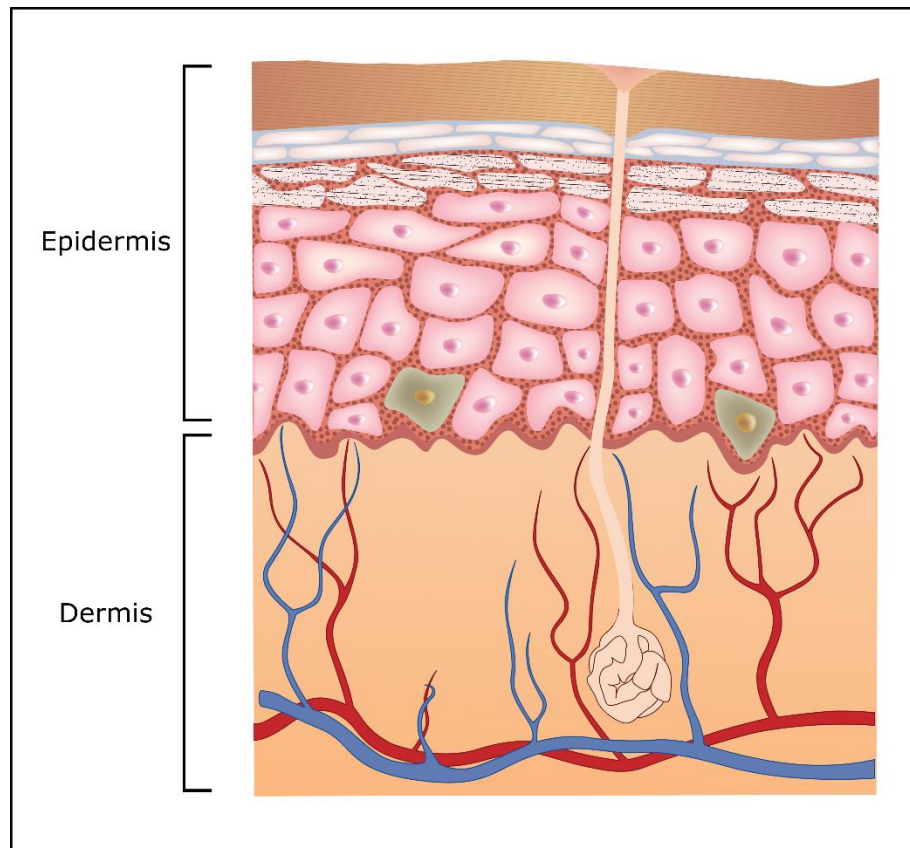


Figure 2.3 Simplified cross section diagram of skin, featuring the epidermis and dermis layers. The four main layers of epithelial cells are presented. Vascularisation is also displayed, as is a sweat gland. (Image purchased from Shutterstock)

Furthermore, each individual cell is further broken up into distinctive structures. Figure 2.4 depicts a generic eukaryotic cell and some of the core organelles. Even at this level, organic cells feature a fluid cytoplasm, numerous sugars and amino acids as well as loose and membrane bound proteins and organelles (Raven & Johnson 2002), all of which can affect and alter light passage through any organic medium.

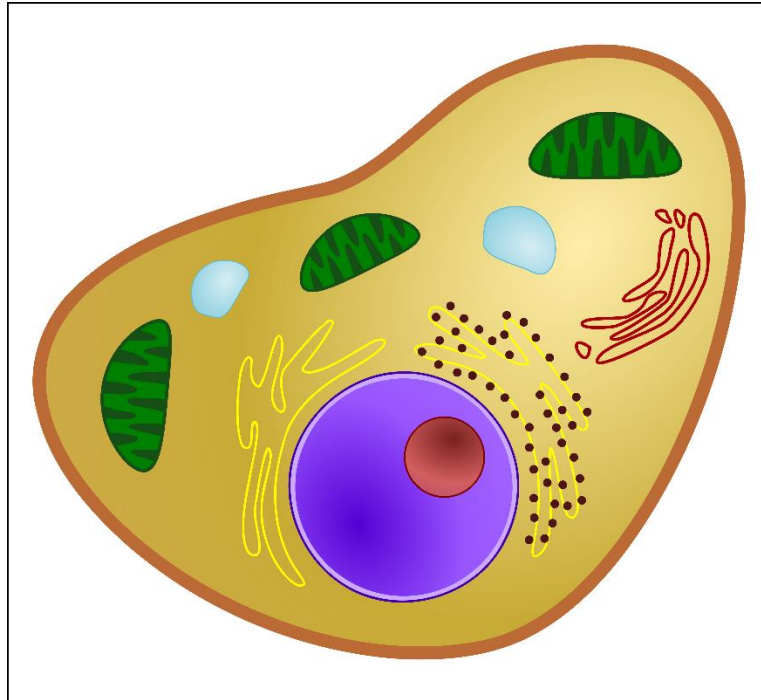


Figure 2.4 Basic 2D schematic of a eukaryotic cell. The image features various organelles floating in the cytoplasm to depict complexity and the numerous interfaces for light scattering and interaction, which are present in even the simplest organic units.

This type of complexity leads to intricate layering throughout all organic tissues. For example, the human bladder will be an important focus of the work described further in this thesis. While it is a relatively simple structure, a fully developed bladder is still comprised of multiple layers. These can, as presented in Figure 2.5, be broken up into four different “coats”: the serous, the muscular, the sub-mucous and the mucous. The serous coat is a partial outer layer and is localised on the superior and lateral regions of the bladder. The muscular coat consists of three layers of muscular fibres, an external and internal layer where the fibres are arranged longitudinally and a middle layer between them with the fibres exhibiting a circular arrangement. The sub-mucous layer is areolar (loose connective tissue) attaching the muscular and mucous layers together. The latter, in turn, is a smooth layer covered by two forms of transitional epithelial cells over the entire inside of the bladder (Gray 2012).

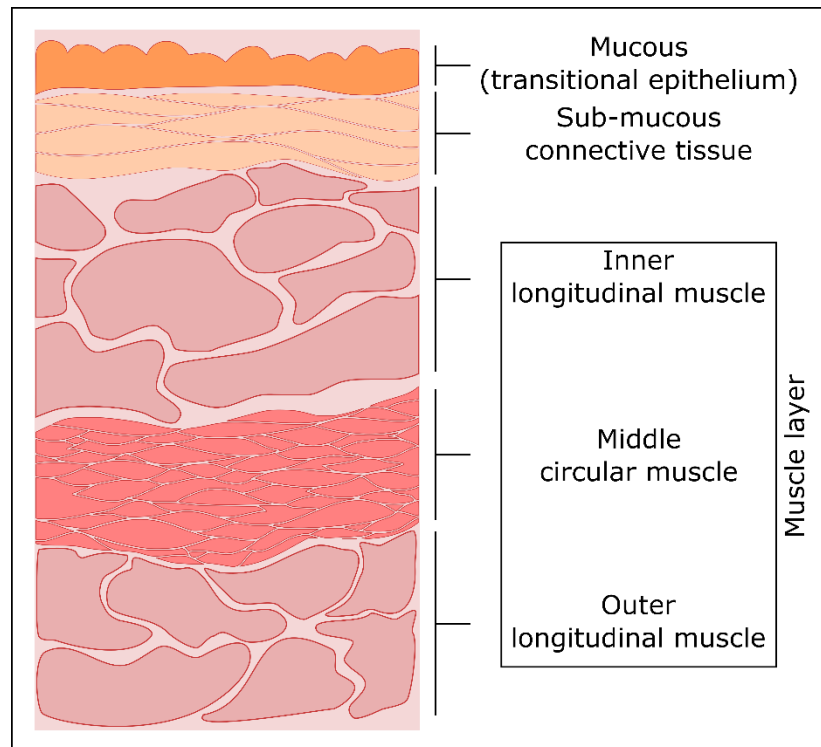


Figure 2.5 Basic schematic of the bladder cell layering.

Through the use of cell layering, tissues throughout the body are made up to serve different and specialised functions. Despite the fact that the specialisation of these different tissues and even organs allows for improved discrimination when observing their function, they still exhibit immense complexity, even in what are relatively simple structures.

2.2.3: Complex light interactions

The reason why it is so crucial to understand the complex, layered and heterogeneous nature of organic tissue when considering light interaction, is due to the increased number of parameters that have to be taken into account as compared to isotropic media. By their very nature, cells not only provide uneven surfaces for the light to interact with upon initial contact, but also further provide media with numerous different refractive indices. The number of events described in 2.2.1 are orders of magnitude higher compared to those in an isotropic medium. Additionally, further interactions become prevalent and need to be taken into account. This is particularly important when considering living tissue, which relies on large amounts of fluid movement, for example in the form of blood.

2.2.3.1 Scattering

In complex structures like tissue, the variation between the multiple refractive indices belonging to different subcellular components as well as the cytoplasm, acts as a major source of scattering. While the wavelength of light passing through the tissue will have specific scattering

characteristics, the sizes, component structures and morphology within the tissue cells are also responsible for the level of scattering (Vo-Dinh 2010). Knowing these sizes and shapes, as well as the values of the refractive indices involved, can technically make it possible to calculate the scattered radiation.

Unlike with singular events however, it is important to note that in complex tissues, the independently scattered light waves will interact not only with the incident wave, but also with each other. Furthermore, it is vital to take note of compounding scattering events (Bohren & Huffman 1998). The most commonly occurring type of scattering in biological objects is known as Rayleigh scattering, where the light is scattered by atoms and molecules smaller than the wavelength of radiation. This type of scattering is heavily dependent on the size of particles encountered by the incident light. Furthermore, as scattered light intensity inversely depends on the fourth power of the wavelength, shorter wavelengths towards the blue end of the visible spectrum undergo stronger scattering than longer wavelengths. This is also the phenomenon behind the sky being blue (Young 1982).

In relation to biological tissues, however, it is also important to take into account the properties of Raman scattering and Raman shift. While Rayleigh scattering exhibits no energy exchange between radiation and scattering particle and accounts for the majority of scattering events, the scatterer molecule or atom can either absorb some radiation energy or lose a portion of energy itself. These events are known as Stokes and anti-Stokes Raman scattering respectively. Such changes in energy result in alteration of the vibrational level of the scatterer particle and a wavelength shift in scattered radiation unique to that particle (Bumrah & Sharma 2016).

2.2.3.2 Reflection: diffuse and specular

Much like with the scattering, the complexity of a medium will also alter the way light reflects off the surface of said medium. The case portrayed in Figure 2.1 above is commonly known as specular reflectance, which happens as a result of a smooth or polished surface. More specifically, this involves the light undergoing reflection at an angle equal to that of the angle of incidence.

However, biological tissue is not a smooth medium. Thus, it is important to understand that in addition to specular reflection, light can undergo diffuse reflection or a combination of both. Diffuse reflection arises when an uneven surface reflects oncoming light in a number of directions at a variety of angles (Juds 1988).

2.2.4 Autofluorescence

In addition to the fundamental light interactions described above, it is important to take into account the events, which occur upon absorption of a photon. Certain molecules, upon absorption of

energy in the form of a photon with a specific wavelength from the UV-visible and near-infrared (IR) spectral ranges, are converted from their ground state to their excited state. These molecules may then release energy, again in the form of a photon. Such a system is not perfect however, resulting in a loss of energy between absorption and emission. Thus, a photon of a different wavelength is emitted. The collective term for such molecules is fluorophores. Fluorophores endogenously present in organic systems, capable of emitting photons upon excitation by specific wavelengths of light radiation without externally added molecules, are distinguished as autofluorophores. The phenomenon relating to autofluorophore action is autofluorescence (Monici 2005).

The autofluorescence of proteins is generally exhibited as a result of increased amounts of various amino acids. Specifically, tryptophan, tyrosine and phenylalanine, though the former usually dominates the protein spectrum. Furthermore, it is vital to understand that the proximity of these amino acids within the protein structure also has an effect on the autofluorescence excitation and emission (Vo-Dinh 2010; Menter 2006; Monici 2005).

2.3 Diagnostic and clinical relevance

The bulk of this chapter has concentrated on the interactions between light and various surfaces, specifically organic tissues. Such interactions are important to consider when developing methodologies and technologies for imaging, monitoring or diagnosis of tissue. For example, observing the way scattering occurs can provide insights into the physical properties of organic tissue. However, as with the case of autofluorescence, directly assessable biomarkers are also available to be used.

2.3.1 Autofluorophores

As already mentioned, specific organic molecules have autofluorescent properties. These molecules can thus be employed as useful biomarkers when spectroscopically analysing organic tissue. For example, epithelial and connective tissues may be distinguished by observing the collagen and elastin fluorescence signals (Vo-Dinh 2010). At this time, the excitation and emission maxima for these biomarkers have been characterised in detail and are well known (Croce & Bottiroli 2014; Huang et al. 2006). Table 2.1 presents these values for some of the most diagnostically and clinically relevant biomarkers.

Table 2.1 Excitation and emission wavelengths of various autofluorophores

Fluorophore	Molecules/localisation	Excitation (nm)	Emission (nm)
Aromatic amino acids	Tryptophan	280	350
	Tyrosine	275	300
	Phenylalanine	260	280
Cytokeratins	Intracellular fibrous protein	280-325	495-525
Collagen	Extracellular fibrous protein	330-340	400-410
Fatty acids	Accumulated lipids	330-350	470-480
Reduced pyridine nucleotides	β -nicotinamide adenine dinucleotide (NADH) (bound)	330-380	440
	NADH (free)		462
Elastin	Connective tissue	350-420	420-510
Flavins	flavin adenine dinucleotide (FAD)	350-370	480-540
Lipofuscin	Miscellaneous (proteins, lipids)	400-500	480-700
Porphyrins	Haemoglobin/myoglobin	500-600	630, 670
Melanin	Melanocytes	785	820-920

Fluorescence spectroscopy is the technique used to measure the emission of this autofluorescence. However, as organic tissue is complex and contains many various biomarkers, the emission spectra do not come out exclusively depicting a specific biomarker. Figure 2.6 shows typical emission spectra for four different excitation wavelengths, as recorded from pure compounds in solution (Dunaev et al. 2015).

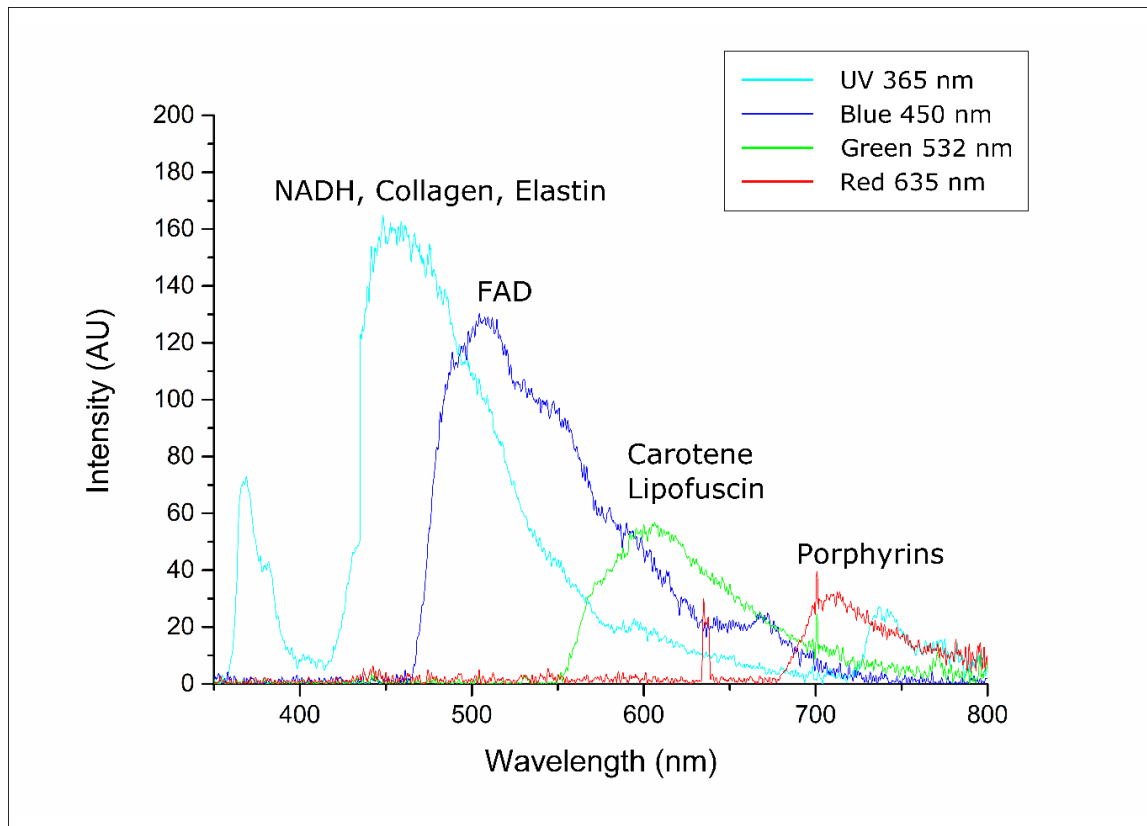


Figure 2.6 A typical example of emission spectra for four different excitation wavelengths (Dunaev et al. 2015). UV (365 nm), blue (450 nm), green (532 nm) and red (635 nm) excitations are presented. Biomarkers excited by the stated wavelengths of light are labelled next to their emission peaks.

As is evident from the figure, emissions of specific autofluorophores are not unique on the spectrum. Wavelengths of light near to the specific excitation wavelength of an autofluorophore may excite it to a lesser extent. This results in the curved spectra with multiple peaks, which display presence of more than one type of biomarker.

2.3.2 Clinically and diagnostically relevant biomarkers

2.3.2.1 NADH and FAD, the redox ratio

Arguably, one of the most important processes for life and the continued survival of organic material is the ability to produce energy. In this respect, organisms and organic tissues produce energy in the form of adenosine triphosphate (ATP) in a process called metabolism. The mainly mitochondria bound reduced pyridine molecule β -nicotinamide adenine dinucleotide (NADH, also commonly known as NAD(P)H) and the oxidised flavoprotein molecule flavin adenine dinucleotide (FAD), thus present themselves as excellent biomarkers for observing metabolic processes (Mayevsky & Chance 2007; Raven & Johnson 2002; Ostrander et al. 2010). Furthermore, it should be noted that the oxidised form of NADH and the reduced form of FAD do not have similar

fluorescent properties. As the process of metabolism involved the net gain of NADH and net consumption of FAD, the two biomarkers are functionally inverse (Kosterin et al. 2005).

In light of the above, a ratio can be used to provide a numeric value describing the metabolism of an organic tissue. This is commonly referred to as the redox ratio (RR) (Ostrander et al. 2010), which is displayed in equation 2.3.

$$RR = \frac{NADH}{FAD} \quad (2.3)$$

The RR can generally indicate an increase in metabolic activity by a rising value and a decrease by falling value.

2.3.2.2 Collagen and elastin, structural proteins

From a diagnostic perspective, structural properties of organic tissue are also of great importance. In this respect, collagen and elastin are great biomarkers for observing potential structural changes under different conditions due to their importance and prevalence in the extracellular matrix (Monici 2005; Kulikov 2014). On its own, collagen fibres can account for as much as 60 – 70 percent of the dry weight of dermal tissue. When considering that structural proteins, such as collagen, will fluctuate in quantity depending on apoptotic conditions of cells or formation of new healthy or even dysplastic cells (Smirnova et al. 2012), the high importance of such biomarkers is easy to see.

It should also be noted that these biomarkers are by no means exclusive and studies conducted by groups such as of Georgakoudi et al. (2002) present evidence that taking various biomarkers into account potentially provides more information from a diagnostic perspective.

2.3.2.3 Porphyrins and melanin

Biomarkers for structural proteins and metabolic processes hold a critical role for observing organic processes, which will be looked at in more detail further on in this thesis. This, however, does not reduce the value of other potential biomarkers in diverse applications. For example, autofluorescence of porphyrin has been used as a marker for determining effectiveness of anti-tumour agents (Gurushankar et al. 2014) by aiding in observation of their anti-angiogenic effect. Protoporphyrin autofluorescence has also been suggested as a potential marker for diabetes mellitus (Fauaz et al. 2010).

A particularly interesting biomarker to note is melanin. Melanin very effectively absorbs light from the UV to the visible spectrum. This results in a suppression of fluorescence signals in areas of high melanin content. As demonstrated by Dunaev et al. (2015), volunteers with high melanin concentrations in their skin displayed largely suppressed autofluorescence signals on shorter

wavelengths, leaving porphyrins as the only clearly evident biomarkers. Analysis by methods utilising longer wavelengths can use melanin as a marker for melanoma (Silveira et al. 2012), however this particular case is a good demonstration that some biomarkers will limit the potential methodologies that are available for a diagnostic application.

2.4 Conclusion

The processes of light interaction with organic tissues are incredibly complex. Decades of research have provided access to many technological advancements. The concepts briefly described in this chapter lie as a foundation for a myriad of photonics techniques, which are currently employed for the study of organic tissues.

References

- Boas, D., Pitris, C. & Ramanujam, N. eds., 2011. Handbook of Biomedical Optics, Boca Raton: CRC Press.
- Bohren, C.F. & Huffman, D.R., 1998. Absorption and Scattering of Light by Small Particles, Wiley-VCH Verlag GmbH. Available at: <http://dx.doi.org/10.1002/9783527618156.ch1>.
- Bumrah, G.S. & Sharma, R.M., 2016. Raman spectroscopy – Basic principle, instrumentation and selected applications for the characterization of drugs of abuse. *Egyptian Journal of Forensic Sciences*, 6(3), pp.209–215.
- Choy, D.S.J., 1988. History of Lasers in Medicine TT - Die Geschichte des Lasers in der Medizin. *Thorac cardiovasc Surg*, 36(S 2), pp.114–117.
- Croce, A.C. & Bottiroli, G., 2014. Autofluorescence spectroscopy and imaging: A tool for biomedical research and diagnosis. *European Journal of Histochemistry*, 58(4), pp.320–337.
- Dougherty, T.J. et al., 1978. Photoradiation therapy for the treatment of malignant tumors. *Cancer research*, 38(8), pp.2628–35. Available at: <http://www.ncbi.nlm.nih.gov/pubmed/667856>.
- Dunaev, A. V et al., 2015. Individual variability analysis of fluorescence parameters measured in skin with different levels of nutritive blood flow. *Medical engineering & physics*, 37(6), pp.574–583. Available at: <http://www.ncbi.nlm.nih.gov/pubmed/25922293>.
- Fauaz, G. et al., 2010. Erythrocyte protoporphyrin fluorescence as a potential marker of diabetes. *Applied Spectroscopy*, 64(4), pp.391–395.
- Finsen, N.R., 1902. Om bekæmpelse af lupus vulgaris med en redegørelse for de i Danmark opnaede resultater, København: Gyldendalske boghandels forlag.
- Georgakoudi, I. et al., 2002. NAD (P) H and Collagen as in Vivo Quantitative Fluorescent Biomarkers of Epithelial Precancerous Changes NAD (P) H and Collagen as in Vivo Quantitative Fluorescent Biomarkers of. , pp.682–687.
- Gøtzsche, P.C., 2011. Niels Finsen's treatment for lupus vulgaris. *Journal of the Royal Society of Medicine*, 104(1), pp.41–42.
- Gray, H., 2012. Gray's Anatomy 15th ed. T. Pickering Pick & R. Howden, eds., London: Bounty Books.
- Gurushankar, K. et al., 2014. Endogenous porphyrin fluorescence as a biomarker for monitoring the anti-angiogenic effect in antitumor response to hesperetin loaded nanoparticles in experimental oral carcinogenesis. *RSC Adv.*, 4(87), pp.46896–46906.
- Huang, Z. et al., 2006. Cutaneous melanin exhibiting fluorescence emission under near-infrared light excitation. *Journal of Biomedical Optics*, 11(3), p.34010. Available at: <http://biomedicaloptics.spiedigitallibrary.org/article.aspx?doi=10.1117/1.2204007>.
- Jameson, D.M., 2014. Introduction to Fluorescence, CRC Press. Available at: <https://books.google.co.uk/books?id=Z53MBQAAQBAJ>.
- Juds, S., 1988. Photoelectric Sensors and Controls: Selection and Application, First Edition, Taylor & Francis. Available at: https://books.google.co.uk/books?id=BkdBo1n_oO4C.
- Kosterin, P. et al., 2005. Changes in FAD and NADH fluorescence in neurosecretory terminals are triggered by calcium entry and by ADP production. *Journal of Membrane Biology*, 208(2), pp.113–124.
- Kulikov, K., 2014. Laser Interaction with Biological Material, Springer. Available at: <http://link.springer.com/10.1007/978-3-319-01739-6>.
- Mayevsky, A. & Chance, B., 2007. Oxidation-reduction states of NADH in vivo: from animals to clinical use. *Mitochondrion*, 7(5), pp.330–9.
- Menter, J.M., 2006. Temperature dependence of collagen fluorescence. *Photochemical & Photobiological Sciences*, 5(4), pp.403–410.
- Møller, K.I. et al., 2005. How Finsen's light cured lupus vulgaris. *Photodermatology Photoimmunology and Photomedicine*, 21(3), pp.118–124.
- Monici, M., 2005. Cell and tissue autofluorescence research and diagnostic applications. *Biotechnology Annual Review*, 11(SUPPL.), pp.227–256.
- OpenStax, 2016. OpenStax, Anatomy and Physiology, OpenStax CNX. Available at: <http://cnx.org/contents/14fb4ad7-39a1-4eee-ab6e-3ef2482e3e22@8.24>.

- Ostrander, J.H. et al., 2010. Optical redox ratio differentiates breast cancer cell lines based on estrogen receptor status. *Cancer research*, 70(11), pp.4759–4766. Available at: <http://www.ncbi.nlm.nih.gov/pubmed/20460512>.
- Peng, Q. et al., 2008. Lasers in medicine. *Reports on Progress in Physics*, 71(5), p.56701.
- Porto, S.P.S. & Wood, D.L., 1962. Ruby optical maser as a Raman source. *Journal of the Optical Society of America*, 52(3), p.251.
- Rashed, R., 1990. A Pioneer in Anaclastics: Ibn Sahl on Burning Mirrors and Lenses. *Isis*, 81(3), pp.464–491.
- Raven, P. & Johnson, G., 2002. *Biology 6th ed.*, McGraw-Hill Science/Engineering/Math.
- Rosenberg, N., Gelijns, A. & Dawkins, H. eds., 1995. *The Changing Nature of Medical Technology Development*, Washington, DC: National Academy Press.
- Silveira, J.L. et al., 2012. Discriminating model for diagnosis of basal cell carcinoma and melanoma in vitro based on the Raman spectra of selected biochemicals. *Journal of Biomedical Optics*, 17(7), p.77003. Available at: <http://dx.doi.org/10.1117/1.JBO.17.7.077003>.
- Smirnova, O.D., Rogatkin, D. a. & Litvinova, K.S., 2012. Quantitative Fluorescent Biomarkers of Abnormal Tissue Changes. *Journal of Innovative Optical Health Sciences*, 5(2), p.1250010.
- Stern, M., 1975. In vivo evaluation of microcirculation by coherent light scattering. *Nature*, 254, pp.56–58.
- Townes, C.H., 1962. Optical Masers and Their Possible Applications to Biology. *Biophysical Journal*, 2(2), pp.325–329.
- Vo-Dinh, T. ed., 2010. *Biomedical photonics handbook*, Boca Raton: CRC Press. Available at: <http://books.google.com/books?hl=en&lr=&id=Pl4wsXCiZdQC&oi=fnd&pg=PP1&dq=Biomedical+Photonics+Handbook&ots=S7F2dZigml&sig=zRAZXvSSJSqO7gFmnl65nYcd3eo> [Accessed October 29, 2013].
- Wolf, K.B. & Krotzsch, G., 1995. Geometry and dynamics in refracting systems. *European Journal of Physics*, 16(1), pp.14–20.
- Young, A.T., 1982. Rayleigh scattering. *Physics Today*, 35(1), pp.42–48. Available at: <http://physicstoday.scitation.org/doi/10.1063/1.2890003>.
- Zaret, M.M. et al., 1961. Ocular Lesions Produced by an Optical Maser (Laser). *Science*, 134(3489), pp.1525–1526.

Chapter 3 : Principles of biophotonics techniques

The previous chapter provided a brief summary on the multiple ways light interacts with various objects, specifically organic tissues. This information is a crucial basis for the development of technology capable of assessing the conditions of such objects. As such, many techniques have been developed, which have been effectively utilised to collect large volumes of data on organic materials in their varying states. The following chapter will concentrate on a number of these techniques. Specifically, powerful techniques that are commonly utilised, the majority of which are relevant to the work described further in this thesis, were selected for this chapter.

3.1 Laser Doppler flowmetry

Laser Doppler flowmetry (LDF), a technique first commercialised in the 1980s, is a non-invasive method of diagnostics utilised predominantly for the measurement of tissue blood perfusion in organic tissues. The concept was initially proposed for measurement of haemodynamics by Stern (1975), by monitoring the scattering of coherent light by static tissues as well as the moving blood cells within a living organism.

To explain further, LDF is specifically based around the scattering of laser radiation (near IR) from moving particles within the organic system. The light will pass through the organic tissue in accordance to this tissue's optical properties until it is scattered by a dynamic particle, which in terms of organic systems will be an erythrocyte. These moving particles will scatter the oncoming photons and alter the frequency of said photons in a process more commonly referred to as the Doppler shift. The size of this Doppler shift depends on the scattering angle, the velocity of the dynamic particle, the wavelength of light within the tissue and the angle between the direction of particle velocity and the scattering vector. It is important to note here, that in an organic system the scattering events will not be unique. Due to the continuous stream of erythrocytes and the varying orientation of microvessels within organic tissue, multiple shifts will occur in the same system even if all the particles travel at an identical speed. Thus, the sum of individual Doppler shift events is used to calculate the average velocity of particles (in this case blood) once the scattered light is ultimately detected by a specialised probe. Ultimately, a continuous monitoring of tissue perfusion is achieved (Leahy et al. 1999; Riva et al. 2010; Rajan et al. 2009; Peng et al. 2008). Figure 3.1 presents a simplified schematic of an LDF device used to calculate the haemodynamics of an organic system.

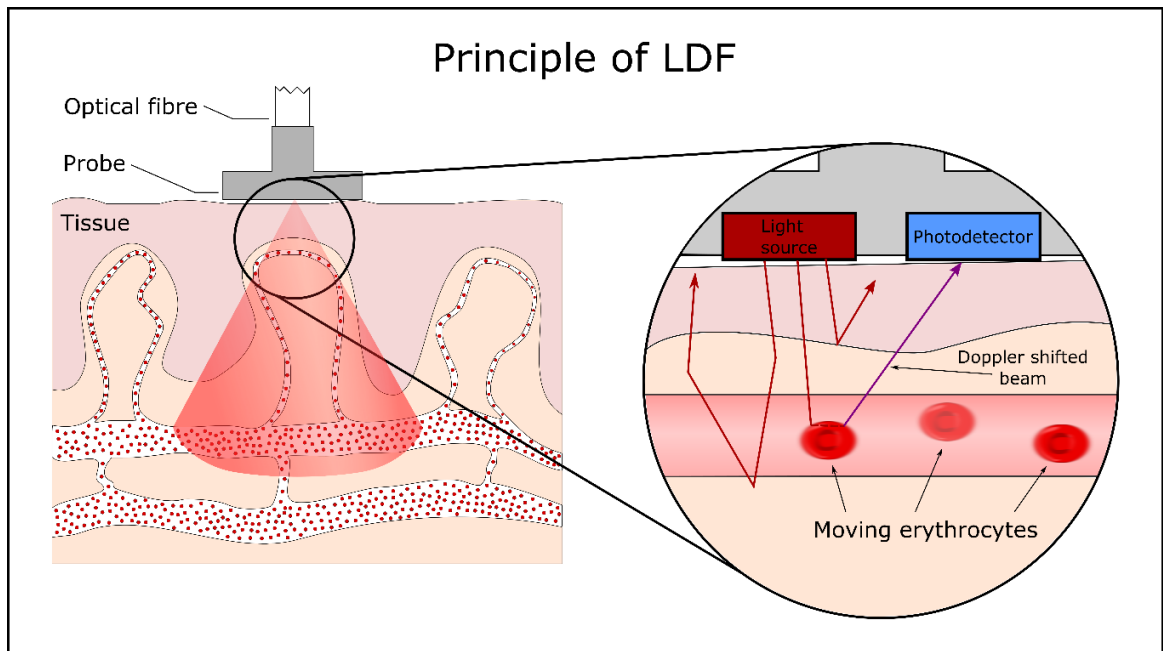


Figure 3.1 Simple schematic of an LDF probe used to calculate the haemodynamics of an organic system.

LDF as a technique, due to the mechanism of its action, is thus able to provide a very sensitive method for non-invasive blood perfusion measurement. The lack of dependence on radioactive markers, as employed in other techniques, stands as one of the major benefits of LDF (Rajan et al. 2009; Riva et al. 2010; Jafarzadeh 2009). Unfortunately, while the technique is being slowly adapted to clinical application, the majority of use is found in the academic and research sectors. This is primarily due to a number of limitations. The nature of the sensitivity of the technique also results in oversensitivity to minute motion and artefacting. This is compounded by a relatively short penetration depth and the occurrence of multiple Doppler shifts, leading to increased noise signal (Leahy et al. 1999; Rajan et al. 2009). Additionally, LDF uses arbitrary perfusion units rather than an absolute measurement (Leitao Ferreira 2007), which clinical practice is often reluctant to employ.

Despite the drawbacks, advances are constantly being made. LDF has been successfully demonstrated in multiple settings such as cancer research (Palmer et al. 2013; Hemingway et al. 1992; Heier et al. 1991), plastic surgery (Alsbjörn et al. 1984), physiological measurements (Dunaev et al. 2014) and even in clinical perfusion monitoring for Raynaud's syndrome and diabetes (Dremin et al. 2016). Further development within the research areas employing LDF, improvement of the technique's metrological support and combination with other diagnostic methodologies (for example Dunaev et al., 2015) could eventually see LDF effectively employed in a clinical setting.

3.2 Spectroscopy

Spectroscopy, in itself, is not a description of a single technique. As a collective term, spectroscopy studies the interactions of electromagnetic radiation and matter. At the simplest level, spectroscopic techniques rely on the use of electromagnetic radiation to elucidate property data about an object of interest through the measurement of absorption, spontaneous emission and/or various types of scattering. Due to the multiple potential optical properties, which can be measured through spectroscopic means, there is naturally a variety of spectroscopic techniques (Campbell & Dwek 1984). Each such technique has benefits and drawbacks, ranging from variations in price and ease of use, to specifics of application (for example for detection of cancer by a combination of fluorescence and diffuse reflectance spectroscopy as described by Zhu et al. (2008)). This section will concentrate on fluorescence spectroscopy due to the importance of the technique further in the thesis as well as introduce the concept of Raman spectroscopy, a powerful technique that is commonly and effectively employed for analysis of organic and biological objects.

3.2.1 Fluorescence spectroscopy

Chapter 1 of this thesis has already mentioned the concept of fluorescent spectroscopy as a tool for observing properties such as autofluorescence. The principle of the technique is relatively simple. As mentioned in the first chapter, certain molecules have the capacity to absorb energy from specific wavelengths of light. These molecules are labelled fluorophores and autofluorophores (when they are endogenous). The absorption of energy is enough to excite fluorophores from their ground electronic state (S_0) to their singlet excitation state (S_1). After excitation, the fluorescent molecule undergoes relaxation back to the ground state by either radiatively or non-radiatively releasing energy. A non-radiative relaxation is characterised by energy dissipating as heat. Radiative relaxation is the principle behind fluorescence. Following a non-radiative relaxation within the excited state, the fluorescing molecule transitions down to the ground state with a release of a photon. The wavelength of the released photon is always red-shifted in comparison to the excitation wavelength, due to the loss of energy occurring as a result of the non-radiative transitions (Ramanujam 2000a; Gillenwater et al. 1998). Figure 3.2 presents this example of emission in a simplified Jablonski diagram.

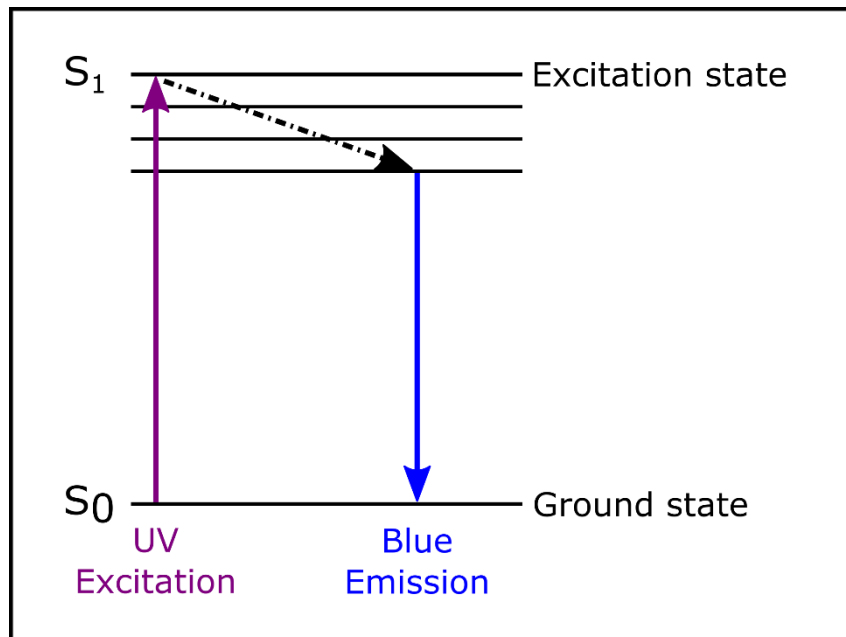


Figure 3.2 Simple Jablonski diagram presenting an example of fluorescence as a result of radiative relaxation. The figure presents UV wavelength excitation followed by blue wavelength emission due to the loss of energy during transition between vibrational levels (depicted as the dotted line). NADH autofluorescence is a real world example of this series of events.

The above physical properties make it possible to excite various autofluorophores within a biological system to determine their relative quantities by employing a photodetector and capturing the emitted, red-shifted wavelengths of light. Chapter 2, table 2.1 provides excitation and emission details of the autofluorophores most relevant to biological and clinical applications. It is, however, important to also mention the potential of exogenous fluorophores. Particularly in the fields of photodynamic therapy, fluorescent molecules (such as 5-aminolevulinic acid and hypericin) can be introduced to a biological system based on their preferential uptake by specific, for example neoplastic tissues (Wagnieres et al. 1998).

While fluorescence spectroscopy is a powerful technique capable of providing a good understanding of the relative levels of desired molecules, it does suffer certain limitations. The output of fluorescence data is in forms of biomarker levels rather than quantitative concentrations of said biomarker. Though an issue, this can be circumvented through the application of biologically relevant ratios (such as the redox ratio mentioned in section 2.3.2.1 of this thesis). It is also important to note that a certain level of distortion is to be expected in any output signal, due to the inevitable series of scattering and absorption events emitted photons will encounter. This effect is compounded in living tissues due to the presence of very strong absorbers such as haemoglobin (Sudhakar et al. 1994).

Despite the various drawbacks, fluorescence spectroscopy has seen successful application in disease diagnostics. Amongst many diseases, cervical and oesophageal dysplasia (Pandey et al. 2012; Georgakoudi et al. 2001), atherosclerosis of the aorta and coronary arteries (Marcu et al. 2001; Calton

et al. 2010) and multiple varieties of cancer (Litvinova et al. 2010; Shahzad et al. 2010; Palmer et al. 2013; Ramanujam 2000b) have all been detected with the aid of the technique.

3.2.2 Raman spectroscopy

While fluorescence spectroscopy relies on the excitation of specific molecules within a system, Raman spectroscopy is a technique that relies on the scattering properties of the objects of interest. The technique employs a monochromatic light source to irradiate the object of interest and generate scattering events as a result of light interacting with vibrating molecules. As already mentioned in section 2.2.3, a small fraction of these scattering events, those undergoing Raman scattering, will be inelastic. More specifically, this scattered radiation exhibits a changed frequency compared to that of the incident radiation. The detection of these Raman shifted scattering events is followed by the construction of Raman spectra (Smith & Dent 2005; Bumbrah & Sharma 2016).

Considering that this technique is capable of monitoring unique and specific molecules within a system and the last few decades have seen a large technological advancement, Raman spectroscopy presents a high potential for clinical applications in diagnostics and monitoring. Though much of the drive has been towards detecting cancer, successful implementation of Raman spectroscopy has been achieved in many various tissue types, including the oesophagus, the gastrointestinal tract, cervix, mouth and many others.

3.3 Tissue reflectance oximetry

Tissue reflectance oximetry (TRO) is a technique most commonly employed to determine the microhaemodynamics, oxygen transport characteristics and utilisation of an organic system in a non-invasive manner. The technique employs a spectroscopic approach in order to calculate levels of oxygenated and deoxygenated haemoglobin (Figure 3.3). These two haemoglobin fractions exhibit unique absorption properties, presenting a possibility of detection by green (530 nm) and red (635 nm) radiation wavelengths respectively (Murkin & Arango 2009; Scheeren et al. 2012; Ferrari & Quaresima 2012). This technique ultimately determines the relative volumes of the above-mentioned haemoglobin fractions, as well as the oxygen saturation of the microvasculature, within the monitored tissue volume. These parameters provide an average level of blood velocity and a tissue oxygen saturation value (Dunaev et al. 2014).

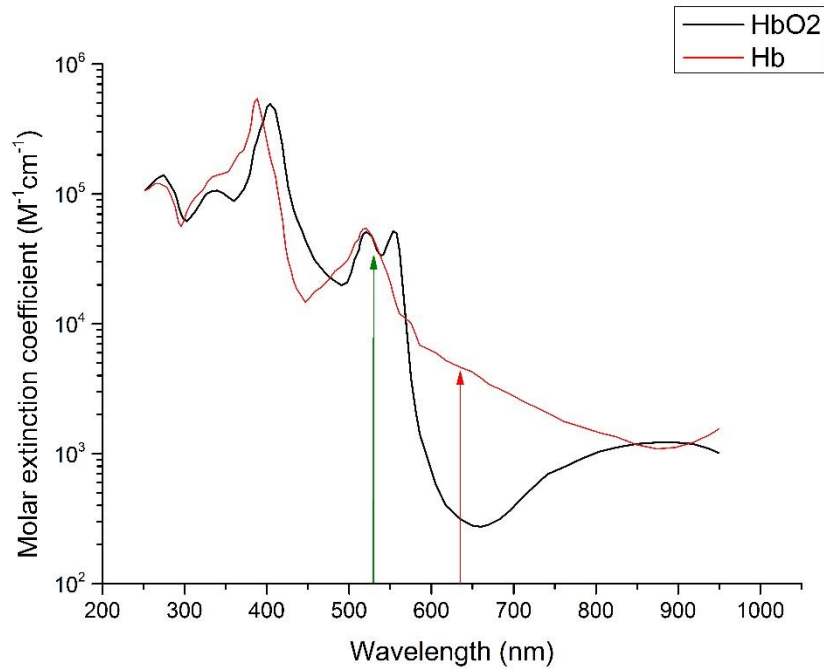


Figure 3.3 A rough graph presenting the absorption spectra of oxygenated (HbO₂) and deoxygenated (Hb) haemoglobin. Red and green arrows indicate the specific absorption wavelengths employed to detect the differing haemoglobin fractions.

It is important to note that similarly to the above techniques discussed in this chapter already, TRO (and other similar methodologies) is also more commonly employed for the purposes of research, though it is finding a place in clinical application. Specifically, this is due to the lack of standardised instrumentation and methodological support for the given techniques (Quaresima et al. 2013). Despite this, as already mentioned for application of LDF, TRO could find a lot of medical application in conjunction with other diagnostic methodologies.

3.4 Optical coherence tomography

Optical coherence tomography (OCT) is a non-invasive, real-time diagnostics technique that was first introduced in the 1980s, but found initial application in optometry in the following decade. The methodology is based on the use of backscattered reflection signals of near IR radiation within the range of 700 – 1300 nm as a tool for constructing structural images. In this, the technique is similar to ultrasound, though with the application of light instead of sound (Zysk et al. 2007; Fercher et al. 2010). This approach allows for the construction of two dimensional images at a high resolution (around 10 – 20 μm), though at a relatively shallow depth (around 2 mm) (Liu et al. 2013; Li et al. 2011).

Though a relatively modern technique, OCT has found extensive application in both biomedical research and clinical diagnostics fields. For example, Maeda et al. (2012) describe the use of OCT to observe microvascular function in *in vivo* rodent models of cancer. Clinically, OCT has been applied extensively in ophthalmology, cardiology and oncology of different organs (including, but not limited to, the mouth and the bladder), as well as other conditions (Zysk et al. 2007; Schmidbauer et al. 2009; Wilder-Smith et al. 2010)

3.5 Other techniques

The above techniques, while powerful, are not the limit of currently available approaches. One of the major benefits they share is the potential for real-time diagnostics or monitoring of living tissues. However, biophotonics techniques exist, which provide a wealth of data from *in vitro* samples and tissue segments. While none of these methodologies are employed in the following work, they bear mention due to their impact on diagnostics and data acquisition abilities.

Flow cytometry is a technique that relies on passing a constant stream of individual cells through a focussed laser beam, with the aim of detecting induced fluorescence and scattering. This is commonly achieved by application of specific fluorophore labels using specific antibodies. While the method requires samples to be taken and carefully prepared for diagnosis, it does provide a large parameter of potential measurements per cell, including size, volume and quantity of RNA/DNA, amongst others. Thus, this technique has seen successful application for diagnosis of such conditions as cancer (Barlogie et al. 1983; Brownstein et al. 2007).

Unlike flow cytometry, confocal laser scanning microscopy (CLSM) is an imaging based technique capable of providing high quality, low blur, three dimensional images constructed from fluorescence properties of tissues of interest (endogenously or with the aid of specific dyes). This technique paved the way for accurately imaging sections of tissue as thick as 50 μm . Ultimately, the technique provides a versatile approach where the quality and resolution of the output image can be enhanced at the cost of acquisition time. This can result in high quality, detailed images. However, the technique is relatively slow, especially when imaging more than one fluorescence channel. It also suffers from a narrow field of view and limited penetration depth (Jonkman & Brown 2015; Jerome 2011).

Multi-photon laser scanning microscopy (MLSM) is a technique that works on a similar principle to CLSM, but relies specifically on IR excitation. This allows for an improved penetration depth and reduced scattering within the sample tissue, providing a better quality output image (Xu et al. 1996; Yeh et al. 2002; Rafailov 2014). One of the major advantages of this technique is the ability to use non-linear scattering (such as second and third harmonic generation) in order to generate contrast (Moreaux et al. 2000; Sun et al. 2000), providing an avenue for imaging active processes in various organisms (Aviles-Espinosa et al. 2014; Débarre et al. 2004). Much like the CLSM however,

MLSM also suffers from slow acquisition times. This ultimately prevents the technique from recording data of samples such as biopsies, which may denature or lose their properties in the time it takes to form a complete, high-resolution image.

3.6 Conclusions

This chapter briefly introduced a number of powerful and commonly employed techniques currently available for analysis of organic tissues. While not all are employed within the work outlined further in this thesis, the current applications in research and clinical practice, as well as the potential future applications of the techniques bears mention.

For the purposes of this thesis, the LDF, TRO and fluorescence spectroscopy techniques have been explained in more detail as they will be the backbone in much of the work outlined in the following chapters.

References

- Alsbjörn, B., Micheels, J. & Sørensen, B., 1984. Laser Doppler flowmetry measurements of superficial dermal, deep dermal and subdermal burns. *Scandinavian journal of plastic and reconstructive surgery*, 18(1), pp.75–79.
- Aviles-Espinosa, R. et al., 2014. Third-harmonic generation for the study of *Caenorhabditis elegans* embryogenesis. *Journal of biomedical optics*, 15(August 2010), p.46020.
- Barlogie, B. et al., 1983. Flow cytometry in clinical cancer research. *Cancer research*, 43(9), pp.3982–97. Available at: <http://www.ncbi.nlm.nih.gov/pubmed/6347364>.
- Brownstein, M. et al., 2007. Biophotonic tools in cell and tissue diagnostics. *Journal of Research of the National Institute of Standards and Technology*, 112(3), p.139. Available at: <http://nvlpubs.nist.gov/nistpubs/jres/112/3/V112.N03.A02.pdf>.
- Bumrah, G.S. & Sharma, R.M., 2016. Raman spectroscopy – Basic principle, instrumentation and selected applications for the characterization of drugs of abuse. *Egyptian Journal of Forensic Sciences*, 6(3), pp.209–215. Available at: <http://linkinghub.elsevier.com/retrieve/pii/S2090536X15000477>.
- Calfon, M.A. et al., 2010. Intravascular near-infrared fluorescence molecular imaging of atherosclerosis: toward coronary arterial visualization of biologically high-risk plaques. *Journal of biomedical optics*, 15(1), p.11107. Available at: <http://biomedicaloptics.spiedigitallibrary.org/article.aspx?articleid=1103245>.
- Campbell, I.D. & Dwek, R.A., 1984. *Biological spectroscopy*, Benjamin/Cummings Pub. Co. Available at: <https://books.google.co.uk/books?id=JofwAAAAMAAJ>.
- Débarre, D. et al., 2004. Velocimetric third-harmonic generation microscopy: micrometer-scale quantification of morphogenetic movements in unstained embryos. *Optics letters*, 29(24), pp.2881–3. Available at: <http://www.ncbi.nlm.nih.gov/pubmed/15645811>.
- Dremin, V. V et al., 2016. The blood perfusion and NADH / FAD content combined analysis in patients with diabetes foot. *SPIE proceedings*, 9698(0), p.969810.
- Dunaev, A. V et al., 2015. Individual variability analysis of fluorescence parameters measured in skin with different levels of nutritive blood flow. *Medical engineering & physics*, 37(6), pp.574–583. Available at: <http://www.ncbi.nlm.nih.gov/pubmed/25922293> [Accessed April 30, 2015].
- Dunaev, A. V et al., 2014. Investigating tissue respiration and skin microhaemocirculation under adaptive changes and the synchronization of blood flow and oxygen saturation rhythms. *Physiological Measurement*, 35, pp.607–621.
- Fercher, A.F. et al., 2010. Optical coherence tomography – development, principles, applications. *Zeitschrift für Medizinische Physik*, 20(4), pp.251–276. Available at: <http://www.sciencedirect.com/science/article/pii/S0939388909001524>.
- Ferrari, M. & Quaresima, V., 2012. Review: Near infrared brain and muscle oximetry: From the discovery to current applications. *Journal of Near Infrared Spectroscopy*, 20(1), pp.1–14.
- Georgakoudi, I. et al., 2001. Fluorescence, reflectance, and light-scattering spectroscopy for evaluating dysplasia in patients with Barrett’s esophagus. *Gastroenterology*, 120(7), pp.1620–1629. Available at: <http://linkinghub.elsevier.com/retrieve/pii/S0016508501013269> [Accessed January 8, 2015].
- Gillenwater, A., Jacob, R. & Richards-Kortum, R., 1998. Fluorescence spectroscopy: A technique with potential to improve the early detection of aerodigestive tract neoplasia. *Head and Neck*, 20(6), pp.556–562.
- Heier, M.S. et al., 1991. Raynaud’s phenomenon after combination chemotherapy of testicular cancer, measured by laser Doppler flowmetry. A pilot study. *British Journal of Cancer*, 63(4), pp.550–552. Available at: <http://www.ncbi.nlm.nih.gov/pmc/articles/PMC1972340/>.
- Hemingway, D.M. et al., 1992. Monitoring blood flow to colorectal liver metastases using laser Doppler flowmetry: the effect of angiotensin II. *British Journal of Cancer*, 66(5), pp.958–960. Available at: <http://www.ncbi.nlm.nih.gov/pmc/articles/PMC1977985/>.
- Jafarzadeh, H., 2009. Laser Doppler flowmetry in endodontics: a review. *International endodontic*

- journal*, 42(6), pp.476–90. Available at: <http://www.ncbi.nlm.nih.gov/pubmed/19459999>.
- Jerome, W.G.J., 2011. The Theory of Fluorescence. In R. L. Price & J. W. Gray, eds. *Basic Confocal Microscopy*. pp. 157–179. Available at: <http://link.springer.com/10.1007/978-0-387-78175-4>.
- Jonkman, J. & Brown, C.M., 2015. Any Way You Slice It-A Comparison of Confocal Microscopy Techniques. *Journal of biomolecular techniques: JBT*, 26(2), pp.54–65. Available at: <http://www.pubmedcentral.nih.gov/articlerender.fcgi?artid=4365987&tool=pmcentrez&rendertype=abstract>.
- Leahy, M.J. et al., 1999. Principles and practice of the laser-Doppler perfusion technique. *Technology and health care: official journal of the European Society for Engineering and Medicine*, 7(2–3), pp.143–162.
- Leitao Ferreira, A.I., 2007. *Laser Doppler Flowmetry*, Coimbra.
- Li, P. et al., 2011. In vivo microstructural and microvascular imaging of the human corneo-scleral limbus using optical coherence tomography. *Biomedical optics express*, 2(11), pp.3109–18. Available at: <http://www.pubmedcentral.nih.gov/articlerender.fcgi?artid=3207379&tool=pmcentrez&rendertype=abstract>.
- Litvinova, K.S. et al., 2010. Chronic Hypoxia as a Factor of Enhanced Autofluorescence of Endogenous Porphyrins in Soft Biological Tissues. *Methods*, 7547, pp.1–6.
- Liu, G. et al., 2013. In vivo, high-resolution, three-dimensional imaging of port wine stain microvasculature in human skin. *Lasers in surgery and medicine*, 45(10), pp.628–32. Available at: <http://www.ncbi.nlm.nih.gov/pubmed/24155140> [Accessed September 5, 2014].
- Maeda, A. et al., 2012. In vivo optical imaging of tumor and microvascular response to ionizing radiation. *PloS one*, 7(8), p.e42133. Available at: <http://www.pubmedcentral.nih.gov/articlerender.fcgi?artid=3425534&tool=pmcentrez&rendertype=abstract> [Accessed September 5, 2014].
- Marcu, L. et al., 2001. Discrimination of Human Coronary Artery Atherosclerotic Lipid-Rich Lesions by Time-Resolved Laser-Induced Fluorescence Spectroscopy. *Arteriosclerosis, Thrombosis, and Vascular Biology*, 21(7), pp.1244–50. Available at: <http://atvb.ahajournals.org/cgi/content/abstract/21/7/1244%5Cnhttp://www.ncbi.nlm.nih.gov/pubmed/11451759>.
- Moreaux, L. et al., 2000. Membrane imaging by simultaneous second-harmonic generation and two-photon microscopy. *Optics letters*, 25(5), p.320. Available at: <http://www.opticsinfobase.org/abstract.cfm?id=366%5Cnhttp://ol.osa.org/abstract.cfm?URI=ol-25-5-320>.
- Murkin, J.M. & Arango, M., 2009. Near-infrared spectroscopy as an index of brain and tissue oxygenation. *British Journal of Anaesthesia*, 103(Supplement 1), pp.i3–i13. Available at: <http://bj.oxfordjournals.org/lookup/doi/10.1093/bja/aep299>.
- Palmer, S. et al., 2013. Technologic developments in the field of photonics for the detection of urinary bladder cancer. *Clinical Genitourinary Cancer*, 11(4), pp.390–396.
- Pandey, K. et al., 2012. Fluorescence spectroscopy: a new approach in cervical cancer. *Journal of obstetrics and gynaecology of India*, 62(4), pp.432–6. Available at: <http://www.pubmedcentral.nih.gov/articlerender.fcgi?artid=3500953&tool=pmcentrez&rendertype=abstract>.
- Peng, Q. et al., 2008. Lasers in medicine. *Reports on Progress in Physics*, 71(5), p.56701.
- Quaresima, V., Ferrari, M. & Fantini, S., 2013. Accuracy of oxygen desaturation of hemoglobin in muscle by near-infrared oximeters [corrected]. *Medicine and science in sports and exercise*, 45(6), p.1217.
- Rafailov, E.U., 2014. *The Physics and Engineering of Compact Quantum Dot-based Lasers for Biophotonics* E. U. Rafailov, ed., Weinheim, Germany: Wiley-VCH Verlag GmbH & Co. KGaA. Available at: <http://doi.wiley.com/10.1002/9783527665587>.
- Rajan, V. et al., 2009. Review of methodological developments in laser Doppler flowmetry. *Lasers in Medical Science*, 24(2), pp.269–283.
- Ramanujam, N., 2000a. Fluorescence spectroscopy in vivo. *Encyclopedia of Analytical Chemistry*, pp.20–56. Available at: <http://onlinelibrary.wiley.com/doi/10.1002/9780470027318.a0102/full>.

- Ramanujam, N., 2000b. Fluorescence Spectroscopy of Neoplastic and Non-Neoplastic Tissues. *Neoplasia (New York, N.Y.)*, 2(1–2), pp.89–117. Available at: <http://dx.doi.org/10.1038/sj.neo.7900077>.
- Riva, C.E. et al., 2010. Ocular blood flow assessment using continuous laser Doppler flowmetry. *Acta Ophthalmologica*, 88(6), pp.622–629.
- Scheeren, T.W.L., Schober, P. & Schwarte, L.A., 2012. Monitoring tissue oxygenation by near infrared spectroscopy (NIRS): Background and current applications. In *Journal of Clinical Monitoring and Computing*. Dordrecht: Springer Netherlands, pp. 279–287.
- Schmidbauer, J. et al., 2009. Fluorescence Cystoscopy with High-Resolution Optical Coherence Tomography Imaging as an Adjunct Reduces False-Positive Findings in the Diagnosis of Urothelial Carcinoma of the Bladder. *European Urology*, 56(6), pp.914–919.
- Shahzad, A. et al., 2010. Diagnostic Application of Fluorescence Spectroscopy in Oncology Field: Hopes and Challenges. *Applied Spectroscopy Reviews*, 45(1), pp.92–99. Available at: <http://www.tandfonline.com/doi/abs/10.1080/05704920903435599>.
- Smith, W.E. & Dent, G., 2005. Chapter 1 Introduction, Basic Theory and Principles. In *Modern Raman Spectroscopy - A Practical Approach*. John Wiley & Sons, Ltd, pp. 1–21. Available at: <http://doi.wiley.com/10.1002/0470011831.ch1>.
- Stern, M., 1975. In vivo evaluation of microcirculation by coherent light scattering. *Nature*, 254, pp.56–58. Available at: <http://www.nature.com/nature/journal/v254/n5495/abs/254056a0.html>.
- Sudhakar, K. et al., 1994. Fluorescent derivatives of human hemoglobin. Differences in interaction of the porphyrin with the protein between the alpha and beta subunits. *Journal of Biological Chemistry*, 269(37), pp.23095–23101.
- Sun, C.-K. et al., 2000. Scanning second-harmonic/third-harmonic generation microscopy of gallium nitride. *Applied Physics Letters*, 77(15), p.2331. Available at: <http://link.aip.org/link/APPLAB/v77/i15/p2331/s1&Agg=doi>.
- Wagnieres, G. a, Star, W.M. & Wilson, B.C., 1998. In Vivo Fluorescence Spectroscopy and Imaging for Oncological Applications. *Photochemistry and Photobiology*, 68(5), pp.603–632.
- Wilder-Smith, P. et al., 2010. Optical diagnostics in the oral cavity: an overview. *Oral Diseases*, 16(8), pp.717–728. Available at: <http://doi.wiley.com/10.1111/j.1601-0825.2010.01684.x>.
- Xu, C. et al., 1996. Multiphoton fluorescence excitation: new spectral windows for biological nonlinear microscopy. *Proceedings of the National Academy of Sciences of the United States of America*, 93(20), pp.10763–8. Available at: <http://www.pubmedcentral.nih.gov/articlerender.fcgi?artid=38229&tool=pmcentrez&rendertype=abstract>.
- Yeh, A.T. et al., 2002. Selective corneal imaging using combined second-harmonic generation and two-photon excited fluorescence. *Optics Letters*, 27(23), pp.2082–2084. Available at: <http://ol.osa.org/abstract.cfm?URI=ol-27-23-2082>.
- Zhu, C. et al., 2008. Diagnosis of breast cancer using fluorescence and diffuse reflectance spectroscopy: a Monte-Carlo-model-based approach. *Journal of Biomedical Optics*, 13(3), p.34015.
- Zysk, A.M. et al., 2007. Optical coherence tomography: a review of clinical development from bench to bedside. *Journal of Biomedical Optics*, 12(5), p.51403. Available at: http://www.ncbi.nlm.nih.gov/entrez/query.fcgi?cmd=Retrieve&db=PubMed&dopt=Citation&list_uids=17994864%5Cnhttp://www.ncbi.nlm.nih.gov/pubmed/17994864%5Cnhttp://biomedicaloptics.spiedigitallibrary.org/article.aspx?doi=10.1117/1.2793736.

Chapter 4 : MLNDS and the LAKK series devices.

The last chapter summarised a number of currently available, photonics enabled techniques for the investigation and imaging of organic tissue parameters. The techniques described are known for their effectiveness; however, all field various disadvantages, whether in the form of limited information, poor penetration depths and slow acquisition times, amongst others. To this effect, diagnostics technology has begun to stream towards the combination of photonics based, non-invasive technology into units capable of complimentary methodologies capable of enhancing the quality of received data while also compensating for each other's limitations (Rogatkin et al. 2011; Kalchenko et al. 2011). Such devices have collectively been termed multifunctional laser-based non-invasive diagnostics systems (MLNDS).

At the current moment, use of combined techniques is indeed presenting itself to be highly effective. Many studies are employing multiple techniques to bolster the usefulness of output data (Kalchenko et al. 2011; Patel et al. 2012; Kuznetsov et al. 2011). However, the integration of multiple such techniques into single MLNDS' is still relatively uncommon and particularly rare on the market. As such, this chapter will concentrate on the LAKK series of commercially available devices created by SPE "LAZMA" Ltd. These devices are a good example of multifunctional diagnostics devices employed in a research and diagnostics capacity. Additionally, this series of devices sees extensive use within the work described in this thesis.

4.1 The LAKK-M

The work in this thesis relates to the use of many various forms of photonics based techniques. However, one device is used in each investigation presented in the following chapters. This device is the LAKK-M, an MLNDS developed by SPE "LAZMA" Ltd, Russia. Following the core idea of MLNDS design, Figure 4.1 shows the schematic structure of the LAKK-M.

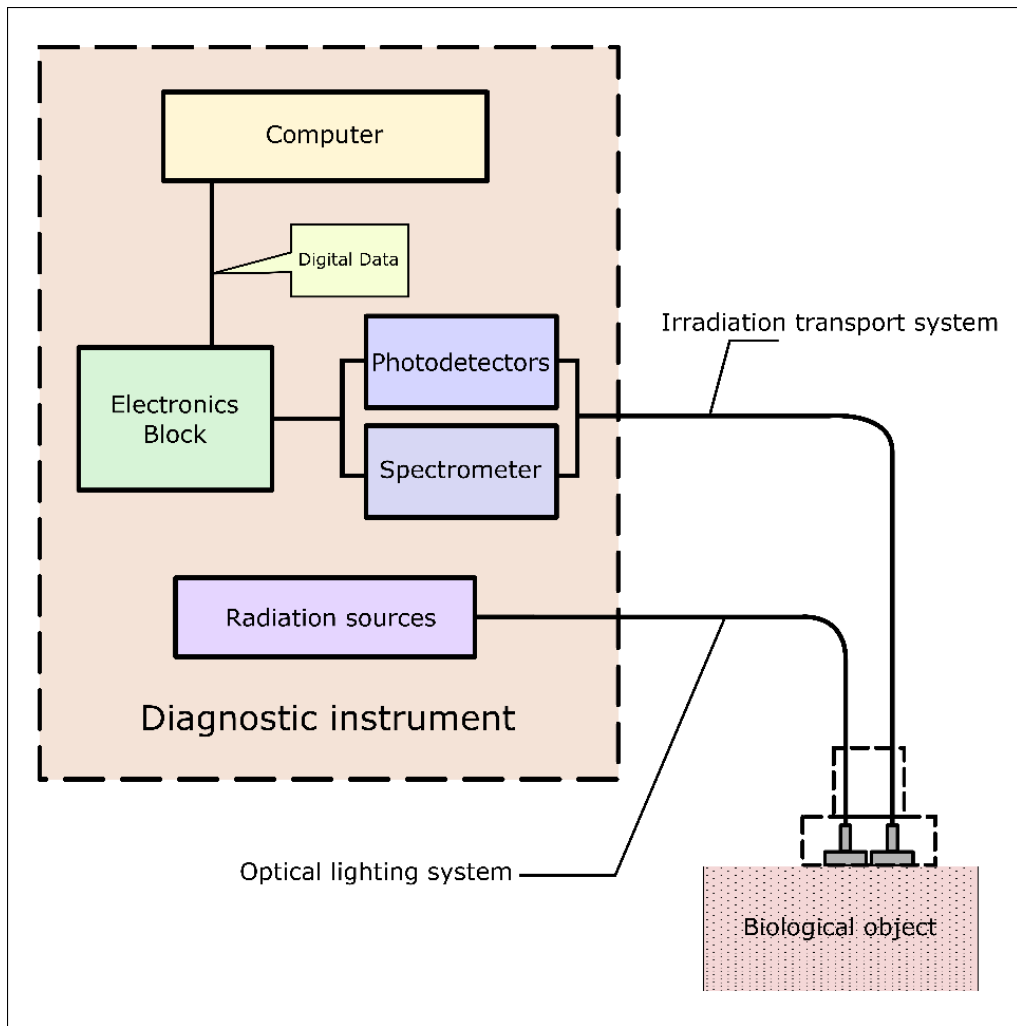


Figure 4.1 Simplified block schematic of the LAKK-M. The device incorporates LDF, TRO, pulse oximetry and fluorescence spectroscopy methodologies. The key internal components are presented.

The reason for such extensive use of the LAKK-M lies in the versatility of the methodologies combined within the system. It provides access to LDF and TRO for measuring microcirculatory parameters such as perfusion and tissue saturation, as well as pulse oximetry (PO) and fluorescence spectroscopy (FS).

The device itself is capable of employing LDF, TRO and pulse oximetry simultaneously. The system is displayed in Figure 4.2 below.

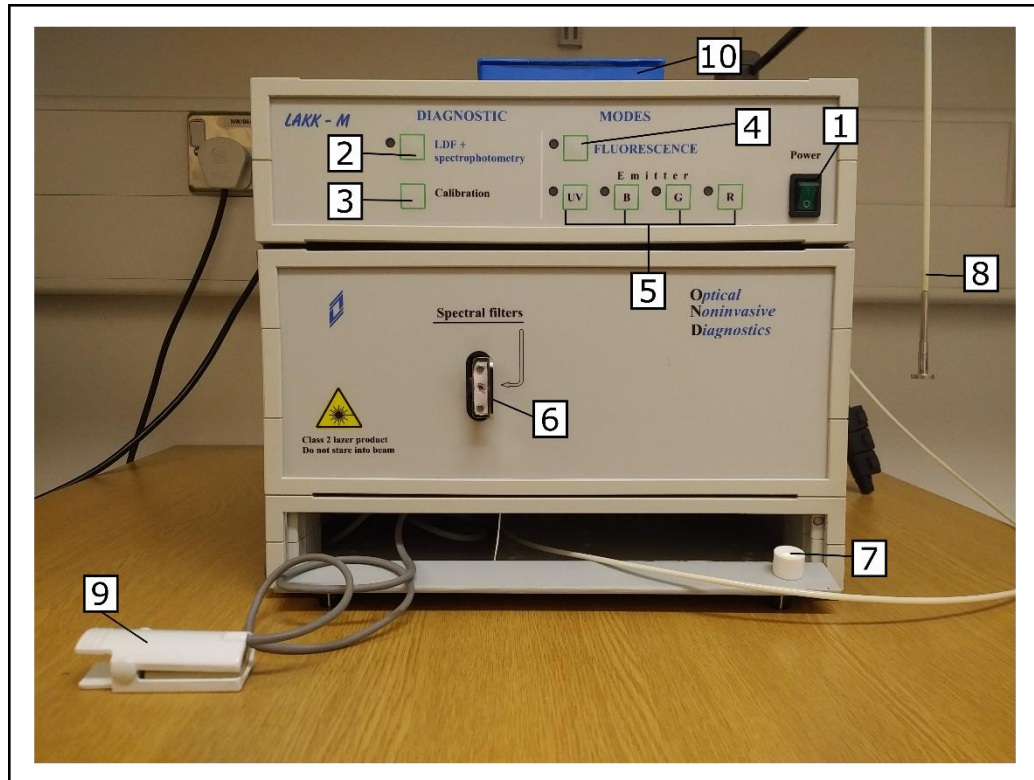
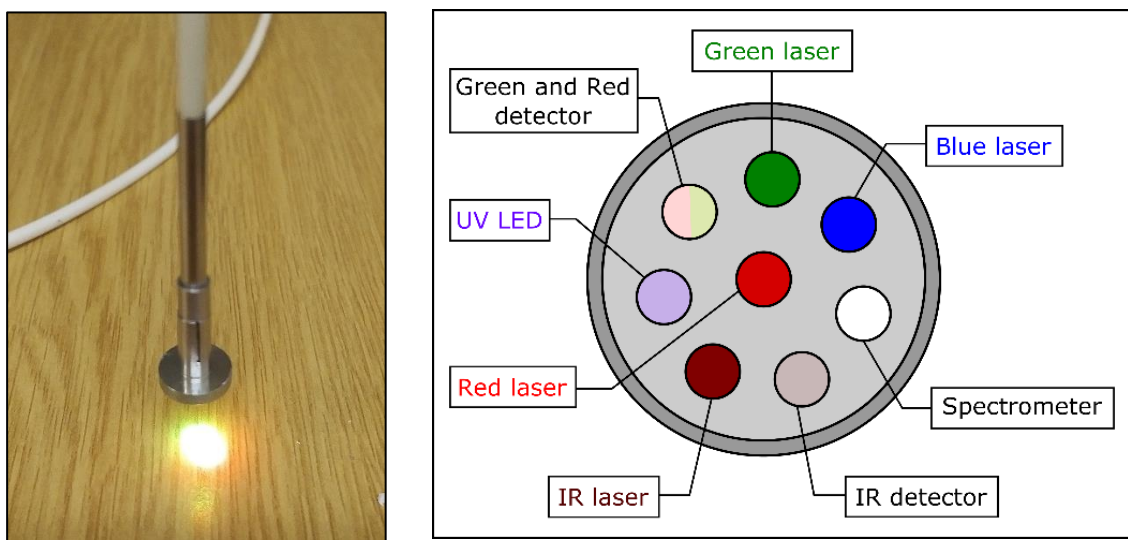


Figure 4.2 The LAKK-M device. 1 – Power switch. 2 – Switch to set device into LDF and TRO recording mode. 3 – Calibration button for LDF mode. 4 – Switch to set device into fluorescence spectroscopy mode. 5 – Excitation wavelength selection buttons. 6 – Filter for fluorescence excitation. 7 – Calibration dock. 8 – Main fibre with probe. 9 – Pulse oximeter finger clamp. 10 – Externally housed filters.



A


B

Figure 4.3 A) External appearance of the main LAKK-M optical fibre probe housing the multiple radiation sources and detector fibres. B) Schematic depiction of the internal arrangement of the multiple radiation sources and detection fibres. Sources and detectors are labelled.

The main fibre (Figure 4.2 – 8) houses a combination of multiple optical fibres, each employed to either deliver or detect light. Figure 4.3 displays a close-up of the probe and the internal arrangement of the fibres.

The wavelengths employed by the LAKK-M are presented below in Table 4.1, with their respective diagnostics channels. It should be noted that all of the radiation sources within the LAKK-M are laser based, except of the fluorescence spectroscopy UV excitation channel, which is achieved by an LED. Furthermore, the output power at the probe-end is around 2 – 3 mW for each light source (LAZMA Ltd. 2011).

Table 4.1 Wavelengths of corresponding LAKK-M channels. All values in nm.

				NIR
FS	365	450	532	635
TRO			532	635
LDF				1064
PO				1064

4.2 Fundamental methodology of the LAKK-M device

Due to the importance of the LAKK-M device in the work described in this thesis, below are outlined standard methodological approaches for recording measurements. As the device has multiple channels, methodology will be described for acquisition of microcirculatory parameters (by LDF, TRO and pulse oximetry) and fluorescence measurements. Before function, the device must be turned on (Figure 4.2 – 1) and the mode must be selected by pressing the corresponding button on the device case (Figure 4.2 – 2 or 4). The device utilises specific software to process the data received by the probes, titled LDF 3v3.1.1.403 (SPE “LAZMA” Ltd). This software must be installed on an associated pc/laptop and accounts for all channels of the device.

A comprehensive database is inbuilt into the software, capable of storing any measurements taken by the device in a dated and timed format. This is the same for both microcirculatory and fluorescence channels, with recordings for each available for storage per database entry. Upon forming a database entry, the device has to be physically switched on, with a correct operating channel selected, to allow for the automatic selection of the correct mode of operation by the software. These steps must be successfully completed before following the methodological approaches outlined below.

4.2.1 Basic measurement of microcirculatory parameters

The measurement of LDF and TRO is conducted simultaneously. Prior to use, the probe of the LAKK-M device must be calibrated using the calibration dock (Figure 4.2 – 7) situated on the panel door, which houses the fibres when the device is off. The calibration dock is made of a specialised polymer designed to exhibit maximal backscattering. The output of this calibration

reading is used to normalise all following measurements. The probe must be calibrated (Figure 4.2 – 3) for at least 5 – 10 seconds. It should be noted that the software, which has been initiated as above, will be in the correct mode and will display a warning if the device has not calibrated. At this point, the device is ready for use. The option to record for a designated time or continuously is provided by the software.

Additionally, the pulse oximeter can also be employed to function simultaneously with the other measurements. The device automatically initiates pulse oximeter function when the microcirculatory assessment mode is activated. The probe for this methodology is located in a separate fibre, with a specialised clamp specifically designed to clip on to a human finger (Figure 4.2 – 9). Pulse oximeter measurements will be registered along with the other methodologies. Due to the construction of the device and design of the probes, while the microcirculatory parameter measurements can be carried out on a diverse selection of tissues and organisms, the pulse oximeter probe is limited to use on humans.

Upon completion of desired measurement time, data must be saved in the software. This data can then be exported in the form of a spreadsheet file or subjected to further analysis (such as a wavelet analysis) within the software. Date and time of the experiment are automatically recorded in the software and are present on any exported data. It should be noted that the probe must be in direct contact with the object being measured, but care must be taken to avoid applying excess pressure, to avoid creation of local occlusion and the corruption of result.

4.2.2 Basic measurement of fluorescence

Upon initiation of the fluorescence spectroscopy software, the device will be ready for use. The probe must be situated on the location of interest. Similarly to the above, excess pressure on the probe should be avoided. Once the probe is in place, device users must ensure a correct filter (provided with the system) is inserted into the body of the device (Figure 4.2 – 6 and 10; Figure 4.4). Once the correct filter is physically inserted into the device, excitation radiation must be initiated by selecting the wavelength of interest and activating it by pressing the corresponding labelled button situated on the body of the diagnostics device (Figure 4.2 – 5).



Figure 4.4 The LAKK-M filters. From left to right - filters for excitation wavelengths of UV (365 nm), green (532 nm), blue (450 nm) and red (635 nm).

Once initiated, the fluorescence channel measurement can be used to either continuously monitor the fluorescence/autofluorescence of the object of interest, or to take a snapshot of the fluorescence value. The software allows the device to record fluorescence measurements from each of the available fluorescence channels without moving the probe, however this is not always required. This is simply achieved by replacing the currently inserted filter for one corresponding to the next wavelength of interest, followed by selection of this wavelength on the body of the device. A snapshot of the new fluorescence curve must also be remembered to save the data. It should be noted that all measurements for the fluorescence channel on the LAKK-M require conditions, which reduce external light. Due to the nature of the technique, light introduces extra noise into the recording, thus limiting such a factor becomes necessary. This is simply achieved by conducting experiments in low light or dark-rooms, or alternatively providing a cuff or cover for the probe which prevents external light entering the area being probed.

Once all the fluorescence readings of interest have been recorded, the recording must be ended and saved. As before, all the data is available for viewing within the software, which immediately displays the amplitude values of various common endogenous fluorophores (such as collagen or NADH), as well as their values normalised to the backscattering peaks. The specific points on the fluorescence curves corresponding to these amplitudes can be manually shifted in order to more accurately obtain the correct values. Once all the spectral peaks of interest are selected to the

approval of the user, data can be exported. This can be done as either a spreadsheet with all the values calculated by the software, or as a data file for the fluorescence curve. The latter allows for the recreation of the measured fluorescence curves to be reconstructed in other software. It should be noted that exporting of data must be done separately for each individual wavelength measured.

4.2.3 Finalising experiments with the LAKK-M

Upon finalisation of the experimental work, care must be taken to turn off the device and store it in a safe manner. The optical fibres (of the combined fibre and the pulse oximeter) must be inserted into the special housing at the base of the device with care. The filters for the fluorescence measurements are stored independently of the device, but it is recommended to keep one filter inserted into the device body. While the device is relatively sturdy, movement should still be carried out with care.

The software aspect of the LAKK-M, as already stated, saves the data after each individual reading. Thus, closing the software after saving data is sufficient. It should be noted that the software incorporates more complex and niche tools for different forms of analysis. These are, however, specialised and do not fall under basic use. As such, they are detailed in the user manual (LAZMA Ltd. 2011).

4.3 Conclusions

This chapter has introduced and explained the methodology of a piece of technology, which is currently set as a bridging tool between research applications and functional diagnostics. As the area of MLNDS is still growing, devices incorporating multiple diagnostics methods will become more readily available. However, at this time, the LAKK-M and other similar devices open avenues to study multiple physiological conditions simultaneously. In light of such capabilities, the following chapters will regularly refer back to the methodologies described above due to the extensive use of the LAKK-M for work carried out in this thesis.

References

- Kalchenko, V. et al., 2011. In vivo characterization of tumor and tumor vascular network using multi-modal imaging approach. *Journal of biophotonics*, 4(9), pp.645–9. Available at: <http://www.ncbi.nlm.nih.gov/pubmed/21714099> [Accessed December 13, 2013].
- Kuznetsov, Y.L., Kalchenko, V.V. & Meglinski, I.V., 2011. Multimodal imaging of vascular network and blood microcirculation by optical diagnostic techniques. *Quantum Electronics*, 41(4), pp.308–313.
- LAZMA Ltd., 2011. LAKK-M Manual. , pp.1–29.
- Patel, R. et al., 2012. Multimodal optical imaging for detecting breast cancer. *Journal of Biomedical Optics*, 17, p.66008.
- Rogatkin, D. a. et al., 2011. Basic principles of design and functioning of multifunctional laser diagnostic system for non-invasive medical spectrophotometry A. Mahadevan-Jansen, T. Vo-Dinh, & W. S. Grundfest, eds. *SPIE proceedings*, 7890, p.78901H–78901H–7. Available at: <http://proceedings.spiedigitallibrary.org/proceeding.aspx?articleid=732816>.

Chapter 5 : Application in cancers: urinary bladder cancer

Cancer is a major long-time worldwide problem and a priority for medical research (Jemal et al. 2009; Jemal et al. 2005; Siegel et al. 2016; Parkin et al. 2005). Considering the strengths of photonics based technologies described above, various forms of cancer present themselves as obvious and highly relevant targets for innovative diagnostics.

5.1 Introduction into bladder cancer

One of the top ten most prevalent cancers worldwide and of interest in this thesis is urinary bladder cancer (BC). It is annually responsible for 7% of all new cases in males and for over 150000 deaths, in the USA alone (Jemal et al. 2009; Parkin et al. 2005). Around 90% of all BC tumours are of epithelial origin (Puzio-Kuter et al. 2009) and can be categorised as low-grade, non-invasive, papillary and superficial or high-grade, muscle invasive carcinoma in situ (CIS). The high-grade tumours account for 15-30% of all tumours and have a poor outcome, with less than a 10% chance of five-year survival. On the other hand, the low-grade tumours account for the other 70-85% of tumours and tend to have a good prognosis after treatment. They do, however, have a 30-50% chance of recurrence post treatment and even a 10-20% chance to progress into high-grade tumours (Jemal et al. 2005; Ahmad et al. 2012; Sylvester et al. 2006). Due to these high rates of recurrence and progression, bladder cancer establishes its role as one of the most expensive cancers to treat on a per-patient basis (Sievert et al. 2009; Jemal et al. 2009).

Currently, the gold standard for the initial diagnosis of BC is the combined use of cystoscopy and urine cytology. Furthermore, carrying out transurethral resection of the bladder tumour (TURBT) serves not only a therapeutic purpose, but also provides extra diagnostic data and aids in disease staging (Palmer et al. 2013). To determine the area of resection, white light cystoscopy (WLC), by rigid or flexible endoscopy, is employed as the primary method for the detection of bladder tumours. This technique exhibits a reliable specificity by allowing the operator/surgeon to directly survey the tissue in question. As such, the method has a very high (85-90%) detection sensitivity for low-grade papillary tumours. However, this is much less efficient at diagnosing CIS, with only an up to 67% chance of detection (reviewed in Karaoglu et al. 2013). Alternatively, photodynamic diagnosis (PDD) may be employed as a detection technique. This method relies on the application of 5-aminolevulinic acid (5-ALA) or a similar molecule such as Hexaminolevulinate (HAL). These are photoactive porphyrin molecules and take time to accumulate, with particular preference, within neoplastic tissue. Upon stimulation by wavelengths of blue light, they emit red fluorescence (Jocham et al. 2005).

One of the primary reasons why WLC maintains its position as the go-to method of bladder cancer detection is due to the relatively low cost, even in comparison to that of PDD, the second most commonly used technique. However, the tumours visible by this method may not reveal the complete extent of the actual tumour and even upon surgical removal may still lead to high cases of recurrence (Brausi et al. 2002). As already mentioned, the method also suffers when faced with CIS tumours. In comparison, PDD has been widely shown to have a more favourable sensitivity for detecting bladder tumours. While chances of detection of low-grade, lower risk tumours are similar between the two methods, PDD has a much higher sensitivity for the more aggressive forms of tumour as well as for detecting CIS (Grossman et al. 2007 and a meta review of multiple papers by Mowatt et al. 2011). The high sensitivity of PDD comes at the price of a reduced specificity compared to WLC. The increased incidence of false-positive outcomes leading to unnecessary surgical procedures must be taken into account before application of the technique (Mowatt et al. 2011). Furthermore, both techniques only provide a surface level visual representation of tissue and cannot indicate any potential molecular changes within. Despite the drawbacks, together with urine cytology, WLC and PDD form the best current methods for detecting new and recurring bladder tumours.

5.2 Bladder cancer tumour background

5.2.1 Anatomy and tumour progression

To ultimately achieve the aim of developing early detection technology for BC, we must first understand the disease and how it interacts with the human body. This includes understanding of the anatomy of the bladder (briefly touched upon in chapter 1). The organ lies posterior to the pubic bone and anterior to the rectum. Largely the same for both sexes, an anterior placement in relation to a uterus is unique to females, while males exhibit a prostate inferior to the bladder. When fully developed, the bladder is comprised of several layers, which can be more simply categorised into four different “coats”: the serous, the muscular, the sub-mucous and the mucous. The serous coat presents itself as a partial outer layer derived from the peritoneum, localising on the superior and lateral regions of the organ. This “dome” is known to project into the abdomen when the bladder is distended with urine, indicating a partial extension outside of the peritoneal cavity (termed retroperitoneal). The following, muscular coat actually consists of three individual layers of detrusor muscle: longitudinally arranged external and internal layers, with an intermediary layer exhibiting a circular arrangement of muscle fibres. Finally, the sub-mucous layer of loose connective tissue attaches the muscular layer to the mucous layer. The latter is a smooth layer consisting of two forms of transitional epithelial cells, making the organ suited to large internal volume fluctuations (Gray 2012; OpenStax 2016).

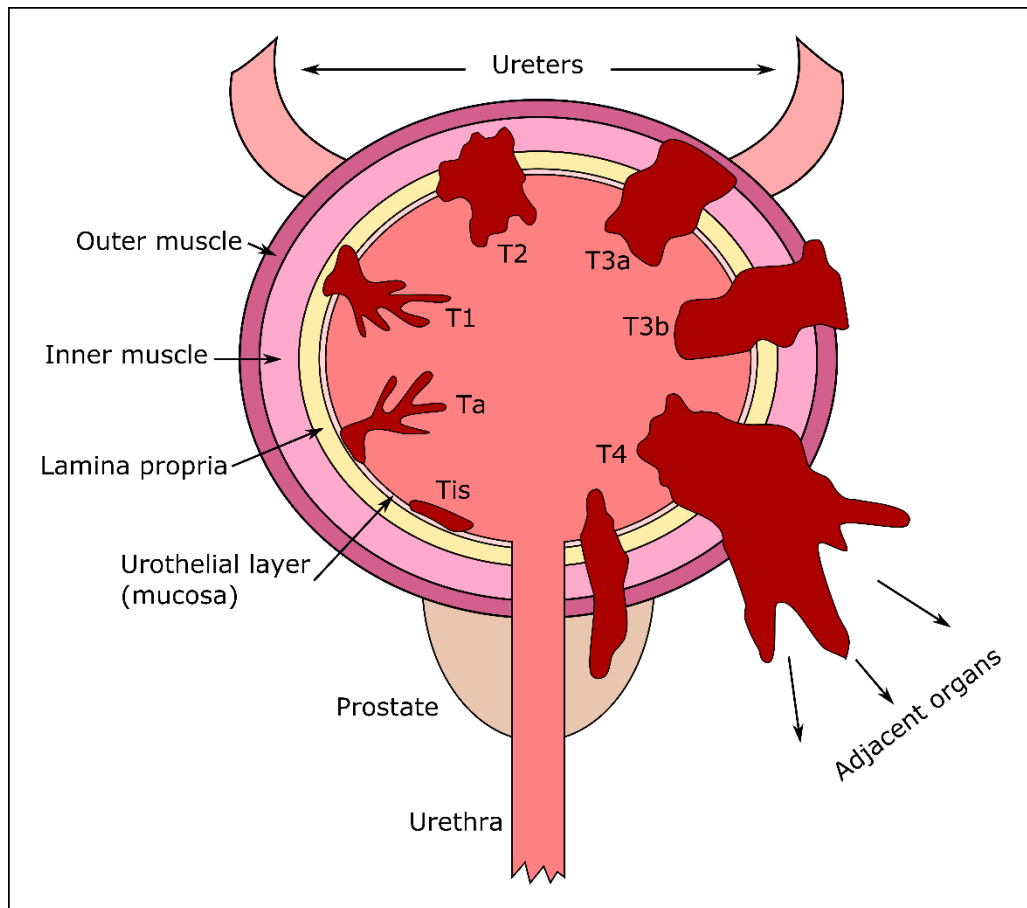


Figure 5.1 A simplified diagram depicting various cancer tumour stages in a male bladder. Level of severity increases from Ta in a clockwise direction.

When it comes to the classification of BC tumours, the extent of progression into the structure of the organ plays a great role. The different stages of BC tumours as characterised by the TNM classification of malignant tumours system are presented in Figure 5.1. These tumours can be relatively simply classified into muscle invasive and non-invasive. The non-muscle invasive tumours consist of the pTa papillary tumours present in the mucosa and the pT1 tumours, which penetrate through to the lamina propria. The Tis tumours, a title used to describe flat tumours growing on the mucosa characterising CIS, are also attributed to this group. Muscle invasive tumours are divided into pT2 – pT4. This is done based on the level of tumour progression and penetration of tissue, with pT4 tumours having spread to neighbouring tissues (Meijden 1998).

5.2.2 Cancer tumour properties

Considering the various stages of bladder cancer, it is important to note the various properties exhibited by the tumours throughout their growth. While many cancers have specific properties

depending on their originating tissue, certain aspects such as vascularisation and metabolism are generally shared by most cancer tumours, including those of the bladder.

A key point to understand is that tumour cell function is distinct from that of regular cells. Like most other tissue, tumours require a sufficient oxygen supply in order to grow. This was further demonstrated by Folkman (1972) in the early 70s, who observed that tumours in isolated perfused organs will only grow up to 2-3mm diameter, failing to develop any further. Through implantation of tumours into non-isolated tissues like muscle, neovascularisation and an expansion beyond the small diameters was observed. Such neovascularisation in tumours is a result of angiogenesis, where new vasculature is developed from that already present in the host tissue (Vaupel et al. 1989; Eatock et al. 2000). It is due to this process that tumour tissues exhibit a large heterogeneity, containing both well vascularised and poorly vascularised (to the point of hypoxic) micro-regions (Secomb et al. 1993). In turn, it is vital to also know that hypoxia in tumours can stimulate the process of angiogenesis (Shweiki et al. 1992), ultimately improving the blood and oxygen supply. In the case of bladder cancer, as with many others, the increasing severity of the disease exhibits an initial tendency towards hypoxic tumours, until they eventually develop their own vasculature allowing for further growth.

The reason for such further development is due to the importance of oxygen consumption and metabolism within tumorous tissue. Tumour growth can be regulated by the oxygen consumption (Chen et al. 2009). Additionally, vascularisation and by relation oxygen consumption, are heavily influenced by the age and stage of the tumour (Secomb et al. 1995).

It is also vital to note the role of tumour metabolic activity in growth and proliferation. Unlike regular cells, which mainly rely on mitochondrial oxidation for their energy production, tumour cells equally utilise glycolysis (Warburg 1956). While this in itself is not exclusive to malignant tumour cells (Vaupel et al. 1989), it is a major mechanism by which tumour cells carry out non-oxygen related metabolism and ultimately proliferate before a more complete and functional vasculature has had time to develop.

5.3 A computational bladder model

With BC so commonplace and such a burden on both individuals and the economy at large, the design, development and substantiation of advanced diagnostic techniques is required. Modern, more sensitive techniques could enhance the potential of already available gold standard approaches.

In light of the anatomical position of the urinary bladder, there is a great potential for photonics based technology to be implemented in a non-invasive diagnostic manner. More specifically, the use of autofluorescence (as described in 1.2.4) measurement has become more widespread as a diagnostics technique. Subsequently, a solid basis and intensive optimisation of this technique for various niche diagnostics applications (such as for bladder cancer) is necessary.

This technique, however, relies heavily on light passage through tissues of interest. Thus, to fully optimise autofluorescence analysis for bladder cancer diagnostics, the effects of various anatomical layers on the probing beam of radiation must be taken into account. Light interactions such as scattering and non-specific absorption of both incident and emitted radiation often obfuscate signals obtained from various forms of tissue. This is a major obstacle and presents an ever-increasing challenge when searching deeper into tissue. This is also the reason why certain early grade bladder tumours like CIS are incredibly difficult to diagnose. It is further important to understand that varying optical properties as a result of different tissues will result in a myriad of unique light interactions, which must all be accounted for before designing a diagnostic technique (Bradley & Thorniley 2006). Furthermore, it is vital to avoid attributing malignancy-induced changes in tissue optical properties to the absolute fluctuations in tissue fluorophores. This is particularly noticeable during matrix degradation or tissue thickening (Tajiri 2007; Izuishi et al. 1999).

Considering the above, this chapter describes the justification, design and development of a computational 3D bladder tissue model for the purpose of simulating the optical properties of multi-layered bladder tissue during irradiation by light of varying wavelengths. Such a model could be employed for comparison of different photonic devices to determine their clinical worth as well as to simulate effects of bladder cancer progression on the host tissue's optical properties, ultimately providing diagnostic benchmarks that can aid in tumour staging and grading criteria.

5.3.1 Justification of developing a model

The use of tissue models, both 3D and otherwise, is rapidly becoming widespread as a tool to aid researchers in simulating experiments and interpreting their outcomes. It has additionally proved itself useful as an initial test for novel photonics based equipment (Bykov et al. 2011; Wróbel et al. 2014; Wróbel et al. 2015; Okada & Delpy 2003). Closer to the topic at hand, 3D models of the bladder have also begun to appear and have become a great source of information employed to design and improve on already existing WLC and PDD techniques. These models, however, often take the form of physical optical phantoms (Lurie et al. 2014). As it stands, no groups employing or developing reliable optical bladder models for the study of tissue autofluorescence were known to the authors at the time the work below was conducted. Thus, a model capable of accounting for distinct endogenous fluorophore contributions could prove incredibly useful in conjunction with minimally invasive diagnostics systems featuring the capacity to record autofluorescence spectra. With a lot of metrological support, backed up by laboratory testing, such technology and such models possess huge potential, which can ultimately be transferred to a clinical setting.

5.3.2 Model requirements for relevance to bladder cancer

When considering the design of such a computational model, one must first consider what it must incorporate into it. Given the tools available from non-invasive photonics based devices (as mentioned in chapters 2 and 3), the model will ideally take into account as many tissue properties as is possible. Due to the use of autofluorescence detection as a diagnostics tool, the biomarkers NADH and FAD used for the redox ratio as well as those for collagen (both described in chapter 1) are the priority. As already indicated, these biomarkers hold key importance within cancers due to their relation to metabolic activity and cell structure. To construct an accurate model, the presence of these biomarkers will need to be accounted for. The model must also be grounded on optical properties of scattering, absorption and transmission of the relevant tissue (Jacques 2013). This is a key feature of the model, which provides the capacity to simulate tissue properties. These parameters can be introduced into the model using their coefficients.

5.4 Methods for computational model development

5.4.1 Proof of concept model

5.4.1.1 Literature review

To obtain the necessary coefficients (attenuation, μ_t ; scattering, μ_s ; absorption, μ_a), the refractive index n and the anisotropy factor g for bladder tissue, a literature analysis was conducted. Using PubMed, searches were made using the following key words: bladder, bladder tissue, optical properties, tissue optical properties, absorption, attenuation, scattering. Data indicating the optical properties of separate bladder tissue layers was preferential to whole bladder recordings, but the latter was not excluded. Priority was given to properties of the bladder mucous and sub-mucous layers.

5.4.1.2 3D model construction

The 3D model was realised and constructed in TracePro (Lambda software). To simulate the core urinary bladder layers, a two-layer set up of the model was chosen. This would simulate the largest mucosa and muscle layers, avoiding the small sub-mucous layer in order to reduce unnecessary complexity. The simulated source and detector were created to mimic parameters of the LAKK-M non-invasive diagnostics device (described in chapter 4). This included a distance of 1 mm between the two components as well as a 0.06 mm diameter for the latter.

To account for instances of scattering and absorption along the total optical path of photons through the simulated tissue, the Monte Carlo modelling was employed. This remains as one of the

most commonly used methodologies to quantitatively describe light distribution within organic tissue.

To account for the biomarkers of interest within tissue, a wavelength range of 300-610 nm was chosen. Further to this, maximum accuracy of the model was insured by simulating criteria for the NADH present in the mucosa (Wang et al. 2009; A' Amar et al. 1997) and the collagen present in the tissue (Wang et al. 2008; Georgakoudi et al. 2001). Table 5.1 compiles the parameters utilised in the model, based on data available in literature (Staveren 1995; Vishwanath & Mycek 2004; Chapman & Reid 1999; Katika & Pilon 2007).

Employing the required parameters, the absorption within the biological tissue is taken into account using the Beer-Lambert law:

$$\Phi = \Phi_0 \exp(-\mu_a t), \quad (5.1)$$

Where Φ and Φ_0 are the transmitted and incident flux, μ_a is the coefficient of absorption and t is the sample thickness.

Fresnel's law is employed to account for the reflection and refraction at the interface between the two simulated layers. The commonly employed Henyey-Greenstein function was selected as the scattering phase function:

$$SDF = p(\theta) = \frac{1-g^2}{4\pi(1+g^2-2g \cos \theta)} \quad (5.2)$$

Where g is the anisotropy factor. This parameter may have a value anywhere between -1 and 1. A positive value of g indicates that rays of light travelling through the media interface are largely scattered in a forward direction, whereas a negative value will result in rays being scattered in a reverse direction. A g value of zero indicates isotropic scattering, meaning it is equal in all directions.

Table 5.1 Model parameters

Layer	Thickness, μm	μ_a, cm^{-1}	μ_s, cm^{-1}	g	Fluorophore	Quantum efficiency (yield)	Peak molar extinction, $\text{M}^{-1}\text{cm}^{-1}$
Mucosa	200	Obtained using the IAD method	Obtained using the IAD method	0.9	NADH	0.05	6220
					FAD	0.05	11300
Muscle	2000			0.9	Collagen	0.3	52940

The beam of light passing through a scattering medium spreads to a random distance x . this is adjustable through the use of a probability distribution:

$$P(x)dx = \exp(-\mu_s x) dx \quad (5.3)$$

Where μ_s is the coefficient of scattering.

When the travelling beam of light interacts with a material that is relatively thin in comparison to the mean free path, that beam will pass through while undergoing negligible scattering. Conversely, a thick material will result in higher likelihood of scattering.

It should be noted in this segment that the computer-based construction of the model was handled by colleagues. While the parameters of the model (including the decision to produce a Monte Carlo model) were made with extensive input from the author, the niche knowledge of specialised software required a collaborative effort.

5.4.1.3 Fluorescence measurement of urinary bladder tissue

To measure the fluorescence of urinary bladder, pig organs were sourced from local distributors. The organs were delivered frozen (freezing conducted immediately after harvesting of the organ, according to distributor) and utilised upon delivery. The bladders were split to separate the dome and trigone segments and further “virtually” divided into 16 sections. Each of these virtual sections on the inner mucosa layer was subjected to optical analysis by the LAKK-M detection device following standard procedure for fluorescence analysis as described in chapter 4. All four available excitation wavelengths (UV 365nm, blue 450nm, green 532nm and red 635nm) were used to measure fluorescence spectra. Work was done at room temperature in a windowless room to limit potential noise in the signal. Bladder sections were maintained on laboratory ice packs during all times they were not actively used in analysis to prevent rapid tissue degradation.

5.4.1.4 Simulation of fluorescence

Fluorescence within the above modelled tissue was simulated with the further aid of the TracePro software. This process utilised the fluorescent and material properties of the modelled tissue in addition to the laws described above. Two major parameters, the relative absorption $ab(\lambda)$ and relative excitation $ex(\lambda)$, can be set and normalised to the molar extinction coefficient K_{peak} and the relative emission $em(\lambda)$. The concentration of the fluorescent material is set through the input of the molar concentration C_{molar} . Absorption coefficient of the fluorophore in media is determined by:

$$\mu_a(\lambda) = ab(\mu)K_{peak}C_{molar} \quad (5.4)$$

With the path length before absorption:

$$d(\lambda) = -\log_{10}(x)/\mu_a(\lambda) \quad (5.5)$$

Where x is a random value between 0 and 1.

The number of photons involved in the simulation process is determined by ascribing quantum efficiency (QE) to the system.

5.4.2 Advanced model

5.4.2.1 Derivation of transport coefficients

The model was advanced by calculating the transport coefficients without having to rely on literature data. Urinary bladders from locally sourced male pigs ($n = 3$) were obtained from an established supplier (WETLAB). The organs were transported refrigerated and vacuum packed to preserve the tissues, and were immediately refrigerated upon reception. A medical grade scalpel was used to separate the superior and lateral surfaces (apical surface) from the antero-inferior surface (basal surface) of the bladder. Sections of tissue around 2 cm^2 (6-10 mm thickness) from each part were excised for analysis. The excised sections were secured in a specialised tissue clamp, which was subsequently screwed into the spectrometer, along the beam path. The Lambda 1050 spectrophotometer, with an additional specialised integrating sphere module, was employed to record the absorption, transmission and diffuse reflectance of the sample tissue. Measurements were taken at 1.5 nm increments along a 350 – 1800 nm wavelength range. The entire set of spectrometer readings was conducted at a room temperature of 22°C . Graphic visualisation of recorded spectrometer data was achieved by using Origin Pro 8 software (Figure 5.2). It should be noted that tissue samples were transported and maintained in small-size, covered petri dishes lying on a bed of dry ice at all times to prevent deterioration and drying. Covers were kept on to reduce effects of air exposure. If samples had to be kept open for extended durations between experiments, parafilm was used to seal the petri dishes and further reduce exposure.

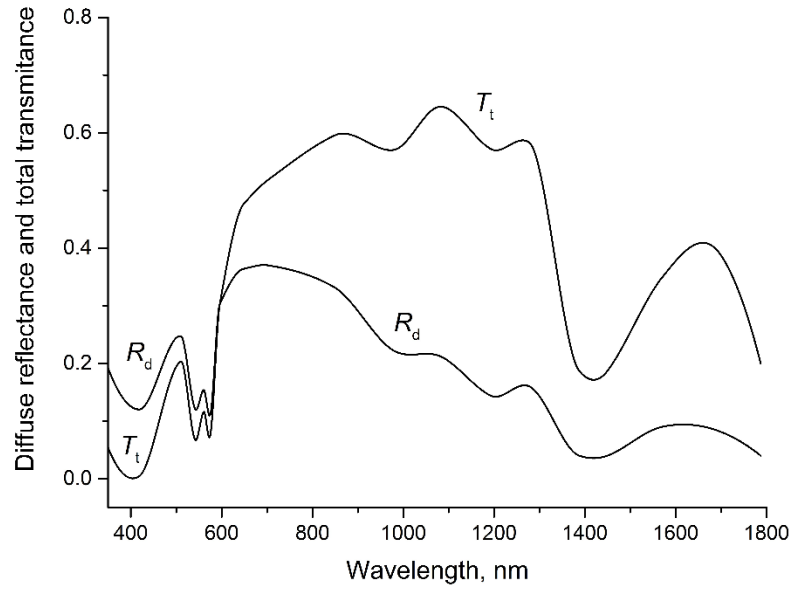


Figure 5.2 Total transmittance (T_t) and diffuse reflectance (R_d) spectra of 2mm thick samples obtained from porcine urinary bladder.

The inverse adding-doubling (IAD) method in conjunction with a corrective Monte-Carlo calculation was utilised to process experimental results and determine the optical parameters of studied tissue (Moffitt 2007; S. A. Prahl et al. 1993). Such an approach is commonly employed in the field of tissue optics, specifically for processing spectrophotometry data derived using an integrating sphere.

The use of the IAD enables the determination of tissue absorption and scattering coefficients, as long as the diffuse reflectance and total transmission are known. Additionally, the anisotropy factor (g) is also required. In the case of this work, the g value was fixed at 0.9 for the calculations as this is most typical for the majority of biological tissues in both the near and the mid infrared spectral wavelengths (Tuchin 2000; Bashkatov et al. 2004).

The initial values for μ_a and μ_s' (which is $= \mu_s(1 - g)$) were calculated by solving the series of equations (5.6) and (5.7):

$$\frac{\mu_s'}{\mu_a + \mu_s'} = \begin{cases} 1 - \left(\frac{1 - 4R_d - T_t}{1 - T_t} \right)^2, & \text{if } \frac{R_d}{1 - T_t} < 0.1 \\ 1 - \frac{4}{9} \left(\frac{1 - R_d - T_t}{1 - T_t} \right)^2, & \text{if } \frac{R_d}{1 - T_t} \geq 0.1 \end{cases}, \quad (5.6)$$

$$(\mu_a + \mu_s')l = \begin{cases} -\frac{\ln T_t \ln(0.05)}{\ln R_d}, & \text{if } R_d \leq 0.1 \\ 2^{1+5(R_d+T_t)}, & \text{if } R_d > 0.1 \end{cases}, \quad (5.7)$$

Where R_d is the measured diffuse reflectance, T_t is the measured total transmission and l is the tissue thickness (S. Prahl et al. 1993).

The initial values of μ_a and μ_s' were subsequently used in an iterative process comparing the calculated values (*calc*) to the experimental values (*exp*) or R_d and T_t . The iterative calculations were conducted until the optical properties “stabilised”, i.e. until there were less than 0.01 mm^{-1} changes between iterations of the calculated absorption and scattering values.

It should be noted that, as there is a certain level of light loss around the edges of the sample which is not collected by the integrating sphere, a Monte-Carlo method of correction was integrated into the calculations. The calculated lost light for a specific set of optical properties was accounted for with each subsequent iteration of the calculations required within the IAD.

The above described iterative calculation process was conducted on each individual wavelength of interest. This enabled the calculation of tissue optical properties for the entire measured spectrum.

5.4.2.2 3D model construction and utilisation

Upon finding the transport coefficients for the experimentally employed tissue, the methodology for constructing the 3D model as well as measurement and comparison of simulated and measured fluorescence results was done identically to that described in section 5.4.1.

5.4.3 Human tumour tissue measurement

Tissue optical properties of human urinary bladder tumours were calculated. Simulated fluorescence was compared to measured fluorescence following the procedures outlined in the advanced model above (5.1.4.2). Two tumour samples, with adjacent non-tumour tissue samples, were measured in this manner. The sample pair sources will be referred to as HB1 and HB2. Each sample was around 0.5 mm thick and all were obtained from Amsbio (AMS Biotechnology (Europe) Ltd.).

The tumour sample from HB1 was a pT3 stage urothelial carcinoma taken after the donor had received two prior courses of chemotherapy. The HB2 donor, conversely, had not undergone any treatment procedures prior to biopsy. Both samples and adjacent normal tissues were snap-frozen upon resection and delivered on dry ice for preservation.

5.5 Computational model construction and utilisation results

5.5.1 Proof of concept model

5.5.1.1 Literature review

To find the transmission, reflectance and absorbance properties of bladder tissue in humans, materials by Vo-Dinh (2010), Cheong et al. (1990) and Sandell & Zhu (2011) were found and employed. The optical properties of the tissues of interest were derived with 532 nm, 633 nm or 1064 nm wavelengths of light (specified in table 5.2). Furthermore, in order to maintain relevancy, optical properties of porcine bladder at multiple wavelengths (Staveren 1995) were also found and specified in table 5.3.

Table 5.2 Optical parameters of human bladder tissues

Tissue	λ (nm)	Absorption μ_a (cm^{-1})	Scattering μ_s (cm^{-1})	Reference
Whole	532	0.27-0.71	1.28-3.30	(Sandell & Zhu 2011)
Whole	633	0.28-0.76	2.5-6.37	(Sandell & Zhu 2011)
Integral	633	1.4	88	(Cheong et al. 1990)
Integral	1064	0.4	116	(Muller & Roggan 1995)
Mucous	1064	0.7	75	(Muller & Roggan 1995)
Wall	1064	0.9	54.3	(Muller & Roggan 1995)

Table 5.3 Optical parameters of pig bladder tissues

λ (nm)	Absorption μ_a (cm^{-1})	Scattering μ_s (cm^{-1})	Reference
458	1.3	255	(Staveren 1995)
488	1.4	248	
514	1.8	240	
532	3.5	277	
630	0.57	214	
630	0.99	258	

The data on transmission, reflectance and absorbance properties of urinary bladder tissue, in addition to the respective coefficients, obtained from the above mentioned sources, was crucial to the construction of the preliminary 3D model.

5.5.1.2 3D Model

The structural properties of the urinary bladder, while relatively simple in comparison to many other organs, is still complex in nature. As such, a simplified dual layer model (featuring mucosa and muscle layers) was constructed for the purposes of theoretical modelling. This model, based on the literature data, is presented in Figure 5.3. Both a three dimensional visual representation

of light passage into modelled tissue and a two dimensional side view of the model are presented. The light penetration depth of around 1 – 1.3 mm is also visible from image 5.3b (Rafailov et al. 2015).

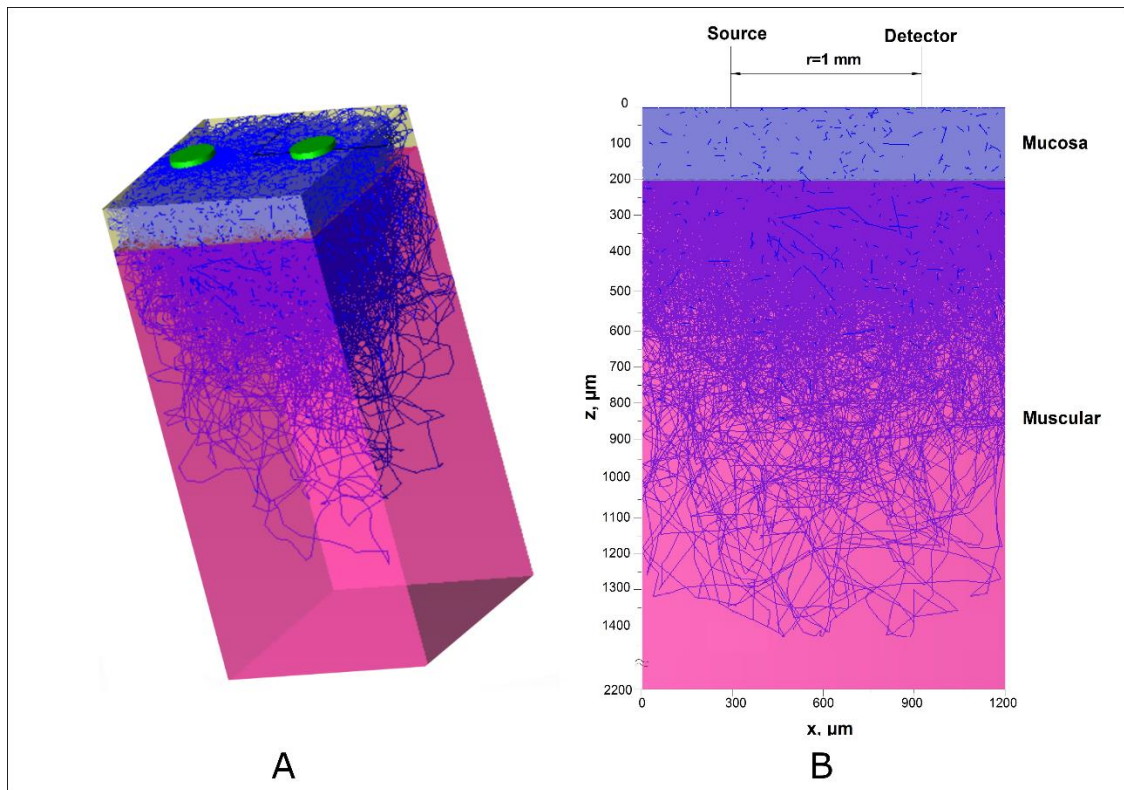


Figure 5.3 (a) Full 3D model view representing photon passage through simulated tissue layers. The green circles represent the source and detector. (b) Side view of the same 3D model. Source, detector and the tissue layers are labelled. The visible darker lines illustrate photons, which are travelling directly towards the visible flat surface.

5.5.1.3 Fluorescence: measured and modelled

Using the generated tissue model, fluorescence by 365 nm wavelength excitation was simulated for comparison to experimentally obtained data. Both NADH and collagen presence within the tissue were accounted for within the model. The comparison of the fluorescence curves is displayed in Figure 5.4 (Rafailov et al. 2015).

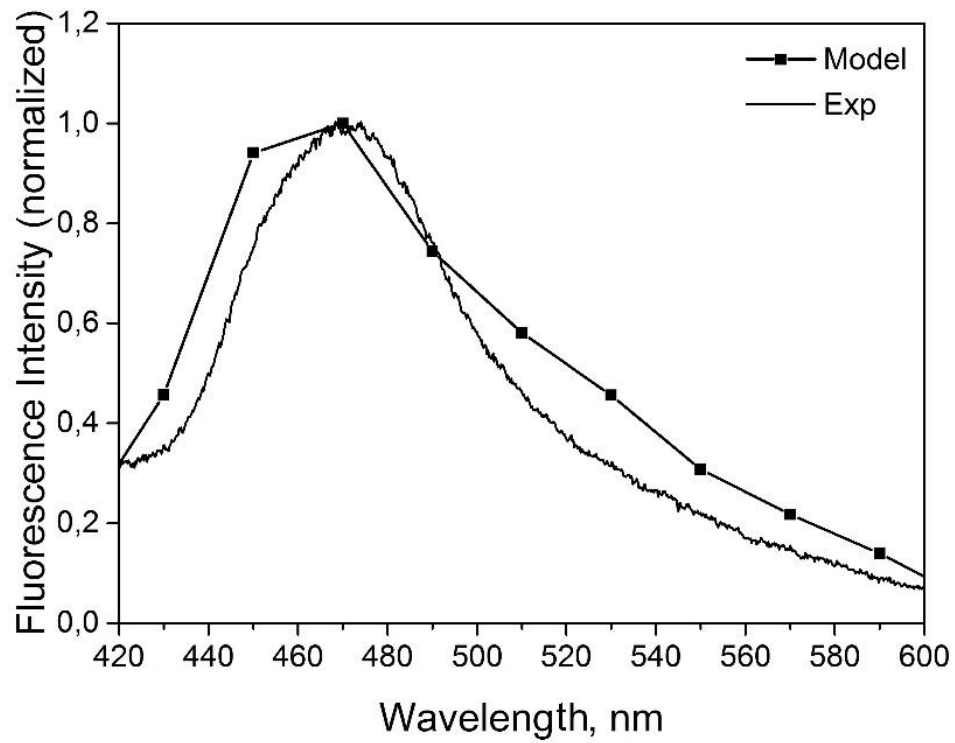


Figure 5.4 Comparison of the modelled and experimentally measured fluorescence at a 365 nm excitation wavelength. NADH and Collagen presence are incorporated into the model.

5.5.2 Advanced model

5.5.2.1 Derivation of transport coefficients: inverse adding-doubling method

The measured transmission and diffuse reflectance values were required for the determination of the transport coefficients through the use of the IAD method. The coefficients of absorption and scattering spectra were reconstructed and presented in Figure 5.5a and 5.5b respectively.

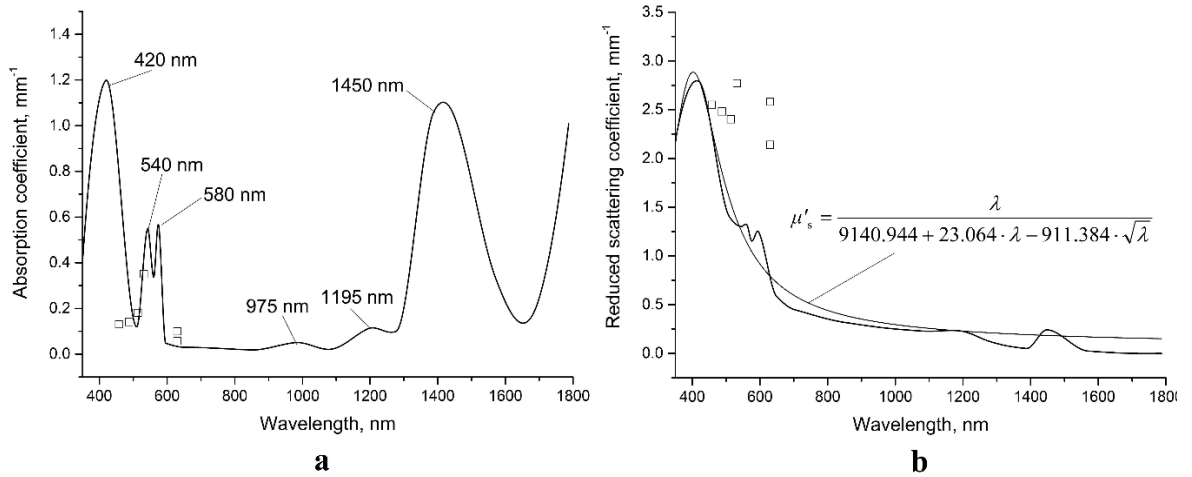


Figure 5.5 Spectra created from (a) the absorption coefficients of porcine urinary bladder and (b) the reduced scattering coefficients of porcine urinary bladder. Experimental data from Staveren (1995) is portrayed on the spectra.

Coefficient values calculated by Staveren (1995) are presented in Figure 5.5 for comparison.

Penetration depth into the biological tissue was also calculated by using the following formula as described in Ritz et al. (2001):

$$\delta = \frac{1}{\sqrt{3\mu_a(\mu_a + \mu'_s)}} \quad (5.8)$$

Where μ_a and μ'_s are the absorption and scattering coefficients (with anisotropy factor). The results of these calculations are presented on Figure 5.6, where it can be observed that the penetration depth of light in the region of interest (400 – 600 nm) is around 1 – 1.2 mm (Rafailov et al. 2016).

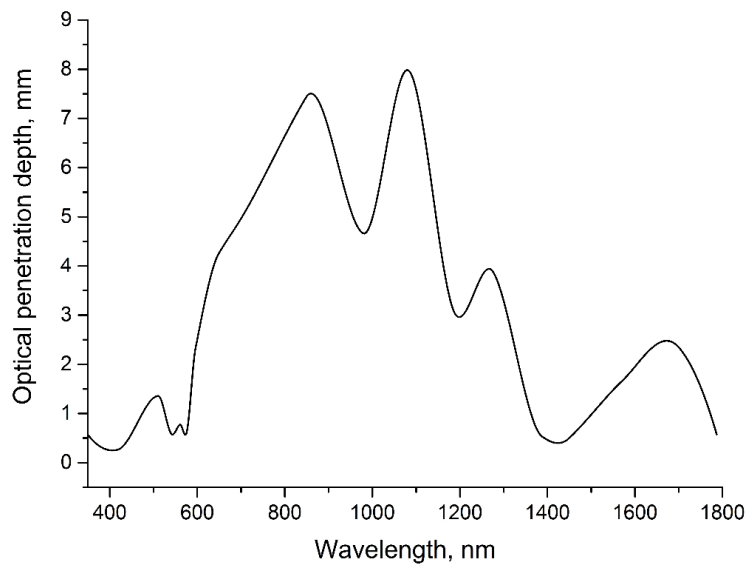


Figure 5.6 Light penetration depth into urinary bladder tissue.

5.5.2.2 Advanced 3D Model

Similarly to the proof of concept model, Figure 5.7 presents a dual layer model featuring the muscle and the mucosa. It should be noted that unlike the initial proof of concept model, two wavelengths of light are simulated and presented on the Figure: 365 nm (a) and 450 nm (b). In turn, the latter is done to further account for the presence of FAD within the simulated tissue (Rafailov et al. 2016).

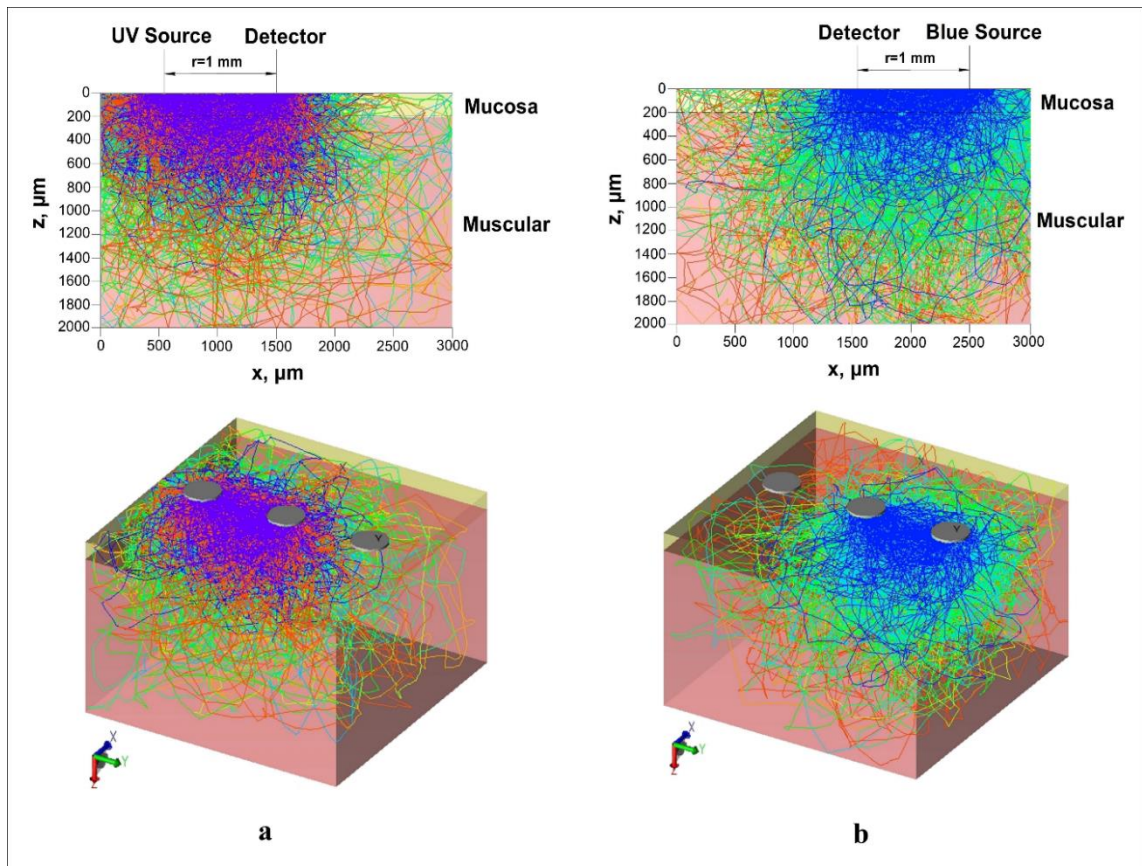


Figure 5.7 (a) Side and full 3D view of model depicting simulated UV light (365nm) within tissue. (b) Side and full 3D view of model depicting simulated Blue light (450nm) within tissue. The source, detector and tissue layers are displayed and labelled. The coloured lines indicate the passage of individual photons through the simulated tissue. These colours within a block are indicative of light intensity. Simulated source light is exclusively UV or blue, but red-shifted paths through the simulated tissue represent photons with lower intensities.

5.5.2.3 Fluorescence: measured and modelled

Again, similarly to the proof of concept model, fluorescence by 365 nm and 450 nm wavelength excitations was simulated using the generated tissue model. This was compared to experimentally obtained fluorescence data from wavelength matched sources. NADH + collagen or FAD + collagen

presence within the tissue were accounted for within the model. The comparison of the fluorescence curves is displayed in Figure 5.8 (Rafailov et al. 2016).

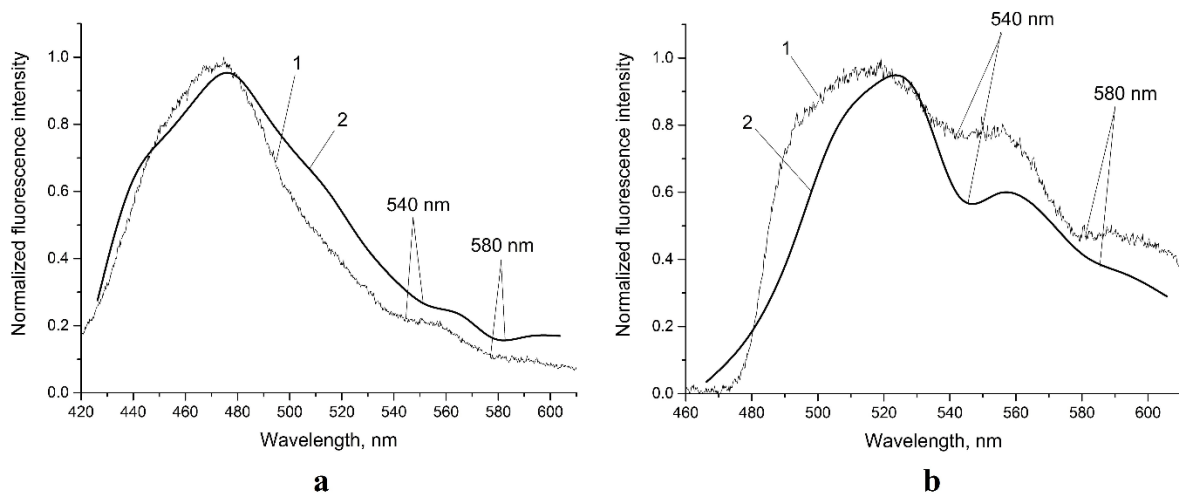


Figure 5.8 Comparison of (1) experimental and (2) model based spectra, calculated using the Monte-Carlo method. Model simulates presence of (a) NADH + collagen or (b) FAD + collagen.

5.5.3 Human tumour tissue measurement

Figures 5.9 and 5.10 display the total transmittance and diffuse reflectance of the intact and tumorous samples from HB1 and HB2 respectively.

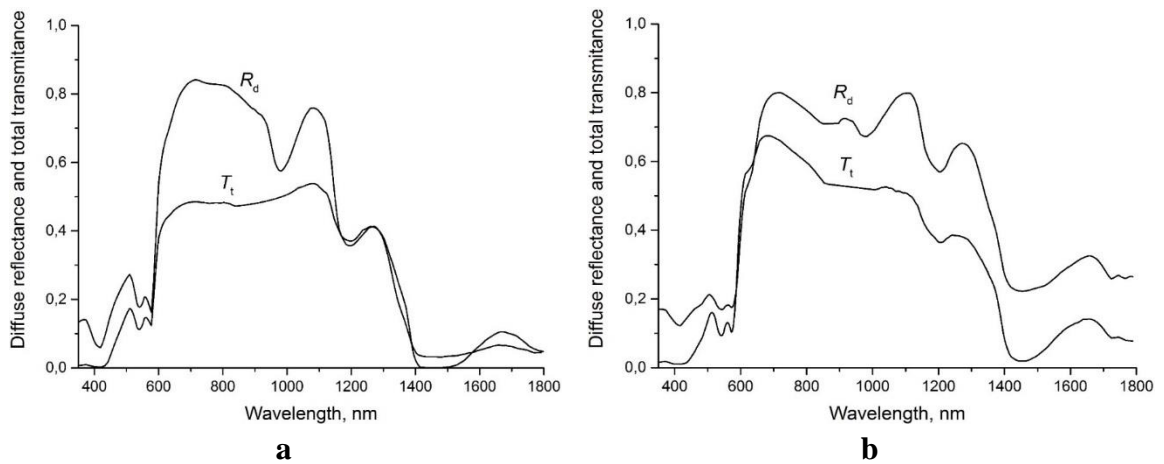


Figure 5.9 Total transmittance (T_t) and diffuse reflectance (R_d) spectra of 0.5 mm thick samples from HR1: (a) intact tissue and (b) tumour tissue.

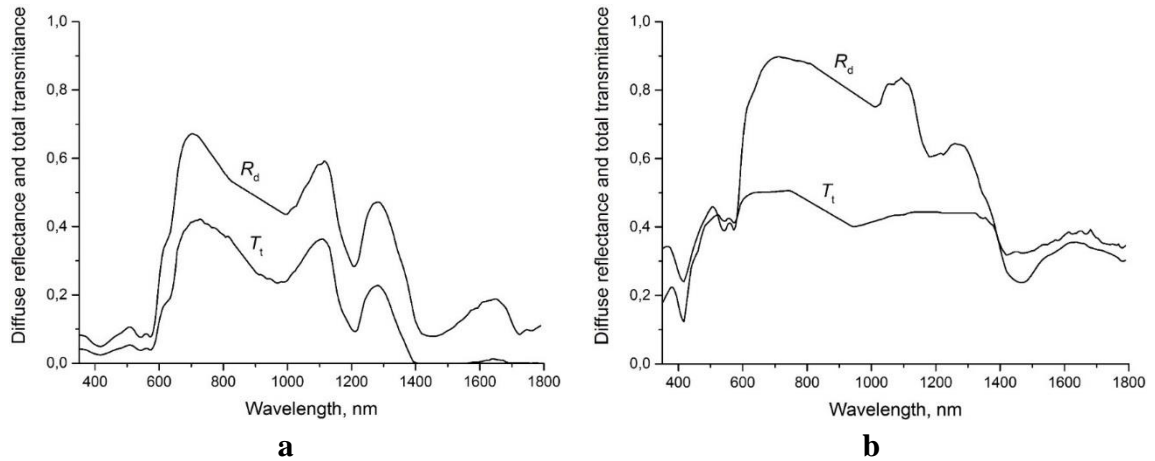


Figure 5.10 Total transmittance (T_t) and diffuse reflectance (R_d) spectra of 0.5 mm thick samples from HR2: (a) intact tissue and (b) tumour tissue.

These values are utilised for the IAD method, outcomes of which are presented in Figure 5.11 for HB1 and Figure 5.12 for HB2.

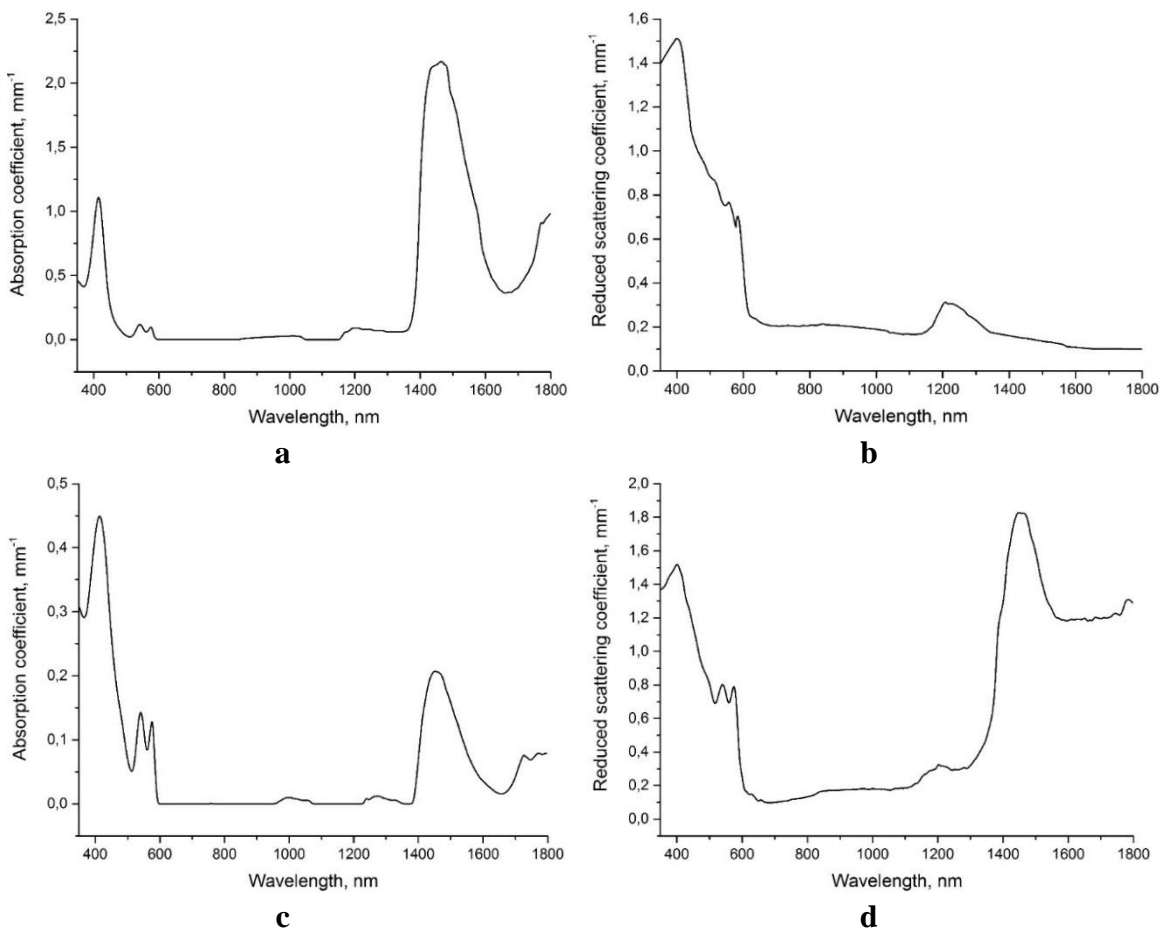


Figure 5.11(a) And (c) portray spectra created from the absorption coefficients of HB1 intact and tumour samples respectively. (b) And (d) portray spectra created from the reduced scattering coefficients of HB1 intact and tumour samples respectively.

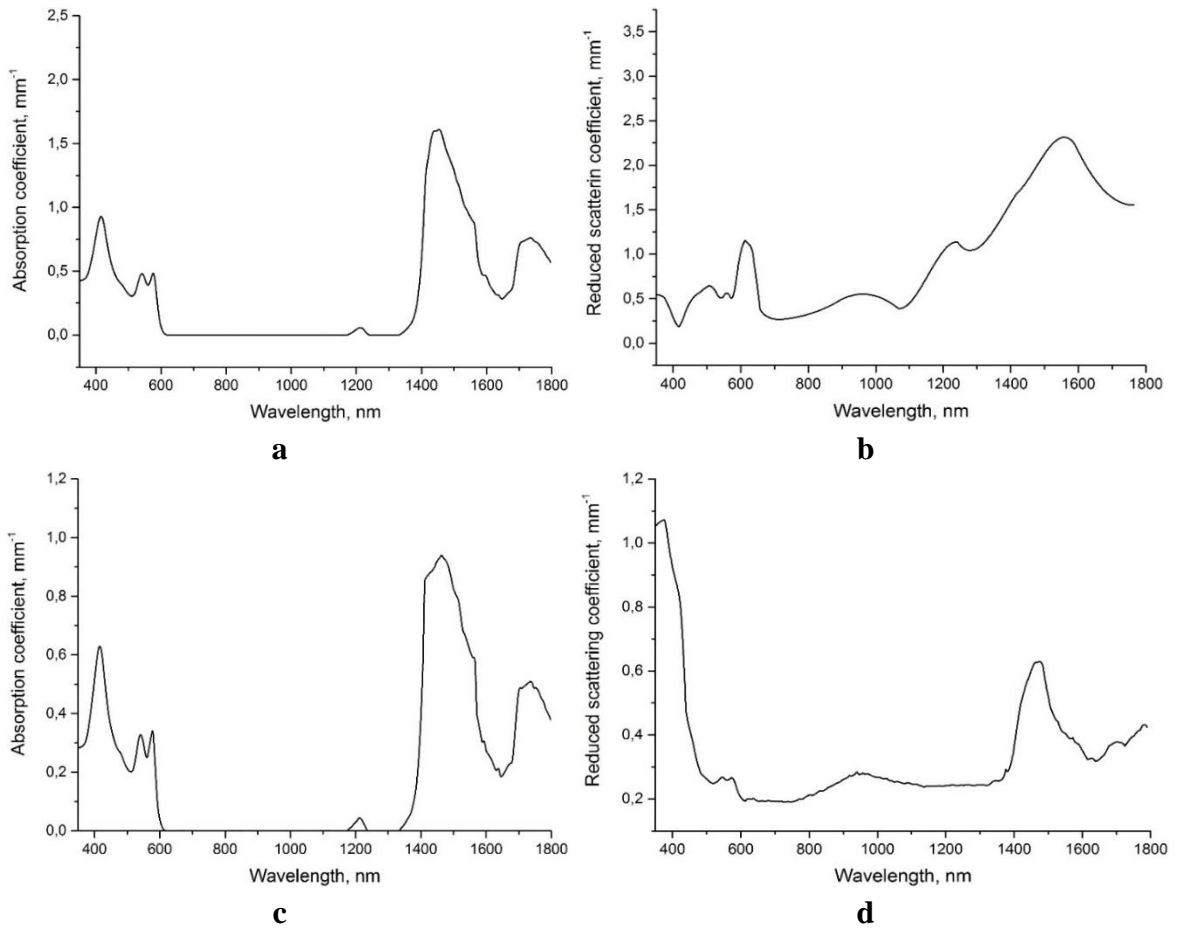
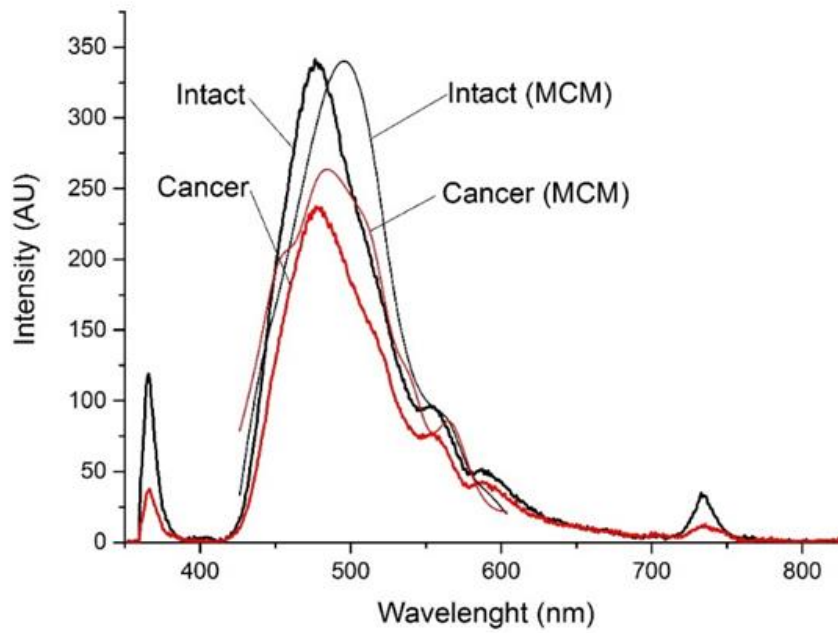


Figure 5.12 (a) And (c) portray spectra created from the absorption coefficients of HB2 intact and tumour samples respectively. (b) And (d) portray spectra created from the reduced scattering coefficients of HB2 intact and tumour samples respectively.

Figure 5.13 below portrays the comparison of simulated and measured fluorescence for HB1 tissue samples at UV and blue excitation wavelengths similar to Figure 5.8. Results for comparison of the HB2 tissue sample fluorescence are also presented in Figure 5.14.

A



B

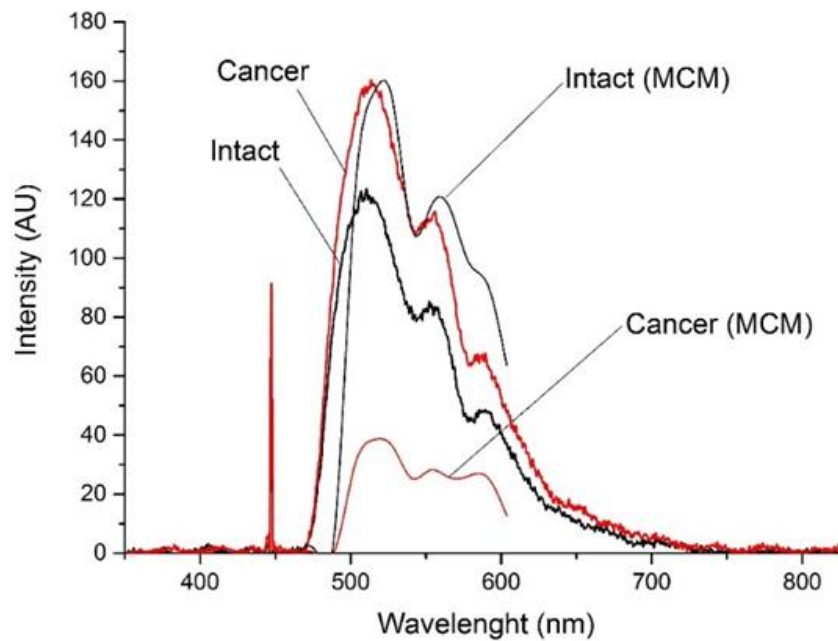


Figure 5.13 Comparison of measured fluorescence and simulated fluorescence for HB1 intact and tumour tissue samples. The curves are labelled, where MCM stands for Monte Carlo Model. Presented are curves for (a) UV excitation at 365 nm and (b) blue excitation at 450 nm.

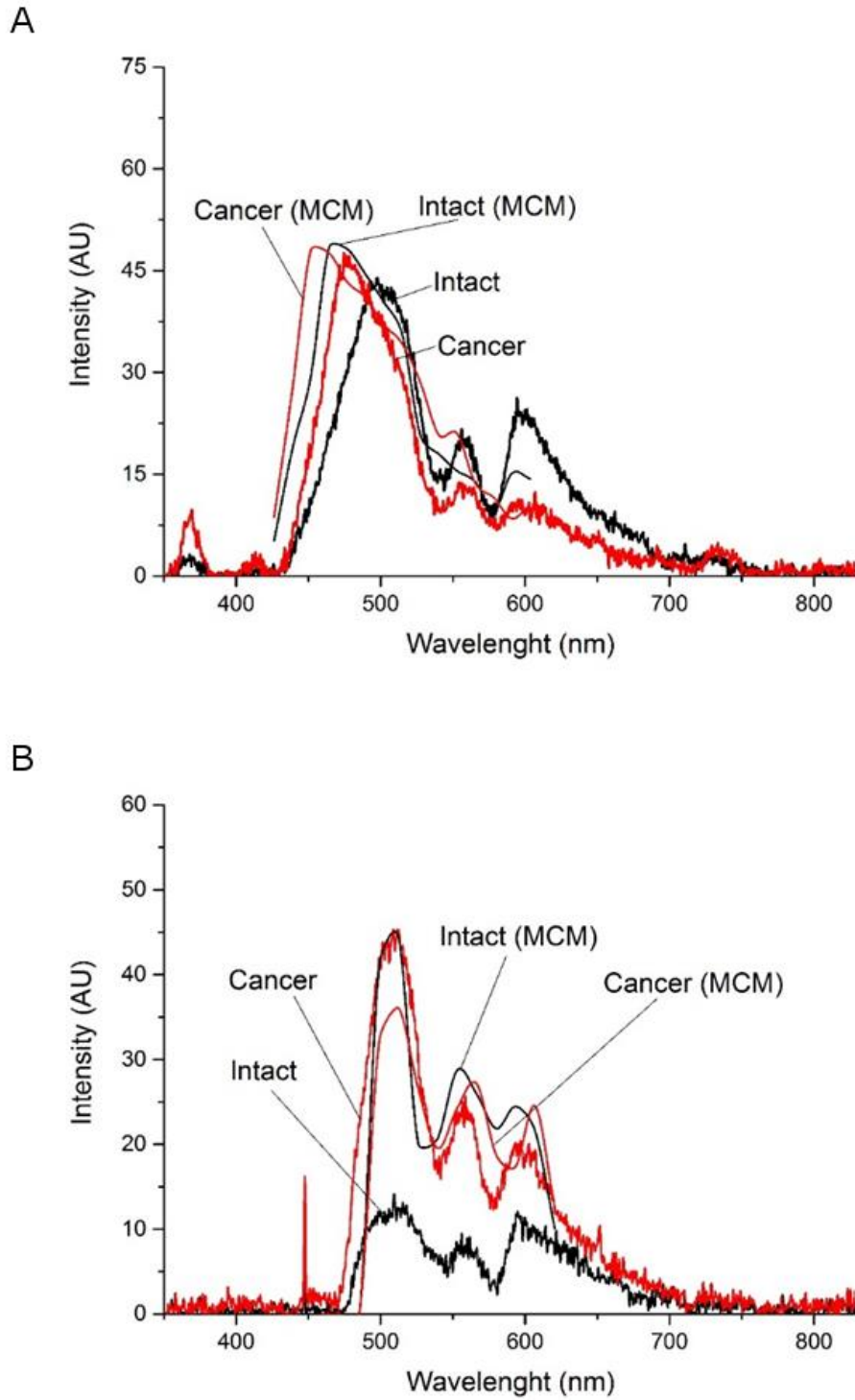


Figure 5.14 Comparison of measured fluorescence and simulated fluorescence for HB2 intact and tumour tissue samples. The curves are labelled, where MCM stands for Monte Carlo Model. Presented are curves for (a) UV excitation at 365 nm and (b) blue excitation at 450 nm.

5.6 Analysis and discussions

5.6.1 Literature analysis

As the proof of concept for the above described model was based on a literature analysis searching for available urinary bladder tissue transport coefficients, it is important to take into account the diversity and quality of the available data. The data sourced from the literature analysis only provided a limited selection of wavelengths, for a limited variation of tissue types. Due to the mucosa and sub-mucosa layers of the urinary bladder acting as hosts for the majority of early BC cases, and accounting for laser based diagnostics device penetration being confined to a similar depth, optical properties of these bladder regions were of special importance. Furthermore, coefficients of interest at wavelengths matching those of biologically important biomarkers were also required. As has been previously mentioned in earlier chapters, these biomarkers (particularly collagen, elastin, NADH and FAD) have excitation wavelengths between 260 – 450 nm and emission wavelengths between 420 – 530 nm (Koenig & Schneckenburger 1994). As the authors of the literature used for the initial model were not concerned with the creation of very specific optical property models, the data available is of only limited use.

Despite the limitations of using literature data, the derived model was still able to provide a huge potential, as will be described further below. However, due to this potential and the investigating groups' eventual access to a spectrophotometer capable of utilising an integrating sphere and thus measuring diffuse reflectance, a more advanced model, tailored to the specific tissue of interest was made possible.

5.6.2 Inverse adding-doubling method: transport coefficients of porcine urinary bladder

Upon the calculation of the absorption and scattering coefficients required for the creation of the above described model, the constructed absorption and scattering spectra presented in Figure 5.5 can be analysed. In doing so, absorption bands of haemoglobin (420, 540 and 580 nm) and water (1450 nm) are evident in the absorption spectra. Less evident, however are the water peaks at 975 nm and 1195 nm.

A noticeable fall in scattering coefficient value is present with the increase of wavelength. This behaviour is, however, consistent with the general biological tissue scattering characteristics (Jacques 2013). The fluctuations visible, even with the consistent drop off, can be attributed to strong absorption from the wavelength regions mentioned above.

Interestingly, a good agreement between data presented by this author and that of previously obtained literature (Staveren 1995) is clearly evident. The observable differences can easily be the

result of differences within the specific experimental data processing, as well as the inevitable property variations in unique organic tissue samples.

It should be noted that the observed dependence of the scattering coefficient within the range of interest, can be accurately approximated ($R^2 = 0.97$) with the aid of the Gunary power function (equation 5.9). This function was the best suited in comparison to multiple others also outlined in the OriginLab manual (OriginLab 2000).

$$\mu'_s = \frac{\lambda}{9140.944 + 23.064\lambda - 911.384\sqrt{\lambda}} \quad (5.9)$$

In the case of determining the capabilities of various non-invasive optical diagnosis methods, including fluorescence spectroscopy, a fundamental parameter to take into account is light penetration depth. Figure 5.6 depicts the range of penetration depths, including the spectral region of interest related to fluorescence spectroscopy (350 – 600 nm), where penetration depth is between 0.5 and 2 mm. This is a suitable depth to successfully stimulate major fluorescent biomarkers (such as NADH, FAD, collagen, etc.).

One major benefit gained from the employment of the IAD method is the improved accuracy compared to literature based coefficient use. Organic tissue samples measured in the spectrometer for reflectance and transmission underwent the same processes and were kept in identical conditions to those which underwent the fluorescence analysis by the LAKK-M. This acts to greatly decrease the potential errors which may arise from alternate experimental practices and laboratory condition variations. There is an added benefit in the form of further calculated data improvement. The sample size of tissue transport coefficients and fluorescence data can be easily expanded on, ultimately improving the accuracy of the model.

5.6.3 Model construction

Regardless of the optical property origin, whether from literature or experimentally derived, the subsequent construction of the 3D model was based on the well-described Monte Carlo methodology. This approach remains as one of the most effective simulation tools in regards to biological tissues, particularly when applied to multi-layered tissues. For this reason, multiple other studies have employed this methodology to construct optical property models (Drezek, Sokolov, et al. 2001; Palmer & Ramanujam 2008; Pavlova et al. 2008; Zhu et al. 2009). These range from a relatively simple one layer model (Palmer & Ramanujam 2008) to a complex five layer model (Pavlova et al. 2009). Despite the widespread use of Monte Carlo enabled modelling, most areas of interest have been easily accessible or external, such as the breast or cervix tissues. This author has not encountered any such modelling to have been produced or optimised for endoscopically reached hollow organs (for example the urinary bladder).

In the case of the model outlined in this thesis, a dual layer setup was selected for a balance of accuracy and simplicity. Though not simple, the physiological structure of the urinary bladder may be “reduced”, without compromising accuracy, into two major component layers: the muscle and the mucosa. These two specific layers are considerably larger than layers that were omitted, such as the connective tissue. The fact that both of the modelled layers constitute the majority of the urinary bladder tissue indicates that they will act as host to the majority of the light-tissue interactions. It is important to note that at the early stage of model development and validation, smaller layers like the already mentioned connective tissue, would not alter the model properties in any significant way, thus explaining their absence.

Due to the intended application of the model for cancer detection, NADH, FAD and collagen were selected as the specific contributing fluorophores. As has been mentioned in chapter 1.3.2.1, these play a key role in accounting for metabolism (with the aid of the redox ratio). Thus they have a key role in tumour growth and the structural makeup of the tumour cells. This author has encountered no other models, excluding Pavlova et al. (2009), including FAD in their parameters. Furthermore, no such models concentrating on the urinary bladder with the same fluorophores of interest were found either.

5.6.4 Three dimensional models

Judging by Figure 5.4, which displays the modelled fluorescence in comparison to that of measured fluorescence as produced by the initial proof of concept model, a good match is clearly visible. While an obvious difference is present in the region of 510 – 570 nm, this can be accounted for by the presence of unaccounted for fluorophores (such as FAD) present in organic tissue. Other chromophores can provide a further contribution to the organically derived spectrum, additionally modifying it in a way not represented by the model. The likeness of the curves in the region of 420 – 490 nm does, however, indicate that the NADH and collagen present in organic urinary bladder tissue heavily influence its fluorescence spectrum.

Figure 5.8 displays a similar level of consistency between measured and simulated values. However, due to the increased accuracy of the model and the introduction of FAD into the simulation, the curves obtained better display nuances of the spectrum. For example, effects of blood are evident in both the modelled and measured spectra (seen from the haemoglobin troughs at 540 nm and 580 nm). As with the initial model, the importance of NADH and collagen are still obvious. However, where the initial model began to diverge at wavelengths expected to display FAD fluorescence, the more advanced model confirms the importance of FAD as a biomarker within the system. Interestingly, similar conclusions were reached by Drezek, Brookner, et al. (2001) and Pavlova et al. (2003) in their work using fluorescence microscopy on cervical tissues. Both authors indicate that mitochondrial NADH and FAD dominate the fluorescence in epithelial cells of the studied tissue.

Relying on these findings and constructing preliminary models on human tumour tissues, we can observe the potential effectiveness of the model. As displayed in Figures 5.13 and 5.14, there are a number of similarities between simulated and measured fluorescence, especially on the UV excitation curves. One of the main features to take into account between the simulated and measured curves (most evidently pronounced on the UV spectra), is the red shifted simulated curve. The shift in peak wavelength is potentially the result of blood, particularly constituents such as the haemoglobin, acting as a form of optical “filter” similar to the physical ones used by the LAKK-M to reduce backscattering. Unfortunately, one of the major drawbacks of using biopsy samples is the fact that size and shape of each sample is neither uniform nor shaped for easy optical analysis. While this would not be an issue in a live tissue or even full excised organ, biopsy samples have varying levels of blood dependent on how much tissue was removed as well as how accurately. The non-uniform nature of such samples may account for the large differences that can be particularly easily observed from the blue spectra of both the HB1 and HB2 samples. Despite this drawback, looking at both the simulated and measured UV fluorescence spectra, we can observe a fall in NADH concentration in tumorous tissues. This is also followed by a general increase in FAD concentration, as seen on the measured blue fluorescence spectra. This could be potentially explained by the presence of hypoxia commonly occurring in tumours. During this hypoxia, only the anaerobic glycolysis pathway is employed, meaning that energy is exclusively generated through NADH metabolism. Additionally, due to the violation of the aerobic pathway of glycolysis, FADH₂ (the reduced form of FAD) formation slows down, leading to a lack of FAD utilisation, and thus accumulation. However, further work must be conducted to improve the simulation capacity for fluorescence spectra derived by blue excitation.

5.6.5 Future prospects and conclusions

The results that this author presents above show great potential and versatility of spectroscopic techniques. They demonstrate the ability to provide large quantities of useful information in regards to non-invasive disease classification. With the application of non-invasive techniques such as fluorescence spectroscopy, in conjunction with the above-described complex modelling, great leaps can be made for detecting dysplasia in urinary bladder. The use of key biomarkers such as NADH, FAD and collagen provides this methodology much of the potential for diagnostics. These biomarkers can be employed to contrast healthy and diseased tissues. However, the described model is not limited to these biomarkers and can, therefore, be further adapted and improved with the introduction of additional relevant ones. As such, this model is not necessarily limited to one organ or one disease and has the capacity to be adapted for further function. Together with a potentially increasing data set and variations in tissues, the model presented has potential to aid in the detection of urinary bladder cancer, especially in conjunction with other optical diagnostics

tools. As a supplement to pre-existing and established methods of cancer detection, utilising such a model and fluorescence analysis may work to reduce the number of problematic false positive diagnoses as well as increase the overall accurate detection rate for early stage cancers.

It is important to note that the model described above is created using porcine bladder tissue. While sufficient for the creation of the model, use of human tissue can greatly improve its functionality in regards to accuracy and relevancy. As is already shown in the experiments above, basing the methodology on healthy and tumorous tissue has the potential to drastically improve upon the viability of the model in specific relation to cancer detection in a clinical setting. The work outlined in this chapter has already demonstrated the crucial first step in perfecting the model. A wide database of tumorous and healthy tissue could provide a fast reference point to measured fluorescence, potentially aiding with early diagnosis. While at this stage, the model is helpful for research purposes, techniques such as the one described above, may become standard in clinical environments with the aid of improved user friendliness. Real time visual feedback for users, such as surgeons or nurses, presents itself as a realistic future application.

Finally, the techniques outlined in this chapter were conducted on bladder tissue due to the pressing need for improved diagnostics for BC. This, however, does not limit them. Similar methodologies can be conducted on tissue from other hollow organs such as the intestine or even from the heart.

References

- A' Amar, O.M. et al., 1997. Autofluorescence Spectroscopy of Normal and Pathological Tissues of the Bladder I. J. Bigio et al., eds. *SPIE proceedings*, 3197, pp.41–49. Available at: <http://proceedings.spiedigitallibrary.org/proceeding.aspx?articleid=931793>.
- Ahmad, I., Sansom, O.J. & Leung, H.Y., 2012. Exploring molecular genetics of bladder cancer: lessons learned from mouse models. *Disease models & mechanisms*, 5(3), pp.323–32. Available at: <http://www.pubmedcentral.nih.gov/articlerender.fcgi?artid=3339826&tool=pmcentrez&rendertype=abstract> [Accessed October 25, 2013].
- Bashkatov, A.N. et al., 2004. Optical properties of mucous membrane in the spectral range 350–2000 nm. *Optics and Spectroscopy*, 97(6), pp.978–983. Available at: <http://link.springer.com/10.1134/1.1843961>.
- Bradley, R.S. & Thorniley, M.S., 2006. A review of attenuation correction techniques for tissue fluorescence. *Journal of the Royal Society, Interface / the Royal Society*, 3(6), pp.1–13. Available at: <http://www.pubmedcentral.nih.gov/articlerender.fcgi?artid=1618480&tool=pmcentrez&rendertype=abstract> [Accessed January 7, 2015].
- Brausi, M. et al., 2002. European Urology Variability in the Recurrence Rate at First Follow-up Cystoscopy after TUR in Stage Ta T1 Transitional Cell Carcinoma of the Bladder: A Combined Analysis of Seven EORTC Studies. *European urology*, 41, pp.523–531.
- Bykov, A. V. et al., 2011. Multilayer tissue phantoms with embedded capillary system for OCT and DOCT imaging. , 8091, p.80911R–80911R–6. Available at: <http://proceedings.spiedigitallibrary.org/proceeding.aspx?articleid=1272385>.
- Chapman, S.K. & Reid, G.A. eds., 1999. *Flavoprotein Protocols* 1st ed., Humana Press.
- Chen, Y. et al., 2009. Oxygen consumption can regulate the growth of tumors, a new perspective on the Warburg effect. *PloS one*, 4(9), p.e7033. Available at: <http://www.pubmedcentral.nih.gov/articlerender.fcgi?artid=2737639&tool=pmcentrez&rendertype=abstract> [Accessed November 6, 2013].
- Cheong, W., Prahl, S. & Welch, A., 1990. A review of the optical properties of biological tissues. *IEEE journal of quantum electronics*, 26(12), pp.2166–2185. Available at: http://www.uta.edu/rfmems/N_041101/Reference/133.pdf [Accessed May 14, 2014].
- Drezek, R., Brookner, C., et al., 2001. Autofluorescence Microscopy of Fresh Cervical-Tissue Sections Reveals Alterations in Tissue Biochemistry with Dysplasia. *Photochemistry and Photobiology*, 73(6), p.636. Available at: [http://doi.wiley.com/10.1562/0031-8655\(2001\)073%3C0636:AMOFCT%3E2.0.CO;2](http://doi.wiley.com/10.1562/0031-8655(2001)073%3C0636:AMOFCT%3E2.0.CO;2).
- Drezek, R., Sokolov, K., et al., 2001. Understanding the contributions of NADH and collagen to cervical tissue fluorescence spectra: Modeling, measurements, and implications. *Journal of Biomedical Optics*, 6(4), pp.385–396. Available at: <http://dx.doi.org/10.1117/1.1413209>.
- Eatock, M.M., Schätzlein, a & Kaye, S.B., 2000. Tumour vasculature as a target for anticancer therapy. *Cancer treatment reviews*, 26(3), pp.191–204. Available at: <http://www.ncbi.nlm.nih.gov/pubmed/10814561>.
- Folkman, J., 1972. Anti-angiogenesis: new concept for therapy of solid tumors. *Annals of surgery*, 175(3), pp.409–16. Available at: <http://www.pubmedcentral.nih.gov/articlerender.fcgi?artid=1355186&tool=pmcentrez&rendertype=abstract>.
- Georgakoudi, I. et al., 2001. Fluorescence, reflectance, and light-scattering spectroscopy for evaluating dysplasia in patients with Barrett's esophagus. *Gastroenterology*, 120(7), pp.1620–1629. Available at: <http://linkinghub.elsevier.com/retrieve/pii/S0016508501013269> [Accessed January 8, 2015].
- Gray, H., 2012. *Gray's Anatomy* 15th ed. T. Pickering Pick & R. Howden, eds., London: Bounty Books.
- Grossman, H.B. et al., 2007. A phase III, multicenter comparison of hexaminolevulinate fluorescence cystoscopy and white light cystoscopy for the detection of superficial papillary lesions in

- patients with bladder cancer. *The Journal of urology*, 178(1), pp.62–7. Available at: <http://www.ncbi.nlm.nih.gov/pubmed/17499283> [Accessed November 21, 2013].
- Izuishi, K. et al., 1999. The Histological Basis of Detection of Adenoma and Cancer in the Colon by Autofluorescence Endoscopic Imaging. *Endoscopy*, 31(7), pp.511–516.
- Jacques, S.L., 2013. Optical properties of biological tissues: a review. *Physics in Medicine and Biology*, 58(14), pp.R37–R61. Available at: <http://stacks.iop.org/0031-9155/58/i=14/a=5007?key=crossref.c531ac37cfa1f77bbc0d33a8e92de8c9> [Accessed July 10, 2014].
- Jemal, A. et al., 2009. Cancer statistics, 2009. *CA: a cancer journal for clinicians*, 59(4), pp.225–49. Available at: <http://www.ncbi.nlm.nih.gov/pubmed/19474385> [Accessed November 10, 2013].
- Jemal, A., Murray, T. & Ward, E., 2005. Cancer statistics, 2005. *CA: a cancer journal for clinicians*. Available at: <http://onlinelibrary.wiley.com/doi/10.3322/canjclin.55.1.10/full> [Accessed November 18, 2013].
- Jocham, D. et al., 2005. Improved detection and treatment of bladder cancer using hexaminolevulinate imaging: a prospective, phase III multicenter study. *The Journal of urology*, 174(3), p.862–6; discussion 866. Available at: <http://www.ncbi.nlm.nih.gov/pubmed/16093971> [Accessed November 19, 2013].
- Karaoglu, I., van der Heijden, A.G. & Witjes, J.A., 2013. The role of urine markers, white light cystoscopy and fluorescence cystoscopy in recurrence, progression and follow-up of non-muscle invasive bladder cancer. *World journal of urology*. Available at: <http://www.ncbi.nlm.nih.gov/pubmed/24166285> [Accessed November 18, 2013].
- Katika, K.M. & Pilon, L., 2007. Feasibility analysis of an epidermal glucose sensor based on time-resolved fluorescence. *Appl. Opt.*, 46(16), pp.3359–3368. Available at: <http://ao.osa.org/abstract.cfm?URI=ao-46-16-3359>.
- Koenig, K. & Schneckenburger, H., 1994. Laser-induced autofluorescence for medical diagnosis. *Journal of fluorescence*, 4(1), pp.17–40. Available at: <http://www.ncbi.nlm.nih.gov/pubmed/24233290>.
- Lurie, K.L. et al., 2014. Three-dimensional, distendable bladder phantom for optical coherence tomography and white light cystoscopy. *Journal of biomedical optics*, 19(3), p.36009. Available at: <http://www.ncbi.nlm.nih.gov/pubmed/24623158> [Accessed April 28, 2014].
- Meijden, A. van der, 1998. Fortnightly review: Bladder cancer. *BMJ: British Medical Journal*, 317(November), pp.1366–1369. Available at: <http://www.ncbi.nlm.nih.gov/pmc/articles/PMC1114251/> [Accessed November 25, 2013].
- Moffitt, T.P., 2007. *Compact Fiber-Optic Diffuse Reflection Probes for Medical Diagnostics*.
- Mowatt, G. et al., 2011. Photodynamic diagnosis of bladder cancer compared with white light cystoscopy: Systematic review and meta-analysis. *International journal of technology assessment in health care*, 27(1), pp.3–10. Available at: <http://www.ncbi.nlm.nih.gov/pubmed/21262078> [Accessed November 20, 2013].
- Muller, G. & Roggan, A. eds., 1995. *Laser-induced interstitial thermotherapy*, Bellingham: SPIE.
- Okada, E. & Delpy, D.T., 2003. Near-infrared light propagation in an adult head model. II. Effect of superficial tissue thickness on the sensitivity of the near-infrared spectroscopy signal. *Applied optics*, 42(16), pp.2915–22. Available at: <http://www.ncbi.nlm.nih.gov/pubmed/12790440>.
- OpenStax, 2016. *OpenStax, Anatomy and Physiology*, OpenStax CNX. Available at: <http://cnx.org/contents/14fb4ad7-39a1-4eee-ab6e-3ef2482e3e22@8.24>.
- OriginLab, 2000. Curve Fitting Functions. *Manual*, pp.1–166.
- Palmer, G. & Ramanujam, N., 2008. Monte-Carlo-based model for the extraction of intrinsic fluorescence from turbid media. *Journal of biomedical optics*, 13(2), pp.1–17. Available at: <http://biomedicaloptics.spiedigitallibrary.org/article.aspx?articleid=1102625> [Accessed July 8, 2015].
- Palmer, S. et al., 2013. Technologic Developments in the Field of Photonics for the Detection of Urinary Bladder Cancer. *Clinical genitourinary cancer*, 11(4), pp.390–6. Available at: <http://www.ncbi.nlm.nih.gov/pubmed/23871799> [Accessed November 20, 2013].
- Parkin, D.M. et al., 2005. Global cancer statistics, 2002. *CA: a cancer journal for clinicians*, 55(2), pp.74–108. Available at: <http://www.ncbi.nlm.nih.gov/pubmed/15761078>.
- Pavlova, I. et al., 2009. Fluorescence spectroscopy of oral tissue: Monte Carlo modeling with site-

- specific tissue properties. *Journal of biomedical optics*, 14(1), pp.1–16. Available at: <http://biomedicaloptics.spiedigitallibrary.org/article.aspx?articleid=1102905> [Accessed July 8, 2015].
- Pavlova, I. et al., 2003. Microanatomical and Biochemical Origins of Normal and Precancerous Cervical Autofluorescence Using Laser-scanning Fluorescence Confocal Microscopy. *Photochemistry and Photobiology*, 77(5), p.550. Available at: [http://doi.wiley.com/10.1562/0031-8655\(2003\)077%3C0550:MABOON%3E2.0.CO;2](http://doi.wiley.com/10.1562/0031-8655(2003)077%3C0550:MABOON%3E2.0.CO;2).
- Pavlova, I. et al., 2008. Understanding the biological basis of autofluorescence imaging for oral cancer detection: high-resolution fluorescence microscopy in viable tissue. *Clinical cancer research: an official journal of the American Association for Cancer Research*, 14(8), pp.2396–404. Available at: <http://www.pubmedcentral.nih.gov/articlerender.fcgi?artid=2773159&tool=pmcentrez&rendertype=abstract> [Accessed December 23, 2014].
- Prahl, S.A., Gemert, M.J.C. Van & Welch, A.J., 1993. Determining the optical properties of turbid media by using the adding-doubling method. *Applied optics*, 32(4), pp.559–568.
- Prahl, S., Gemert, M. van & Welch, A., 1993. Determining the optical properties of turbid using the adding–doubling method. *Applied optics*. Available at: <http://www.opticsinfobase.org/ao/fulltext.cfm?uri=ao-32-4-559&id=40827> [Accessed December 9, 2014].
- Puzio-Kuter, A.M. et al., 2009. Inactivation of p53 and Pten promotes invasive bladder cancer. *Genes & development*, 23(6), pp.675–80. Available at: <http://www.pubmedcentral.nih.gov/articlerender.fcgi?artid=2661614&tool=pmcentrez&rendertype=abstract> [Accessed October 30, 2013].
- Rafailov, I. et al., 2015. A novel excitation-emission wavelength model to facilitate the diagnosis of urinary bladder diseases B. Choi et al., eds. *SPIE proceedings*, 9303(0), p.93030W. Available at: <http://proceedings.spiedigitallibrary.org/proceeding.aspx?doi=10.1117/12.2077554> [Accessed April 30, 2015].
- Rafailov, I.E. et al., 2016. Computational model of bladder tissue based on its measured optical properties. *Journal of Biomedical Optics*, 21(2), p.25006. Available at: <http://biomedicaloptics.spiedigitallibrary.org/article.aspx?doi=10.1117/1.JBO.21.2.025006>.
- Ritz, J.P. et al., 2001. Optical properties of native and coagulated porcine liver tissue between 400 and 2400 nm. *Lasers in Surgery and Medicine*, 29(3), pp.205–212.
- Sandell, J. & Zhu, T., 2011. A review of in vivo optical properties of human tissues and its impact on PDT. *Journal of biophotonics*, 4, pp.773–787. Available at: <http://onlinelibrary.wiley.com/doi/10.1002/jbio.201100062/abstract> [Accessed May 30, 2014].
- Secomb, T.W. et al., 1993. Analysis of oxygen transport to tumor tissue by microvascular networks. *International Journal of Radiation Oncology*Biophysics*Physics*, 25(3), pp.481–489. Available at: <http://www.sciencedirect.com/science/article/pii/036030169390070C>.
- Secomb, T.W. et al., 1995. Analysis of the effects of oxygen supply and demand on hypoxic fraction in tumors. *Acta oncologica (Stockholm, Sweden)*, 34(3), pp.313–6. Available at: <http://www.ncbi.nlm.nih.gov/pubmed/7779415>.
- Shweiki, D. et al., 1992. Vascular endothelial growth factor induced by hypoxia may mediate hypoxia-initiated angiogenesis. *Nature*, 359, pp.843–845. Available at: <http://www.med.upenn.edu/timm/documents/DunaiefTIMMShweikietal-1.pdf> [Accessed December 2, 2013].
- Siegel, R.L., Miller, K.D. & Jemal, A., 2016. Cancer Statistics, 2016. *CA: a cancer journal for clinicians*, 66(1), pp.7–30.
- Sievert, K.D. et al., 2009. Economic aspects of bladder cancer: what are the benefits and costs? *World journal of urology*, 27(3), pp.295–300. Available at: <http://www.pubmedcentral.nih.gov/articlerender.fcgi?artid=2694315&tool=pmcentrez&rendertype=abstract> [Accessed April 7, 2014].
- Staveren, H. van, 1995. Integrating sphere effect in whole bladder wall photodynamic therapy at violet, green, and red wavelengths. *SPIE proceedings*, 2323, pp.13–20. Available at: <http://proceedings.spiedigitallibrary.org/proceeding.aspx?articleid=978626> [Accessed December 9, 2014].

- Sylvester, R.J. et al., 2006. Predicting recurrence and progression in individual patients with stage Ta T1 bladder cancer using EORTC risk tables: a combined analysis of 2596 patients from seven EORTC trials. *European urology*, 49(3), pp.466-5-7. Available at: <http://www.ncbi.nlm.nih.gov/pubmed/16442208> [Accessed November 7, 2013].
- Tajiri, H., 2007. Autofluorescence endoscopy for the gastrointestinal tract. *Proceedings of the Japan Academy. Series B, Physical and biological sciences*, 83(8), pp.248–55. Available at: <http://www.pubmedcentral.nih.gov/articlerender.fcgi?artid=3859293&tool=pmcentrez&rendertype=abstract> [Accessed January 7, 2015].
- Tuchin, V.V., 2000. *Tissue Optics: Light Scattering Methods and Instruments for Medical Diagnosis. SPIE Tutorial Text in Optical Engineering.*, Washington: SPIE Press.
- Vaupel, P., Kallinowski, F. & Okunieff, P., 1989. Blood flow, oxygen and nutrient supply, and metabolic microenvironment of human tumors: a review. *Cancer research*, 49(23), pp.6449–65. Available at: <http://www.ncbi.nlm.nih.gov/pubmed/2684393>.
- Vishwanath, K. & Mycek, M.-A., 2004. Do fluorescence decays remitted from tissues accurately reflect intrinsic fluorophore lifetimes? *Opt. Lett.*, 29(13), pp.1512–1514. Available at: <http://ol.osa.org/abstract.cfm?URI=ol-29-13-1512>.
- Vo-Dinh, T. ed., 2010. *Biomedical photonics handbook*, Boca Raton: CRC Press. Available at: [http://books.google.com/books?hl=en&lr=&id=Pl4wsXCiZdQC&oi=fnd&pg=PP1&dq=Bio medical+Photonics+Handbook&ots=S7F2dZigml&sig=zRAZXvSSJSqO7gFmnI65nYcd3eo](http://books.google.com/books?hl=en&lr=&id=Pl4wsXCiZdQC&oi=fnd&pg=PP1&dq=Bio+medical+Photonics+Handbook&ots=S7F2dZigml&sig=zRAZXvSSJSqO7gFmnI65nYcd3eo) [Accessed October 29, 2013].
- Wang, H.-W., Wei, Y.-H. & Guo, H.-W., 2009. Reduced Nicotinamide Adenine Dinucleotide (NADH) Fluorescence for the Detection of Cell Death. *Anti-Cancer Agents in Medicinal Chemistry*, 9(9), pp.1012–1017. Available at: <http://www.eurekaselect.com/openurl/content.php?genre=article&issn=1871-5206&volume=9&issue=9&spage=1012>.
- Wang, Q. et al., 2008. Measurement of internal tissue optical properties at ultraviolet and visible wavelengths: Development and implementation of a fiberoptic-based system. *Optics Express*, 16(12), p.8685. Available at: <http://www.opticsinfobase.org/abstract.cfm?URI=oe-16-12-8685>.
- Warburg, O., 1956. On respiratory impairment in cancer cells. *Science (New York, NY)*, 124(3215), pp.267–272. Available at: <http://www.ncbi.nlm.nih.gov/pubmed/13351639> [Accessed December 2, 2013].
- Wróbel, M.S. et al., 2014. Multi-layered tissue head phantoms for noninvasive optical diagnostics. *Journal of Innovative Optical Health Sciences*, 8(3), p.1541005. Available at: <http://www.worldscientific.com/doi/abs/10.1142/S1793545815410059>.
- Wróbel, M.S. et al., 2015. Use of optical skin phantoms for preclinical evaluation of laser efficiency for skin lesion therapy. *Journal of Biomedical Optics*, 20(8), p.85003. Available at: <http://biomedicaloptics.spiedigitallibrary.org/article.aspx?doi=10.1117/1.JBO.20.8.085003>.
- Zhu, C. et al., 2009. Model based and empirical spectral analysis for the diagnosis of breast cancer. *Optics express*, 16(19), pp.14961–14978.

Chapter 6 : Application in cardiovascular disease

While cancer remains as one of the most devastating diseases humans currently face, the application of photonics based diagnostics devices has the capacity to be applied to unrelated diseases as well. Along with cancer, conditions such as cardiovascular disease (CVD) or even diabetes affect hundreds of millions worldwide. This chapter will cover the use of photonics based diagnostics technology for development of diagnosis methods in pre-eclampsia, a CVD prevalent in pregnant women around the world. Furthermore the chapter will begin from a validation of the previously described methodology (chapter 4) on an animal model.

6.1 Viability of the LAKK-M in CVD diagnostics on mouse models

The LAKK-M device available for completion of experiments in the work outlined by this thesis was effectively employed on human tissue as presented in the last chapter. However, human tissue is the intended target for measurement by the LAKK-M device. This fact introduces a particular challenge into experimental CVD investigation, as much of the work studying CVD's is conducted on animal models. In light of this, a number of experiments were completed in order to determine the effectiveness of the available technology in observing small changes in disease models and the best measurement protocols to employ. This work was required as a basis to conduct more in-depth analysis of murine CVD models.

6.1.1 Optimal recording areas on mice: introduction and methodology

One of the first steps required to ensure high quality measurements of mice was distinguishing the best areas from which to record. A series of measurements was carried out on two available groups of mice. Both a CSE (cystathionine γ -lyase) deficient group and a wild type C57 group of mice had six animals each. All animals were female, between 7 – 11 weeks old and grown at Aston University. Using the standard measurement methodology for microcirculatory parameter recording described in chapter 4, all the animals were measured for perfusion (I_m), saturation (S_tO_2) and blood velocity (V_b). These measurements were conducted on the tail, the ear and the neck of the animals (which required the removal of animal hair in the probed area). The index of oxygen saturation to perfusion of microvascular blood flow (S_m) was also calculated from the measured data.

6.1.2 Optimal recording areas on mice: results and outcomes

Figure 6.1 below depicts the outcomes of the LAKK-M microcirculatory parameter measurements on various areas of the mice.

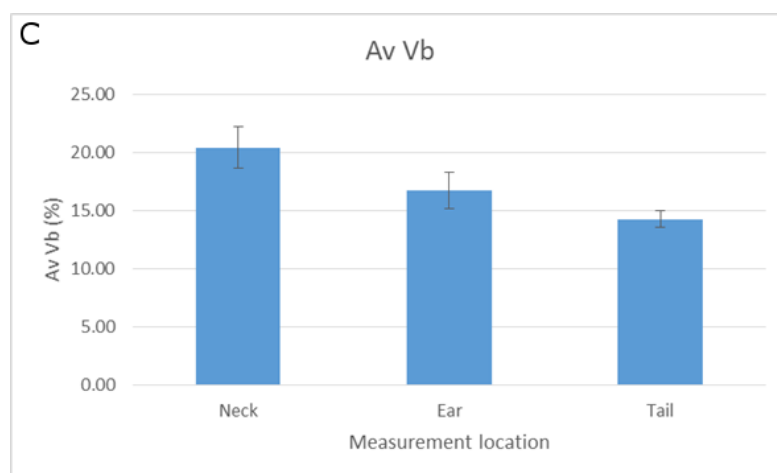
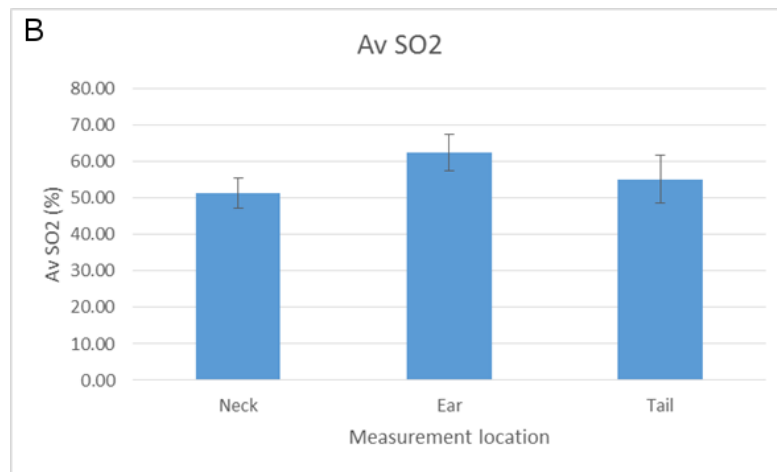
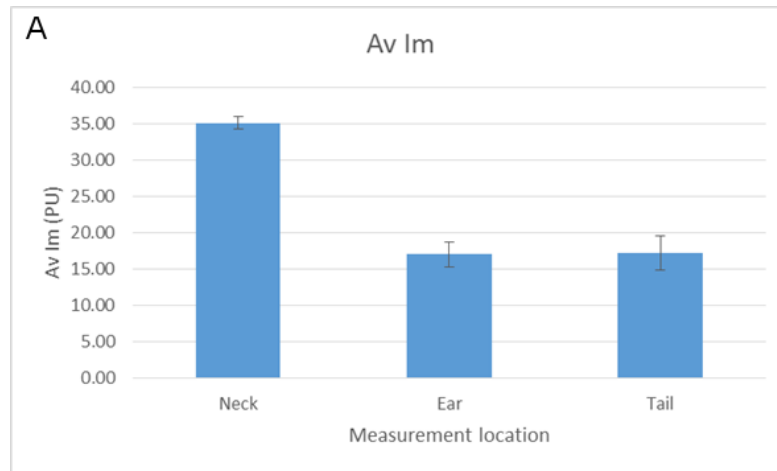


Figure 6.1 Outcomes of the LAKK-M microcirculatory parameter measurements on various areas of the mice. The perfusion (Im), saturation (StO₂) and blood velocity (Vb) are presented in images (A), (B) and (C) respectively.

The above results indicate the sensitivity of the LAKK-M device employed in the experiment to microcirculatory parameters of the different animals. As can be seen from the graphs, stable and large signals can be obtained even in murine models of disease. Ultimately, this is an important basis to further investigate the potentials of the LAKK-M diagnostics on murine models.

6.1.3 Effectiveness in murine disease models: introduction and methodology

Considering the above section established knowledge that viable recordings can be taken employing the equipment and methodologies outlined in chapter 4, it was important to test such application in observing differences in active disease models. As such, comparisons were made between wild type mice and mice with gene knockouts relating to factors important in cardiac function and organism development. Once again, CSE deficient mice were used to compare to wild type (WT) counterparts. CSE functions in a signalling pathway with hydrogen sulphide (H₂S), which is ultimately thought to be responsible for atherosclerosis, myocardial infarction, hypertension and shock in a variety of cardiovascular diseases (Wang, Ahmad, Cai, Rennie, Fujisawa, Fatima Crispi, et al. 2013; Yang et al. 2008; Pan et al. 2012). Additionally, haem oxygenase-1 (HO-1) knockout (KO) mice and their wild type counterparts were compared due to the importance of HO-1 in mammalian embryo survival (Fraser et al. 2011). The primary aim of this preliminary work was to observe the potential for the described methodology at recording present dysfunctions in KO animals.

The animal groups included 3 HO-1 WT and 3 HO-1 KO as well as 5 CSE WT and 5 CSE KO mice. Using the standard methodology described in chapter 4, the microcirculatory perfusion (I_m), saturation (S_tO_2) and blood velocity (V_b) parameters were recorded. Additionally, the autofluorescence of NADH and FAD was also recorded to calculate the redox ratio (RR) as already mentioned in chapter 1. These parameters were recorded on the tails of the animals on two consecutive days. Differences between WT and KO animals were statistically analysed using a two-sample t-test for significant differences.

6.1.4 Effectiveness in murine disease models: results and outcomes

Figure 6.2 displays the day 1 and day 2 recordings of microcirculatory parameters I_m .

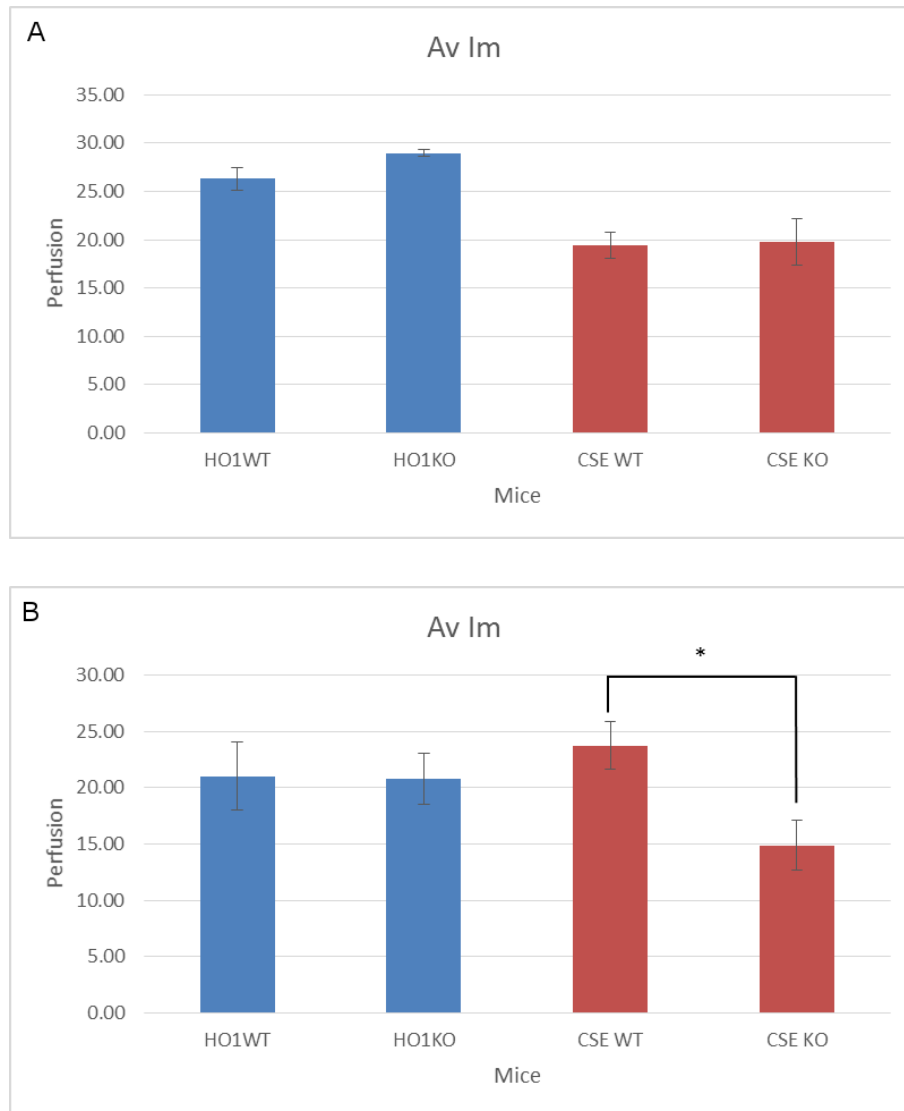


Figure 6.2 Comparison of the I_m values between HO1 WT and KO mice as well as CSE WT and KO mice on day 1 (A) and day 2 (B).

* Significant difference ($p < 0.05$) between the CSE WT and CSE KO, calculated using a t-test.

Figure 6.3 displays the day 1 and day 2 recordings of microcirculatory parameters S_tO_2 . Both of these parameters displayed significant differences. The V_b parameter is not shown as no significance was observed.

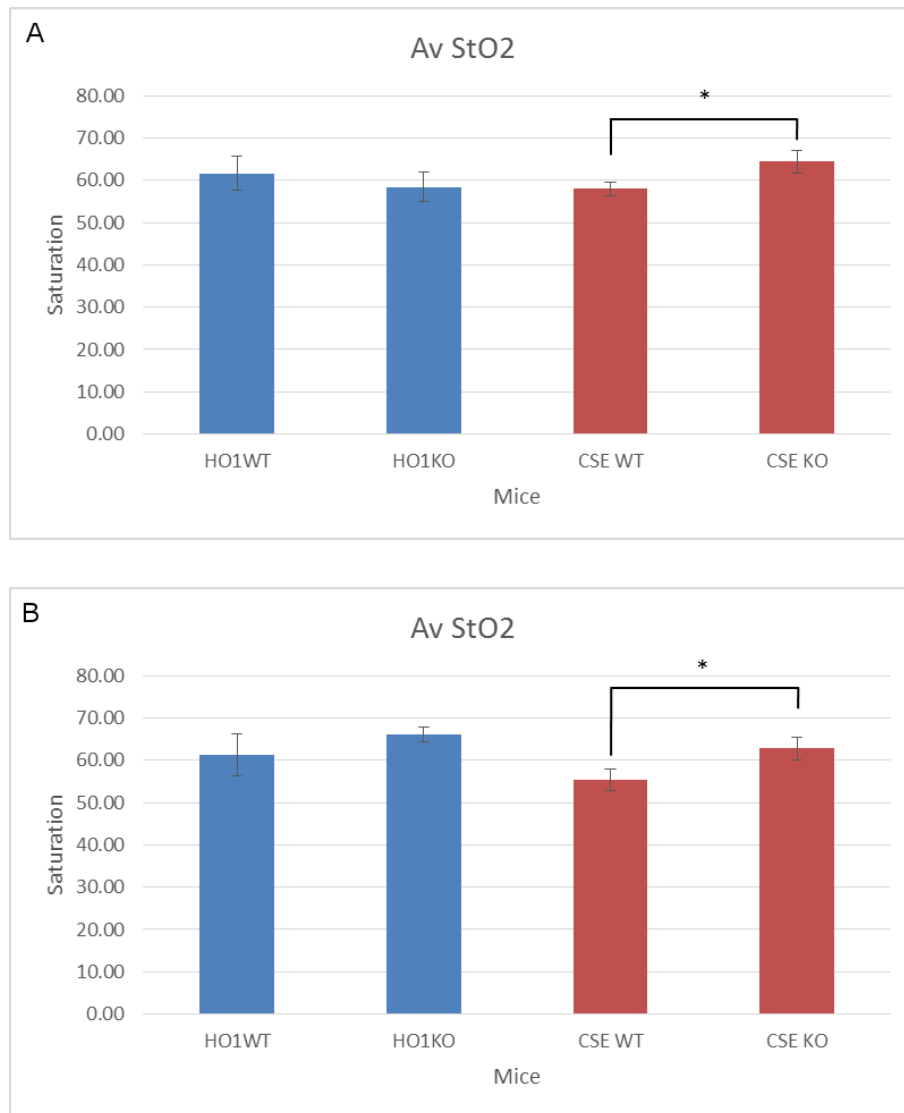


Figure 6.3 Comparison of the StO₂ values between HO1 WT and KO mice as well as CSE WT and KO mice on day 1 (A) and day 2 (B).
 * Significant difference ($p < 0.05$) between the CSE WT and CSE KO, calculated using a t-test.

As seen from the above images, measurement of microcirculatory parameters on animals yields viable results, which can be used to compare mice with knockout-induced deficiencies. The appearance of changes upon day two (as can be easily observed in Figure 6.2) may stem from the knockout induced altered physiological function. Further to the microcirculatory parameters, Figure 6.4 displays the calculated redox ratio comparisons for the various animal groups over the course of two days.

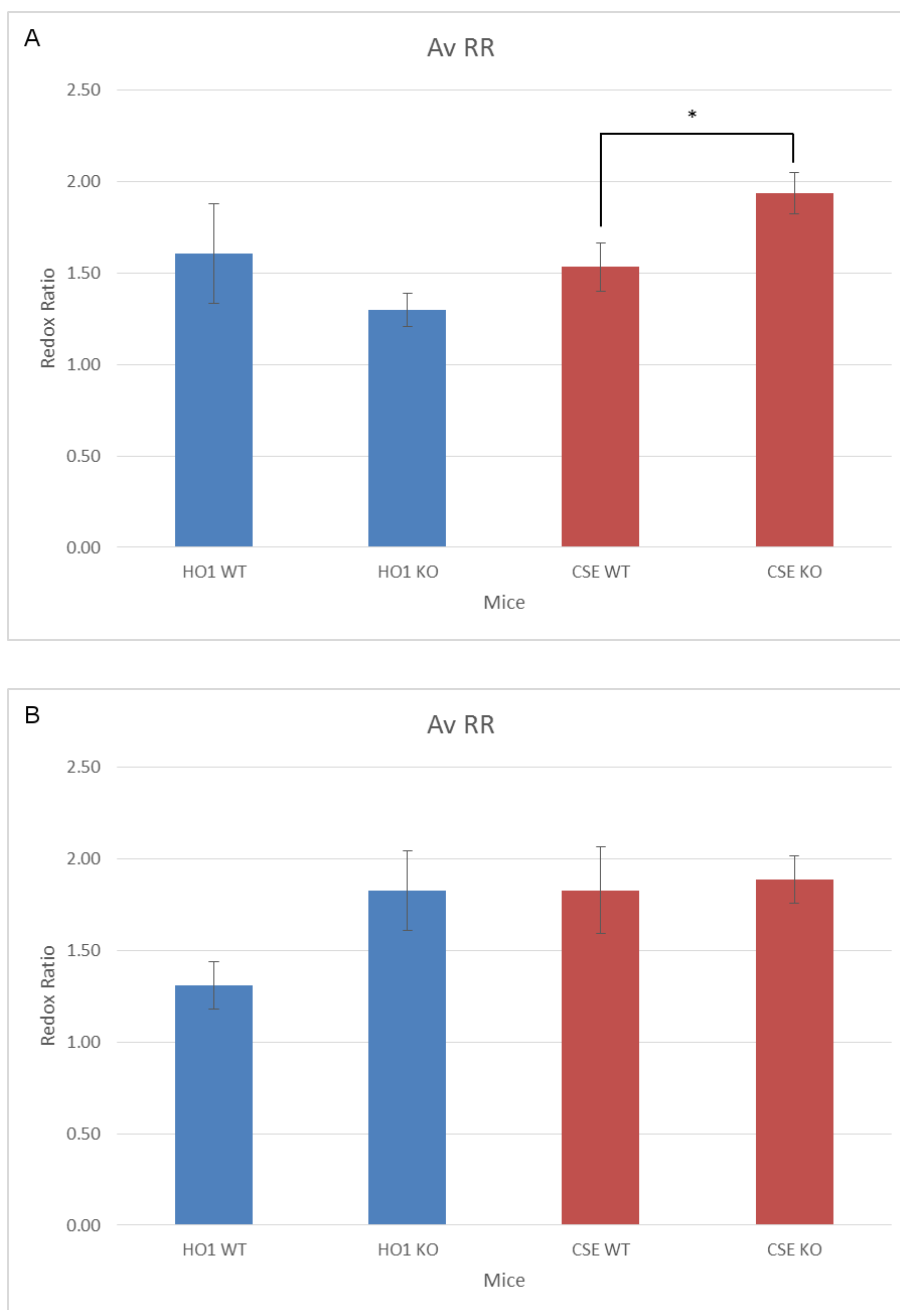


Figure 6.4 Comparison of the RR values between HO1 WT and KO mice as well as CSE WT and KO mice on day 1 (A) and day 2 (B). It should be noted that while not statistically significant, there is an observable tendency towards significance between the HO1 WT and KO mice observable on the second day.

* Significant difference ($p < 0.05$) between the CSE WT and CSE KO, calculated using a t-test.

The autofluorescence data recorded from metabolic cofactors NADH and FAD provides further viability in employing this form of diagnostic technique on animals. The results demonstrated above indicate that the methodology employed has a great potential in distinguishing between animal disease models. This initial validation is crucially important as it provides a support basis for utilising a human-based tool on animals.

In light of the successful implementation of the device on simple animal models, the work was further expanded into a complete experiment. Due to the effective diagnostics potential of the device to deficiencies affecting cardiac function, pre-eclampsia was selected as a suitable target for diagnosis in an established mouse model.

6.2 Application in Pre-eclampsia

6.2.1 Introduction to Pre-eclampsia

Pre-eclampsia is a condition affecting pregnant women worldwide, responsible for one of the major causes of preterm births, as well as perinatal and maternal morbidity. Typically, 3% to 7% of nullipara pregnancies exhibit this condition in the western world. This number drops to 1% to 3% for multiparas. Despite this, different locations with ethnic and social characteristic variations may exhibit up to three times the incidence rate (Noris et al. 2005; Uzan et al. 2011).

The disease is a multifactorial hypertensive condition, thus leading to a large body of work conducted to elucidate the risk factors. However, this is complicated by the fact that presence of risk factors does not necessarily go on to develop the condition. The individuals, who do develop the condition, tend to have it manifest around 20 weeks into pregnancy, with the onset of hypertension and proteinuria. As it stands, however, the pathophysiology of pre-eclampsia is still poorly explained and there is no gold standard for treatment, with the best-known therapy coming in the form of active childbirth (Noris et al. 2005; Bidwell & George 2014).

While pre-eclampsia is still poorly understood, our knowledge on the disease is expanding. To better understand the condition, it is important to know the role of nitric oxide (NO) in normal pregnancy. Its function as a vasodilator of the maternal circulation system and role in increasing foetoplacental and uterine blood flow ensures an adequate and healthy childbirth (Sladek et al. 1997). However, disruption of processes such as endothelial homeostasis (Roberts 1998), oxidative stress (Rodgers et al. 1988) and a loss of vascular endothelial growth factor (VEGF) activity (Ahmed & Cudmore 2009; Maynard, Karumanchi & Ananth. 2011; Powe et al. 2011) all present themselves as key contributors to preeclampsia.

Considering the above, pre-eclampsia remains incredibly difficult to predict or prevent. Due to the mechanisms undertaken by the organism in the presence of pathology, however, pre-eclampsia presents itself as a condition susceptible to non-invasive monitoring. Furthermore, the ability to monitor such a condition using photonics-based diagnostics techniques has the potential to develop earlier diagnosis. In order to observe the effectiveness of any such diagnostic ability, work must be conducted on an effective model of the disease.

Currently, one particular model of interest for pre-eclampsia is based on the function of soluble fms-like tyrosine kinase-1 (sFlt-1). The molecule sFlt-1 is an endogenous antagonist of

VEGF as well as placental growth factor (PlGF). It acts in an anti-angiogenic capacity. During disease progression, this molecule is observed to be produced in larger volumes from the placenta prior to development of the disease (Bidwell & George 2014; Powe et al. 2011; Wang, Ahmad, Cai, Rennie, Fujisawa, F Crispi, et al. 2013). Thus, upregulation of sFlt-1 in rodents can lead to symptoms similar to that of pre-eclampsia (Bergmann et al. 2010).

Basing on the success of the LAKK-M (SPE LAZMA Ltd.) to observe changes within mouse models of CVD, this section outlines the application of the multifunctional non-invasive diagnostics device in monitoring the microcirculatory conditions, as well as fluorescence levels of endogenous biomarkers in an animal model of pre-eclampsia. The selected model utilised adenoviral (Ad-) mediated overexpression of sFlt-1 (Ad-sFlt-1) to closely mimic symptoms often observed in pre-eclampsia. The ultimate goal was to determine the capacity of photonics based diagnostics technologies to detect and successfully monitor hypertensive conditions such as pre-eclampsia.

6.2.2 Methods and materials

6.2.2.1 Animals

The experiment required the use of live animals exhibiting symptoms observable in pre-eclampsia. As such, all procedures were conducted with the approval of the Aston University Ethical Review Committee, in accordance with the United Kingdom Animals (Scientific Procedures) Act 1986.

The study employed 12 female wild-type (WT) C57/black mice. The animals were grown at Aston University, housed in cages and supplied with unrestricted food and water. Each animal was between the ages of 12 – 14 weeks and were not pregnant. A 12 hour light/dark cycle was maintained in an air-conditioned (20-25°C) environment.

6.2.2.2 Experimental design

The 12 animals used in this experiment were divided into two major groups, in line with the conditions of the experiment. The first group (referred to as the Gas group) included six animals which were monitored under isoflurane gas anaesthesia. The second group (referred to as the No-Gas group) consisted of the remaining six animals and did not undergo anaesthesia prior to monitoring. Within both of these groups, half the animals were selected as controls and were injected with empty adenovector containing a CMV promoter (Ad-CMV). The remaining three animals in each group were injected with adenoviral sFlt-1 (Ad-sFlt-1). As there is no easily identifiable visible phenotype, viral expression was ensured with the aid of the collaborating group by Western Blotting

and ELISA analysis according to procedures described in Bergmann et al. (2010) and Mayer et al. (2005). A visual explanation of the experimental groups is presented in Figure 6.5.

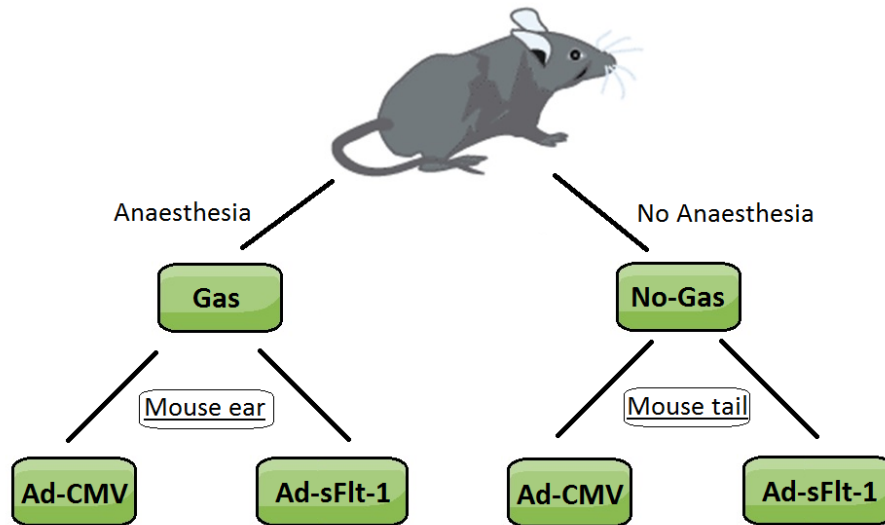


Figure 6.5 Visual explanation of the four groups used in this experiment.

The LAKK-M device was used in this study. Setup of the device was conducted in accordance to the methodology described in chapter 4. Only the LDF, TRO and the UV (365 nm) and blue (450 nm) fluorescence channels were employed to measure animal parameters.

The Gas group animals were placed on a non-heated pad, with microcirculatory and fluorescence parameter data recorded from the ear of the animals. To reduce recording noise and error arising from excessive movement, unanaesthetised animals of the No-Gas group had to be contained in a mouse restraint tube. Recordings were taken from the tails of these animals due to the restraint tube restricting access to the ears. To ensure minimal movement, the tail tips were extended and lightly held down for the duration of the recordings. Figure 6.6 displays the overall layout of the experimental procedure, with data recorded from an unanaesthetised mouse. It should be noted that black covering was placed under the mouse tails to reduce potential unwanted fluorescence signals.



Figure 6.6 Data recording from tail of unanaesthetised mouse of the No-Gas group.

An initial set of measurements was taken from all animals, prior to the injection of control vector Ad-CMV and the Ad-sFlt-1. Such data will further be labelled as “Pre”. Data was recorded again after a period of five days, which will from this point, be referred to as “Post”. Each microcirculatory measurement using LDF and TRO methodologies was done for 20-30 seconds. Fluorescence measurements were recorded for 5-10 seconds per excitation wavelength.

6.2.2.3 Statistical analysis

All data presented below are means \pm SEM. When the data was normally distributed (checked using the Shapiro-Wilk test for a p value of 0.01), group comparisons were conducted using a parametric unpaired t-test. All data was analysed and graphed in OriginPro 9.0 (OriginLab).

A priori calculation of sample size was also conducted, despite having a limited access to animals. The calculation was carried out for a power of 0.8 and a medium effect size of 0.5. Recommended sample size per group was 64 animals.

6.2.2.4 Calculated parameters

After obtaining the initial data sets and conduction of statistical analysis, further parameters were calculated. Comparison of the data was done through normalised parameters. The index of oxygen saturation to perfusion of microvascular blood flow (S_m) was calculated by normalising the obtained saturation (S_tO_2) values to the perfusion (I_m) values, shown in the equation below:

$$S_m = \frac{S_tO_2}{I_m} \quad (6.1)$$

Fluorescence data was used for the calculation of the basic redox ratio (RR) following the methodology already mentioned in chapter 1 (repeated for convenience in equation 6.2).

$$RR = \frac{k_{NADH}}{k_{FAD}} \quad (6.2)$$

Finally, the metabolic parameter described by the RR was normalised to the perfusion (I_m) in a combined parameter for metabolic rate (MR) using the following equation:

$$MR = \frac{RR}{I_m} \quad (6.3)$$

All the parameters were calculated and presented as means \pm SEM, in a similar manner to measured parameters.

6.2.3 Results

6.2.3.1 Measured parameters

Table 6.1 below displays the averages of measured parameters of perfusion and saturation for each of the measured animal groups (Litvinova et al. 2016).

Table 6.1 Averages of measured microcirculatory parameters

Mice		I_m Av \pm SEM		$S_tO_2 \pm$ SEM	
Group n = 3		Pre	Post	Pre	Post
Gas	Control	18.09 \pm 1.55	18.02 \pm 2.86	58.32 \pm 5.44	64.52 \pm 12.33
	sFlt	18.06 \pm 0.89	13.67 \pm 0.15* [§]	63.42 \pm 4.43	58.80 \pm 13.98*
No-Gas	Control	12.39 \pm 2.91	14.75 \pm 1.10	67.76 \pm 5.28	57.64 \pm 7.18
	sFlt	12.02 \pm 2.44	16.66 \pm 1.92*	66.68 \pm 2.16	57.28 \pm 4.51

* Significant difference ($p < 0.05$) Pre vs. Post groups, calculated using a t-test.
[§] Significant difference ($p < 0.05$) Post-Control vs. Post-sFlt, calculated using a t-test.

Figures 6.7 and 6.8 are a visual representation of this data for I_m and S_tO_2 respectively. The significant differences are presented.

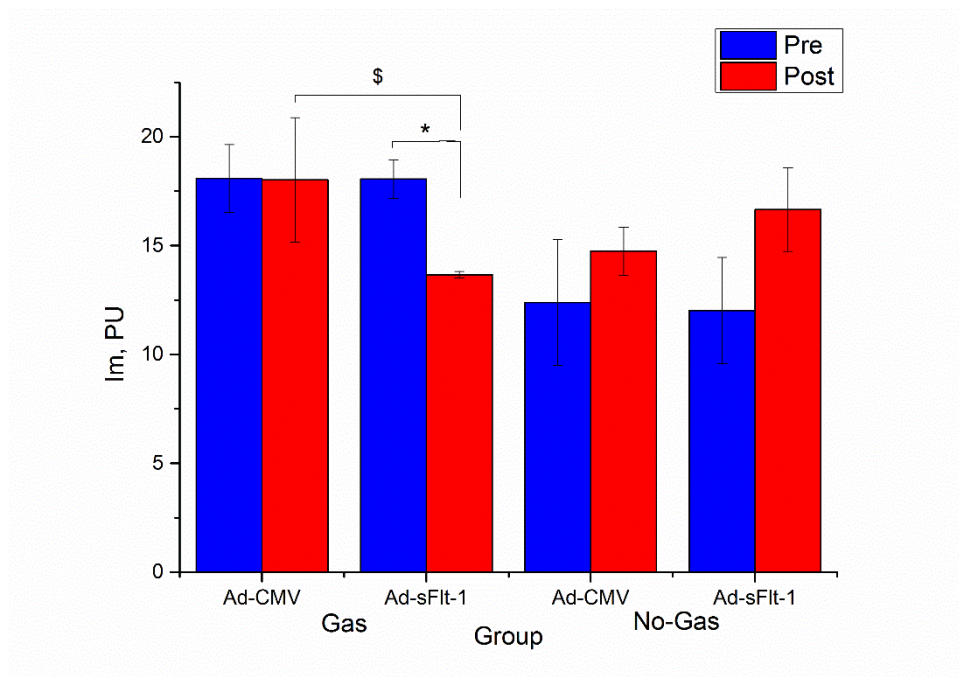


Figure 6.7 Comparison of the I_m values in the Gas and No-Gas groups, at the Pre and five days Post injection of CMV control and Ad-sFlt-1.

* Significant difference ($p < 0.05$) between the Pre vs. Post Ad-sFlt-1 group in the Gas set of animals, calculated using a t-test.

§ Significant difference ($p < 0.05$) between the Pre-Control vs. Pre-sFlt groups in the Gas set of animals, calculated using a t-test.

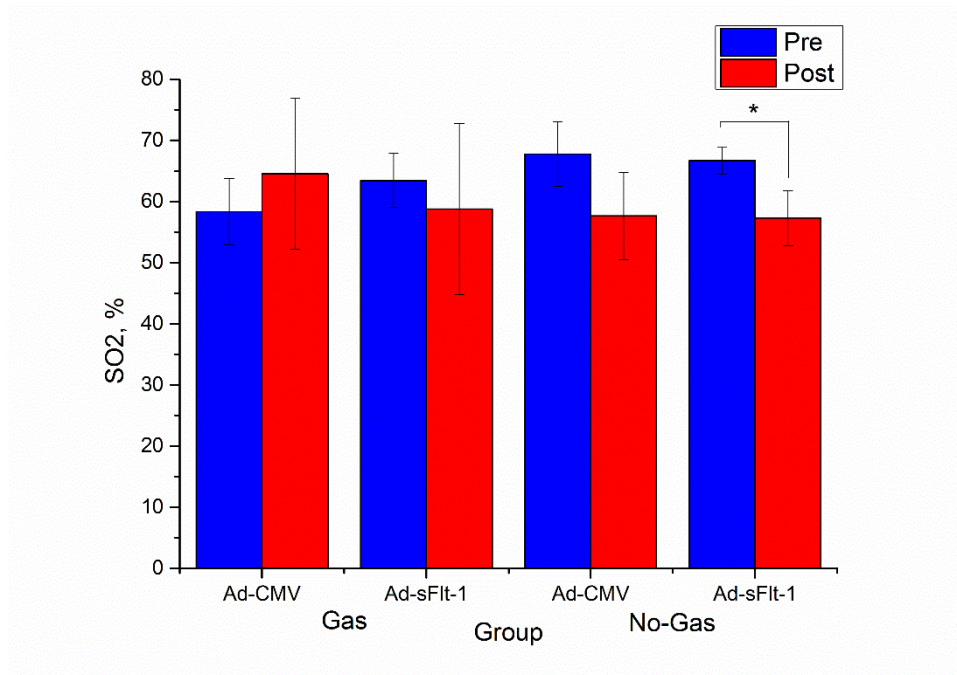


Figure 6.8 Comparison of the StO₂ values in the Gas and No-Gas groups, at the Pre and five days Post injection of CMV control and Ad-sFlt-1.

* Significant difference ($p < 0.05$) between the Pre vs. Post Ad-sFlt-1 group in the No-Gas set of animals, calculated using a t-test.

Table 6.2 displays the averages of measured fluorescence coefficient values for each of the measured animal groups (Litvinova et al. 2016).

Table 6.2 Averages of measured metabolic parameters

Mice		$k_{\text{NADH}} \pm \text{SEM}$		$k_{\text{FAD}} \pm \text{SEM}$	
Group n = 3		Pre	Post	Pre	Post
Gas	Control	1.49 ± 0.25	0.89 ± 0.11	0.53 ± 0.06	0.63 ± 0.26
	sFlt	1.06 ± 0.14	0.43 ± 0.05	0.29 ± 0.04	0.69 ± 0.06
No-Gas	Control	0.97 ± 0.06	0.91 ± 0.04	0.61 ± 0.10	0.49 ± 0.09
	sFlt	0.93 ± 0.08	0.92 ± 0.01	0.43 ± 0.02	0.49 ± 0.03

6.2.3.2 Calculated parameters

Upon registration of the microcirculatory and metabolic parameters, values were normalised using the equations described in part 6.2.2.4. This process was conducted for each animal, with the averages presented in table 6.3.

Table 6.3 Averages of calculated parameters

Mice		$S_m \pm SEM$		$RR \pm SEM$		$MR \pm SEM$	
Group n = 3		Pre	Post	Pre	Post	Pre	Post
Gas	Control	3.31±0.53	3.54±0.12	2.89±0.97	1.76±0.43	0.16±0.04	0.11±0.04
	sFlt	3.51±0.20	4.30±1.03	3.83±0.87	0.61±0.03* [§]	0.21±0.04	0.04±0.00* [§]
No-Gas	Control	6.17±1.53	4.19±0.57	1.70±0.35	2.00±0.37	0.15±0.03	0.14±0.03
	sFlt	6.00±1.13	3.98±0.63*	2.17±0.08	1.89±0.15	0.19±0.03	0.11±0.00* [§]

* Significant difference ($p < 0.05$) Pre vs. Post groups, calculated using a t-test.
[§] Significant difference ($p < 0.05$) Post-Control vs. Post-sFlt, calculated using a t-test.

A visual representation of the S_m , RR and MR parameters are depicted in Figures 6.9, 6.10 and 6.11 respectively. Significance is indicated (Litvinova et al. 2016).

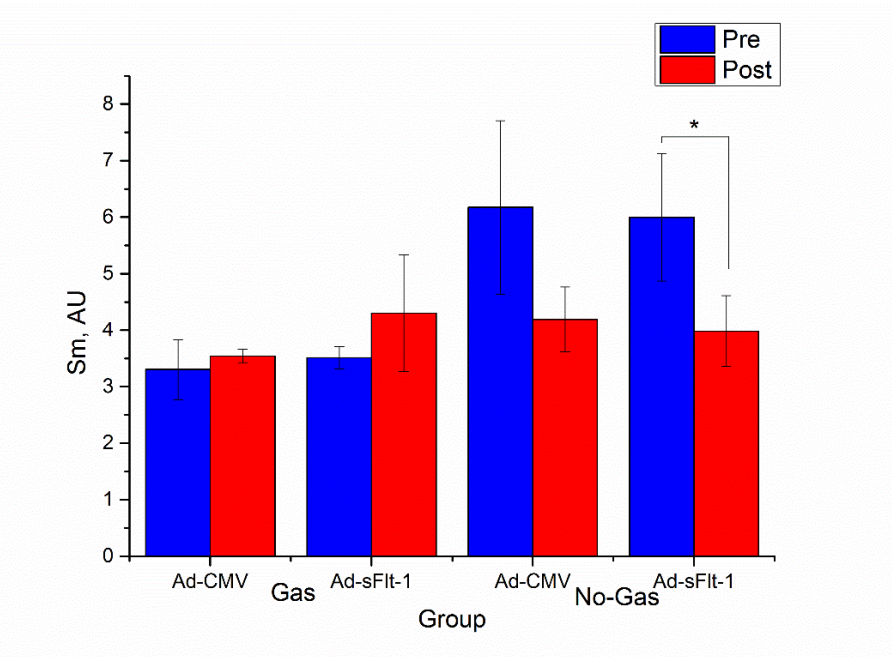


Figure 6.9 Comparison of the S_m values in the Gas and No-Gas groups, at the Pre and five days Post injection of CMV control and Ad-sFlt-1.

* Significant difference ($p < 0.05$) between the Pre vs. Post Ad-sFlt-1 group in the No-Gas set of animals, calculated using a t-test.

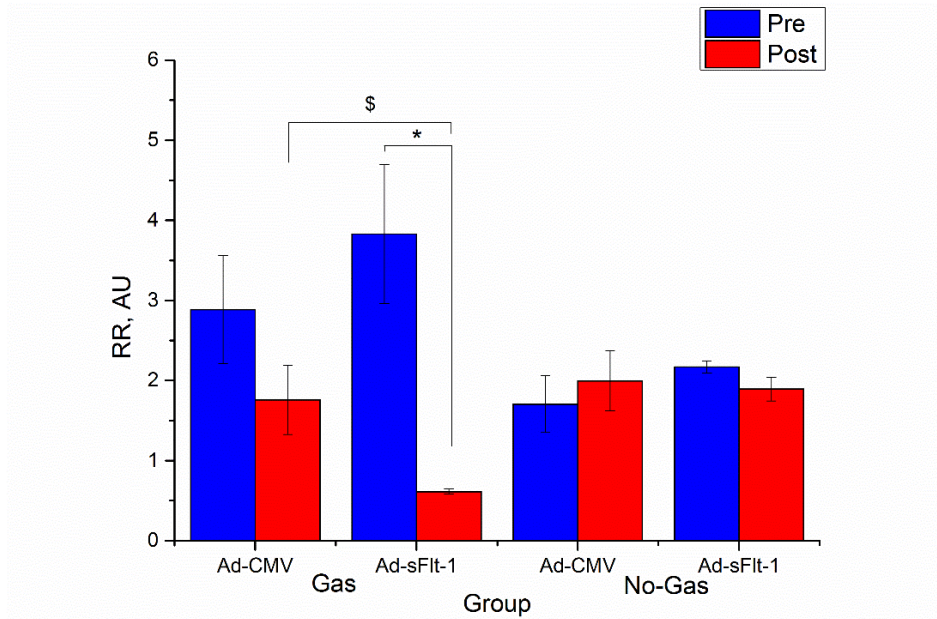


Figure 6.10 Comparison of the RR values in the Gas and No-Gas groups, at the Pre and five days Post injection of CMV control and Ad-sFlt-1.

* Significant difference ($p < 0.05$) between the Pre vs. Post Ad-sFlt-1 group in the Gas set of animals, calculated using a t-test.

\$ Significant difference ($p < 0.05$) between the Pre-Control vs. Pre-sFlt groups in the Gas set of animals, calculated using a t-test.

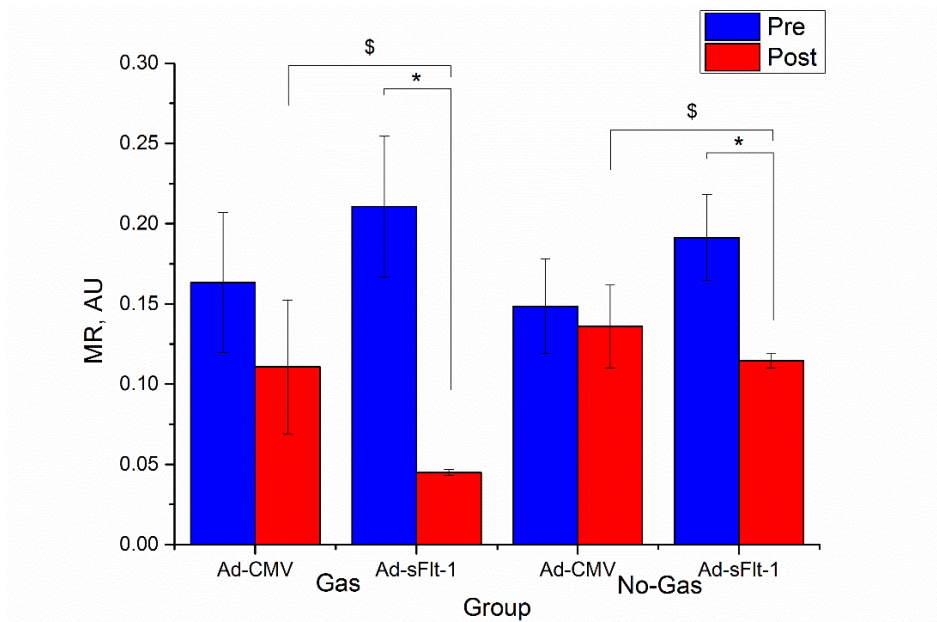


Figure 6.11 Comparison of the MR values in the Gas and No-Gas groups, at the Pre and five days Post injection of CMV control and Ad-sFlt-1.

* Significant difference ($p < 0.05$) between the Pre vs. Post Ad-sFlt-1 groups, calculated using a t-test.

\$ Significant difference ($p < 0.05$) between the Pre-Control vs. Pre-sFlt groups, calculated using a t-test.

6.2.4 Discussion

When assessing the parameters calculated in the above experiment, the authors avoided conducting comparisons of animals between the Gas and No-Gas groups. This was done because any potential outcomes would be the result of multiple variables and would not provide a clear conclusion. The conditions at which the animals were measured would account for many potential differences in recorded values. For example, the metabolic function of animals under anaesthesia is altered, affecting the measured NADH and FAD values. Due to the limited possible output data from such comparisons, the groups were analysed separately with the intention of determining the sensitivity of tested measurement parameters on different conditions.

After initial examination of the parameters obtained from photonics based monitoring of the experimental animals, significant differences in blood perfusion were observed only in the Gas group (Figure 6.7). This involved differences between Ad-sFlt-1 animals pre- and post- injection of the virus, as well as differences between control and virus-injected animals five days after injections. The No-Gas group showed no such differences. It did, however, display significant differences in S_tO_2 between pre- and post- Ad-sFlt-1 animals (Figure 6.8). The lack of significance in S_tO_2 measurements within the Gas group could be explained by the presence of anaesthesia, which suppressed the signal of blood oxygen saturation. It should also be noted that, as expected, Ad-CMV did not elicit any visible changes over the course of the five-day incubation.

To improve the analysis and derive more value from the measured parameters, further normalisation of these parameters was required. This is especially important considering the slight variations in the experimental approach used on animals of the Gas and No-Gas groups. The first parameter of interest was S_m – the index of oxygen saturation to perfusion of microvascular blood flow. As is evident from Figure 6.9, animals of the Gas group did not display any visible difference. Due to the heavy reliance on the S_tO_2 for the calculation of S_m , a similar observable pre- and post-injection difference is present in the Ad-sFlt-1 treated mice of the No-Gas group. While this, in itself is a similar result, it is vital to employ the S_m parameter for a viable comparison of both the Gas and No-Gas group results. The normalisation of oxygen saturation to the perfusion in a measured volume of blood allows for measurements from the tail to be compared to those taken from the ear.

Upon calculation of the redox ratio parameter, significant differences are evident in the Gas group (Figure 6.10). This includes differences between pre- and post- virus injected animals as well as between control and virus animals five days after injection. One possible reason for such differences may be a critical disturbance of cellular metabolism as a result of injected Ad-sFlt-1 action. Similar significant differences were not observed within the No-Gas group, however. Potentially, this may be the result of measurement variation arising from altered experimental approaches undertaken on the two groups. A certain level of error could exist due to the interaction of the monitoring probe with the animal tails. While measurements from the ear (as done for the Gas

group) allow for complete contact with the relatively flat tissue, complete contact with the tail of the animals from the No-Gas group was not always possible due to the round shape of the extremity. Such an issue may be circumvented in the future by using optical probes with a smaller diameter.

The most interesting parameter, relating the metabolic parameters to the microcirculatory parameters, was the metabolic rate (Figure 6.11). Much like with the redox ratio, the Gas group displays visible significant differences between pre- and post- virus injected animals as well as between Ad-CMV and Ad-sFlt-1 animals, post-injection. Importantly, however, these differences are simultaneously observable for the No-Gas group. As such, MR presents itself as the most informative parameter that relies both on the measurements of blood microcirculation as well as metabolic activity in the form of the redox ratio. The parameter provides a capacity for comparison of various tissue types, while also allowing for leeway in the conditions of studied organisms. The reliance on both metabolic and microcirculatory factors for the determination of MR also means measurements on animals with signal suppressing factors such as anaesthesia are still able to provide useful data.

Despite the promising results, it is important to take into account the relatively low number of animals involved in the study. While the approaches described above seem to be viable, the quantity of studied animals will need to be increased to match the calculated sample size in order to fully confirm the effectiveness of the techniques.

6.2.5 Conclusion

Ultimately, the work described above demonstrates the ability of photonics-based technologies such as the LAKK-M to carry out real-time monitoring of vital parameters on animals under a variety of different conditions. The methods described outline the acquisition of a number of key physiological characteristics (I_m , S_tO_2 , NADH and FAD fluorescence) and their use in calculation of informative parameters (S_m , RR and MR). With the use of such parameters, above is displayed a method for monitoring the changes induced through the injection of Ad-sFlt-1 into mice. Injection of Ad-CMV is also observed to have no effect on the status of the animals, further validating the analytical approach. It is also important to note that application of complex parameters such as MR also allows for measurement flexibility, as evident from the presence of observable differences in both anaesthetised and unanaesthetised animals.

Despite the minor difficulties, which arose from a number of fluorescence measurements on the mouse tails, the work above is the first step towards improved monitoring and detection. Further study of pre-eclampsia symptoms in larger quantities of mice are required to fully realise the potential available with the described for of diagnostics. Additionally, while the most immediate step forward would be to increase the number of tested animals, employing pregnant transgenic rodents would further improve the capacity for the above methodology to distinguish presence of pre-eclampsia

symptoms. The methodology can also be expanded to other disease models, and ultimately lead to novel and effective new ways of detecting various diseases.

References

- Ahmed, A. & Cudmore, M.J., 2009. Can the biology of VEGF and haem oxygenases help solve pre-eclampsia? *Biochemical Society Transactions*, 37(6), pp.1237–1242. Available at: <http://biochemsoctrans.org/lookup/doi/10.1042/BST0371237>.
- Bergmann, A. et al., 2010. Reduction of circulating soluble Flt-1 alleviates preeclampsia-like symptoms in a mouse model. *Journal of Cellular and Molecular Medicine*, 14(6 B), pp.1857–1867.
- Bidwell, G.L. & George, E.M., 2014. Maternally sequestered therapeutic polypeptides - A new approach for the management of preeclampsia. *Frontiers in Pharmacology*, 5 AUG(September), pp.1–9.
- Fraser, S.T. et al., 2011. Heme oxygenase-1: A critical link between iron metabolism, erythropoiesis, and development. *Advances in Hematology*, 2011(Figure 1).
- Litvinova, K.S. et al., 2016. A pilot study using laser-based technique for non-invasive diagnostics of hypertensive conditions in mice. *SPIE proceedings*, 9689(0), p.96893H. Available at: <http://proceedings.spiedigitallibrary.org/proceeding.aspx?doi=10.1117/12.2213026>.
- Mayer, H. et al., 2005. Vascular endothelial growth factor (VEGF-A) expression in human mesenchymal stem cells: Autocrine and paracrine role on osteoblastic and endothelial differentiation. *Journal of Cellular Biochemistry*, 95(4), pp.827–839.
- Maynard, Karumanchi & Ananth., 2011. Angiogenic factors and preeclampsia. *Seminars in nephrology*, 31(1), pp.33–46.
- Noris, M., Perico, N. & Remuzzi, G., 2005. Mechanisms of Disease: pre-eclampsia. *Nature Clinical Practice Nephrology*, 1(2), pp.98–114.
- Pan, L.L. et al., 2012. Role of Cystathionine γ -Lyase/Hydrogen Sulfide Pathway in Cardiovascular Disease: A Novel Therapeutic Strategy? *Antioxidants & Redox Signaling*, 17(1), pp.106–118. Available at: <http://online.liebertpub.com/doi/abs/10.1089/ars.2011.4349>.
- Powe, C.E., Levine, R.J. & Karumanchi, S.A., 2011. Preeclampsia, a Disease of the Maternal Endothelium: The Role of Antiangiogenic Factors and Implications for Later Cardiovascular Disease. *Circulation*, 123(24), pp.2856–2869.
- Roberts, J.M., 1998. Endothelial dysfunction in preeclampsia. *Seminars in reproductive endocrinology*, 16(1), pp.5–15.
- Rodgers, G.M., Taylor, R.N. & Roberts, J.M., 1988. Preeclampsia is associated with a serum factor cytotoxic to human endothelial cells. *American journal of obstetrics and gynecology*, 159(4), pp.908–914.
- Sladek, S.M., Magness, R.R. & Conrad, K.P., 1997. Nitric oxide and pregnancy. *The American journal of physiology*, 272(2 Pt 2), pp.R441-63.
- Uzan, J. et al., 2011. Pre-eclampsia: Pathophysiology, diagnosis, and management. *Vascular Health and Risk Management*, 7(1), pp.467–474.
- Wang, K., Ahmad, S., Cai, M., Rennie, J., Fujisawa, T., Crispi, F., et al., 2013. Dysregulation of hydrogen sulfide producing enzyme cystathionine γ -lyase contributes to maternal hypertension and placental abnormalities in preeclampsia. *Circulation*, 127(25), pp.2514–2522.
- Wang, K., Ahmad, S., Cai, M., Rennie, J., Fujisawa, T., Crispi, F., et al., 2013. Dysregulation of hydrogen sulfide producing enzyme cystathionine γ -lyase contributes to maternal hypertension and placental abnormalities in preeclampsia. *Circulation*, 127(25), pp.2514–22. Available at: <http://www.ncbi.nlm.nih.gov/pubmed/23704251>.
- Yang, G. et al., 2008. H₂S as a physiologic vasorelaxant: hypertension in mice with deletion of cystathionine gamma-lyase. *Science (New York, N.Y.)*, 322(5901), pp.587–590.

Chapter 7 : Application in non-disease monitoring

7.1 Lighting effects on biological function

7.1.1 Introduction

Almost everyone in the world is affected by either natural or artificial light sources on a daily basis. These sources play a critical role in a number of biological systems vital for continued healthy function, including circadian, neurobehavioural and neuroendocrine responses (An et al. 2009; Turner et al. 2010; Vandewalle et al. 2009). The exposure to different intensities and volumes of light can directly affect organic systems in both positive and negative ways. From the body's master biological clock to vitamin formation and other hormonal interactions, these effects could be minor or result in critical health complications. Nevertheless, such effects tend to develop in the long-term, when conditions are persistent. Relatively short exposures to varying wavelengths of light, however, may affect the heart rate, alertness and psychological condition of individuals exposed to it. As short as 30 minutes of light exposure has been mentioned as a minimum required time for light to affect cognitive function (Vandewalle et al. 2009). There is even evidence to indicate that an individual's creativity could be affected by the light they are exposed to (Weitbrecht et al. 2015). Despite the fact that light emitting devices such as televisions, smart phones, street illumination and ambient lighting are commonplace around the world, the physical and psychological influences of such illumination are only now receiving attention. As such, there is an untapped area of research, focusing on understanding how lights affect the physiology and psychology of humans based on the intensity and wavelength.

This study aimed to measure the effects of varying wavelengths, temperatures and intensities of light upon human volunteers by employing a tuneable multicolour illumination panel. This was done by conducting simultaneous measurements of individuals' microcirculatory parameters (tissue perfusion and oxygenation) and metabolic parameters (fluorescence of NADH and FAD as a marker of metabolic activity), recorded using the MLNDS LAKK-M. Additionally, a cognitive function measurement was recorded using a computer-based visual search reaction-time task. This is a commonly used psychological test (Trick & Enns 1998), which is done to measure the attention (looking at both reaction time and accuracy) of the volunteers.

7.1.2 Methods and materials

7.1.2.1 Ethical approval

This study was reviewed and given favourable opinion by the Aston University's Ethics Committee. Due to the nature of the study, no higher ethical approval was necessary.

7.1.2.2 Experimental equipment setup

The experiment was carried out in a laboratory with no windows, to ensure no extra unwanted light penetrated through to experimental areas. The area of the laboratory was relatively small to ensure illumination from the light panel was sufficient without use of external light sources. The multicolour illumination panel (developed by M-Squared Lasers and OSRAM) employed as the primary source of controllable light is presented in Figure 7.1.

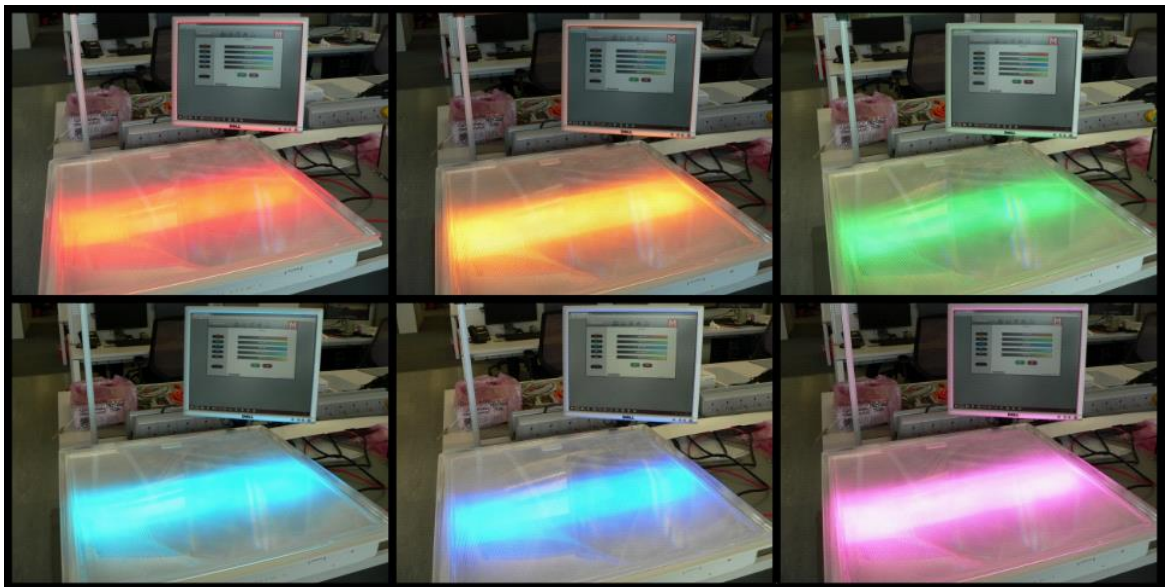


Figure 7.1 Colour-tuneable LED panel developed by M-Squared Lasers and OSRAM. Image displays some of the light wavelengths produced by the panel as well as the control electronics (enabled through ethernet connection).

A table was placed near the illumination source, containing free space, a laptop and the LAKK-M diagnostics device (set up for function and calibrated according to steps described in chapter 4). Laptops were all set to low screen brightness to minimise the effects of their screens on the experimental procedure. Standard room light provided by ceiling mounted fluorescent tube (temperature around 6200K), “cold” light (temperature of 9800K) and “warm” light (temperature of 1820K) were selected as the experimental light sources.

7.1.2.3 Sample size

To test the effects of varying light colour temperature on populations, sample size was calculated for a power of 0.8 and a relatively small effect size of 0.25. Effective sample size was 28 volunteers.

However, due to the potential of practice effects, comparison would also have to be conducted between two sets of volunteers exposed to lights in different order. With a power of 0.8 and a medium effect size of 0.5, each group was calculated to need 64 volunteers.

7.1.2.4 Participants

Overall, 10 volunteers (6 male, 4 female) between the ages of 26 – 57 participated in the study. Selection was done through internal Aston University advertisement and email circulation. Criteria for selection stated that these volunteers must be healthy with no longstanding diagnosed medical conditions (such as heart disease/angina, diabetes, circulatory conditions/diseases and epilepsy/seizures). There was also preference for individuals with no visual impairments, as they could hinder the ability of participants to carry out the computer based visual trial section of the experiment (heavily reliant on differentiating and locating a small coloured shape in a field of distractors).

All volunteers were provided an information sheet briefly detailing the experiment and were asked to sign a consent form (appendix 1a and 1b). They were also informed that they could terminate participation at any time without any consequences or reasons. Should such occur, no data already gathered on the participant would be stored.

Every volunteer that consented to the study was asked to avoid ingestion of caffeinated or alcoholic beverages for at least three hours prior to their allocated session, or during the break within the experiment. Furthermore, they were asked to avoid consumption of food for the duration of the break. Finally, they were asked to avoid altering their daily routine on the day of the experiment (for example cycling to work, if they usually drive or commute).

Finally, volunteers were asked to have reading material such as printed out journal papers of their choice. The reading material was to be employed during the non-testing phases of the experiment, ensuring that volunteers do not sit idly. Once a volunteer signed the consent form and arrived for experimentation, they were introduced to the experiment and had the following methodology described to them.

7.1.2.5 Visual search task

The procedure described in 7.1.2.6 involved the use of a visual search task. This was accomplished with the aid of a free online resource provided by GoCognitive (GoCognitive - Educational tools for cognitive neuroscience 2017). The task involved the participant finding a specific shape (in this case a blue triangle) in a field of distractors (blue squares, red squares and red triangles).

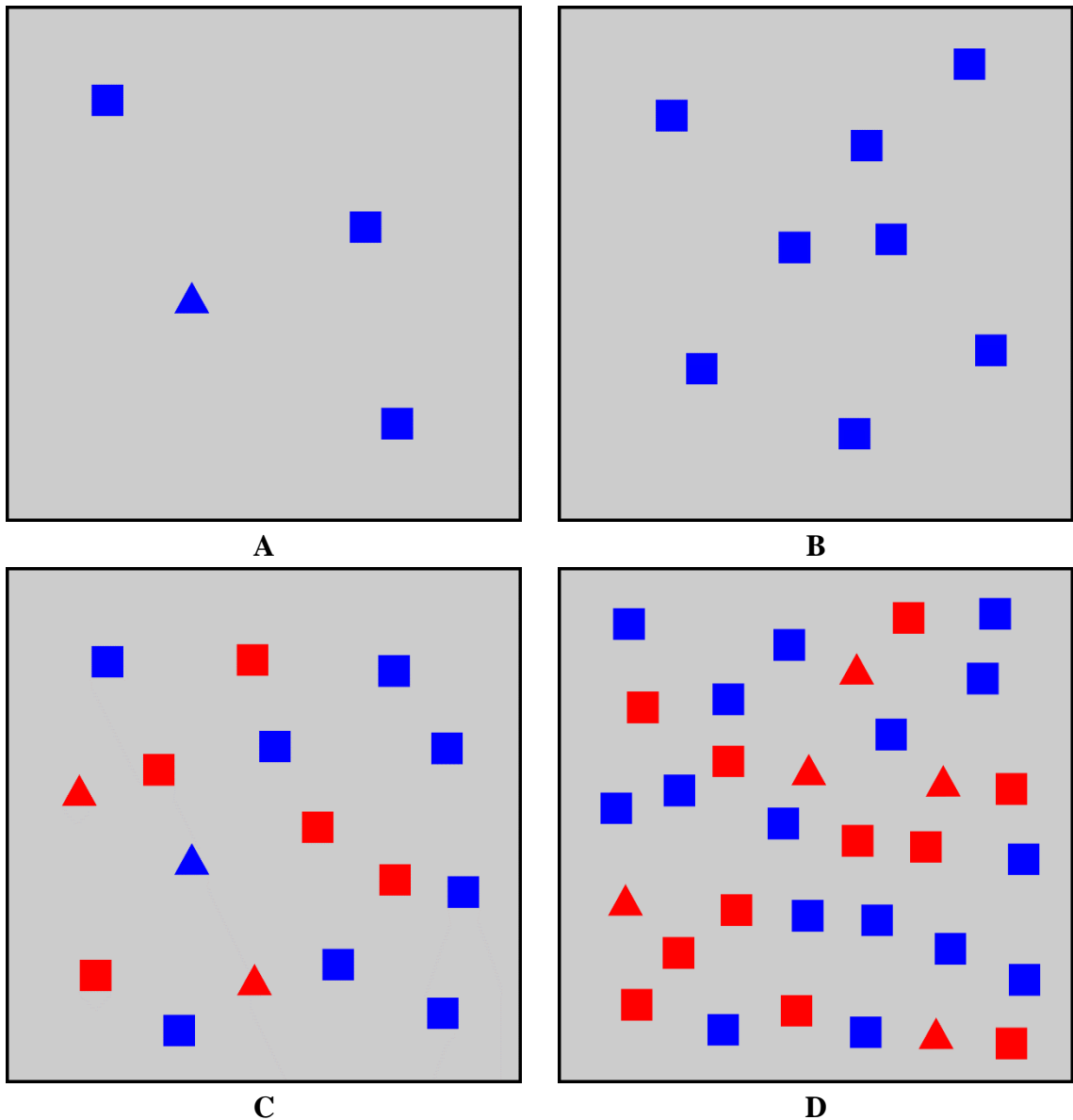


Figure 7.2 Reproduction of the visual search task depicting the various possible paradigms. The blue triangle is the desired target shape in this example. A – The single-search with target fielding 4 shapes. B – The single-search with no target fielding 8 shapes. C – The conjunction-search with target fielding 16 shapes. D – The conjunction-search with no target fielding 32 shapes. Note that the number of shapes was not exclusive to the paradigms above; the presented images are examples.

Four paradigms were employed in the task: single-search with target (target present on a background of same-colour distractors), single-search with no target (no target on a background of same-colour distractors), conjunction-search with target (target present on a background of distractors varying in colour) and conjunction-search with no target (no target on a background of distractors varying in colour). Furthermore, each individual task varied the number of distractors, presenting a total of 4, 8, 16 or 32 shapes to the participant. Examples of the visual search task are reproduced in Figure 7.2.

The procedure was repeated 144 times, alternating the paradigm each time. Ultimately, the data of each individual task was combined into one exportable spreadsheet recording the time taken to provide an answer, the correctness of the answer, the paradigm employed and the number of distractors. Each participant, while not having the same exact trials, had the same number of trials within each individual paradigm.

7.1.2.6 Experimental protocol

At the beginning of the experiment, volunteers underwent perfusion, saturation and autofluorescence measurement by the LAKK-M (following procedures described in chapter 4). This was done under standard illumination by room light. The volunteers were then asked to complete the visual search task as described above. The option to have a short practice with the visual search task was provided for all volunteers.

Upon completion of the tests, the volunteers would be subjected to either warm or cold light (Figure 7.3). This exposure would last for 30 minutes. During this time, volunteers would be encouraged to read the materials they were asked to bring with them. To minimise external light influence on the subjects, volunteers were also encouraged to avoid using their mobile phones. Additionally, laptops within the area of study were closed to prevent screen brightness.

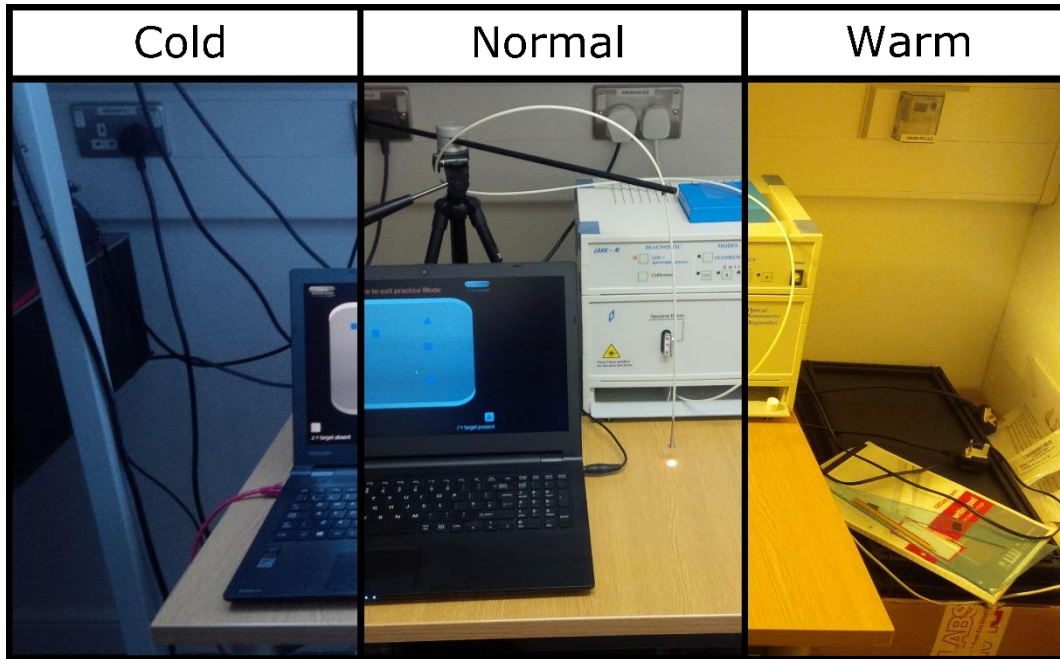


Figure 7.3 Unprocessed photographs of the testing area illuminated by the three tested light settings. Standard room light was categorised as “normal”. Cold light was measured at 9800K. Warm light was measured at 1820K.

When the exposure period was completed, volunteers were once again measured with the LAKK-M for the same parameters and were asked to complete the visual search task again. These measurements were completed while still under illumination by either warm or cold light.

Once the initial light exposure was completed, the volunteers were allowed to take a break. During the space of an hour, the volunteers were to acclimatise back to regular light. As mentioned before, volunteers were asked to avoid ingesting food or any caffeinated or alcoholic beverages. After the hour break, the volunteers returned to the testing room and the experiment was repeated with the opposite light setting (for example if the initial exposure was cold light, volunteers returned and repeated the experiment in warm light). The entire experiment, not accounting for break time, took around 2 hours per participant. It should be noted that the experiments were conducted in the mornings to maintain a schedule. They were finished before regular lunchtime of participants in order to prevent food from having an effect on the measurements.

By the end of the experiment, two groups of participants were created in accordance to the starting light exposure temperature. Seven volunteers were initially subjected to “cold” light, while three volunteers were initially subjected to “warm” light.

7.1.2.7 Data analysis

Analysis of data for the physiological parameters measured by the LAKK-M and the psychological parameters measured by the visual search task were done separately. Analysis of the

physiological parameters was done by calculating the index of oxygen saturation to perfusion of microvascular blood flow, redox ratio and metabolic rate parameters described above in section 6.1.2.4 as well as in Litvinova et al. (2016). Psychological data was presented according reaction times (in ms). The number of errors was used as an indication of attention.

7.1.3 Results

7.1.3.1 Initial “cold” light exposure group

An outlier was discovered in the initial results analysis, calculated as more than 1.5 IQRs (interquartile ranges) below the first quartile or above the third quartile. As such, the data of this volunteer was removed from the following results.

The results for parameter averages recorded under different light colour exposures are presented in Figures 7.4 and 7.5. “Cold” light exposure was first, while “warm” light was used after the hour-long break.

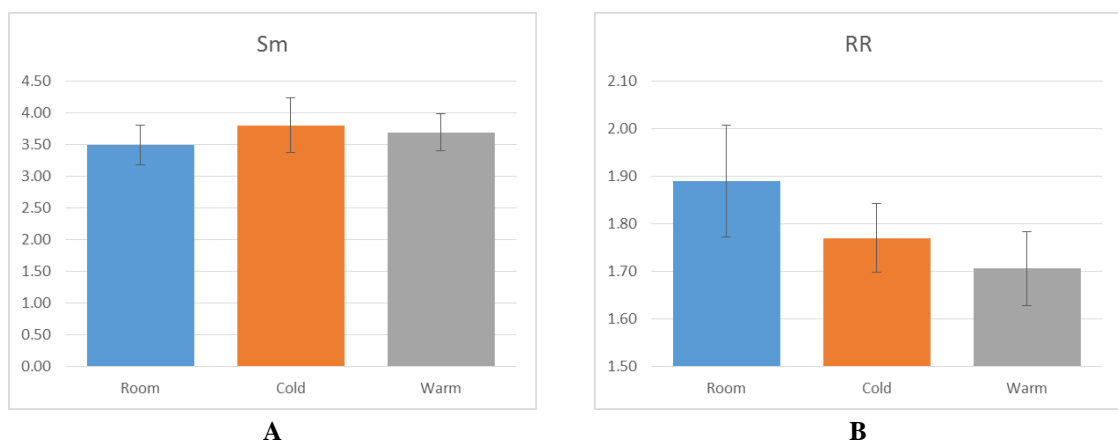


Figure 7.4 The average comparisons of the index of oxygen saturation to perfusion of microvascular blood flow (A) and redox ratio (B) between different light colour temperatures. Initial exposure by “cold” light.

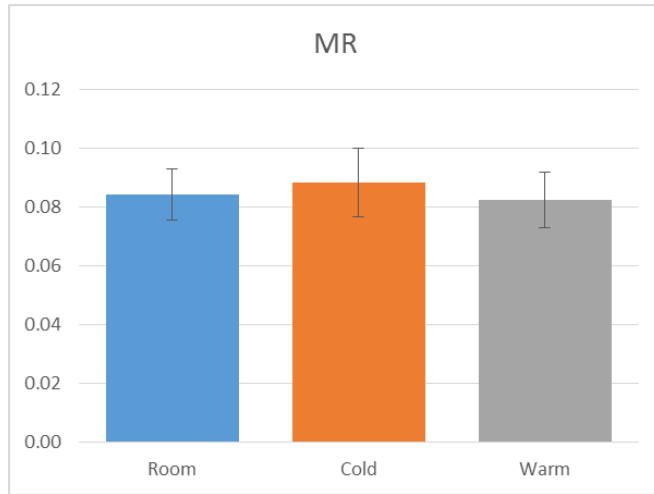
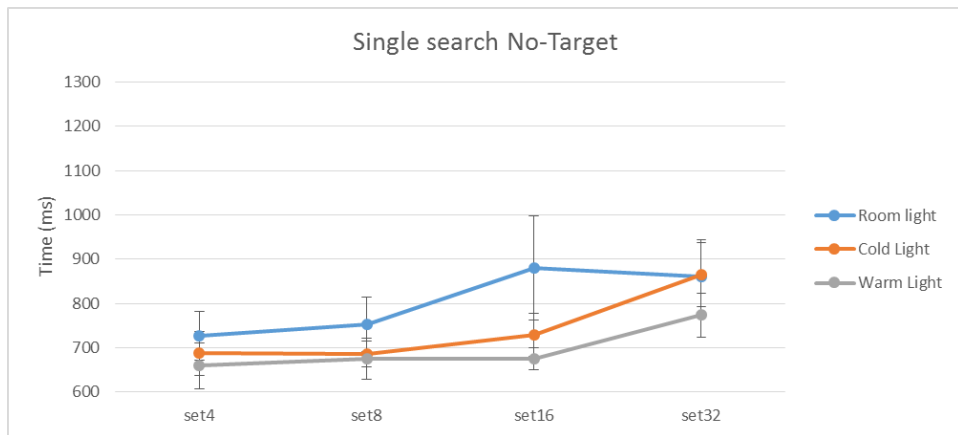


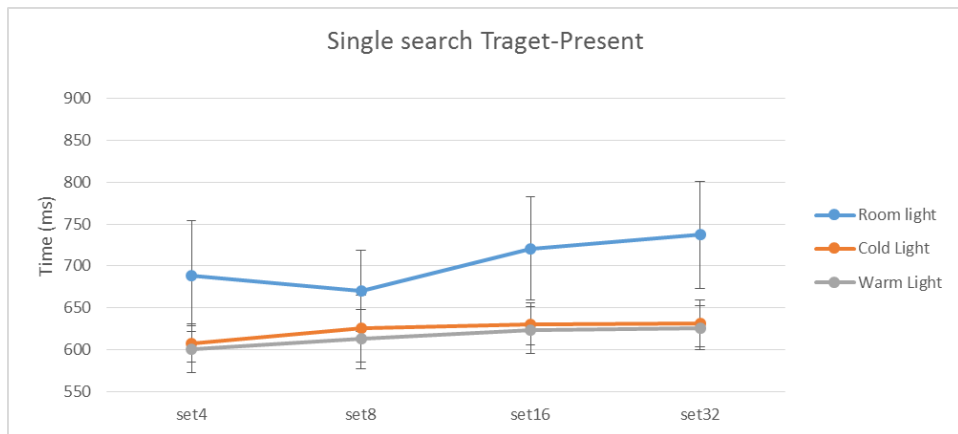
Figure 7.5 The average comparison of the metabolic ratio between different light colour temperatures. Initial exposure by “cold” light.

The times recorded during the visual search task are presented in Figure 7.6. Times taken to provide an answer to “can you see the blue triangle, yes or no?” in a field of distractors are provided for each of the four different paradigms employed by the assessment.

A



B



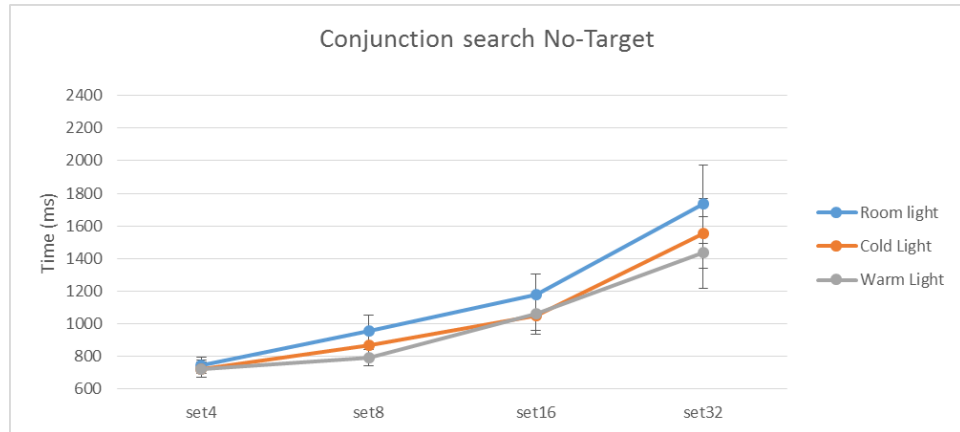
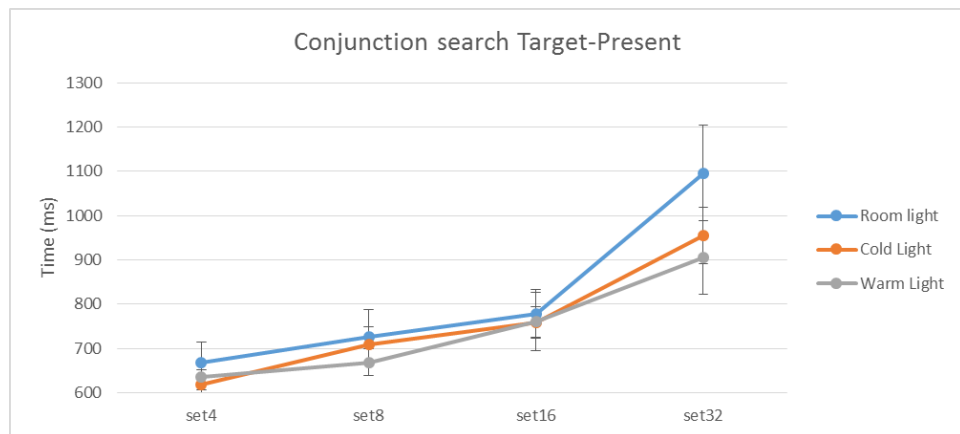
C**D**

Figure 7.6 Results of the visual search task. Initial room light followed by “cold” then “warm” lights. (A) and (B): Field containing distractors of same colour as target shape, no target present and target present respectively. (C) and (D): Field containing distractors of same as well as different colour, no target present and target present respectively.

7.1.3.2 Initial “warm” light exposure group

The results for parameter averages recorded under different light colour exposures are presented in Figures 7.7 and 7.8. “Warm” light exposure was first, while “cold” light was used after the hour-long break.

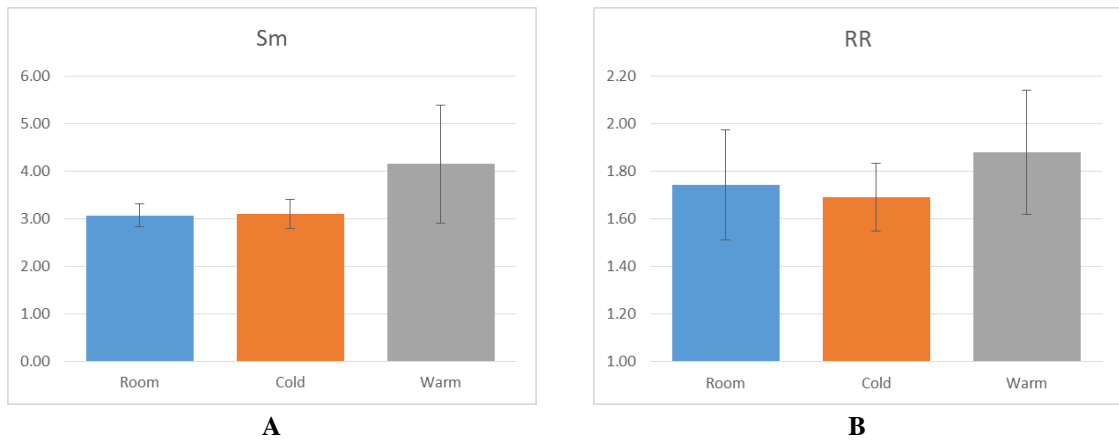


Figure 7.7 The average comparisons of the index of oxygen saturation to perfusion of microvascular blood flow (A) and redox ratio (B) between different light colour temperatures. Initial exposure by “warm” light.

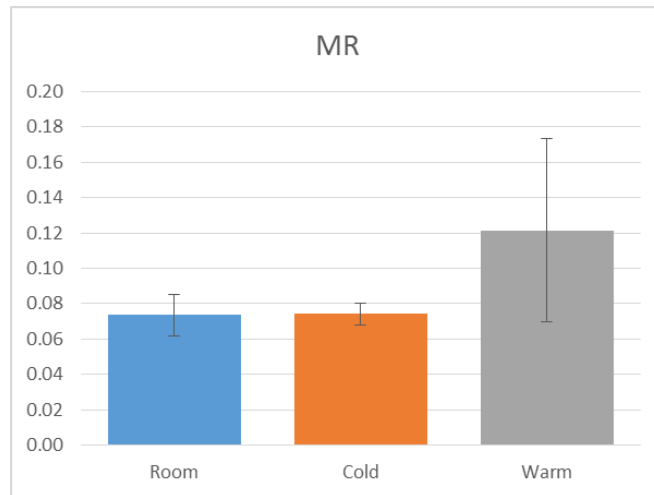
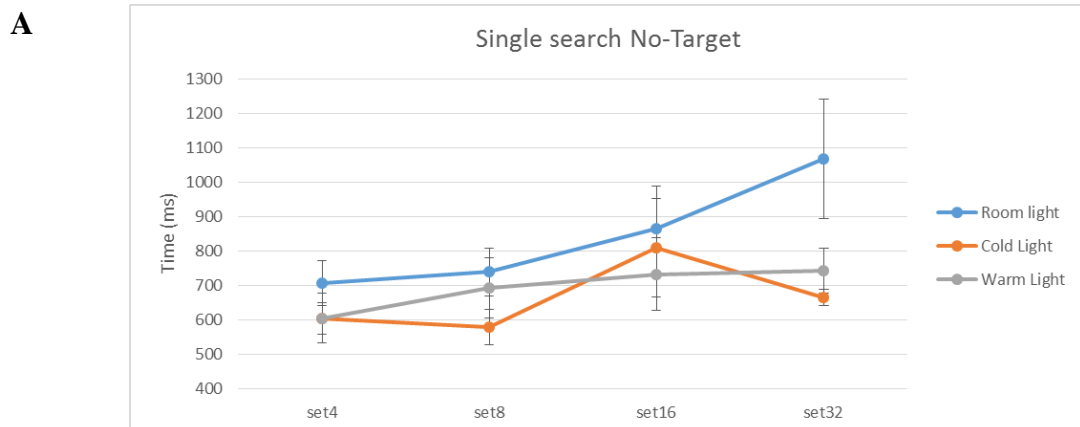


Figure 7.8 The average comparison of the metabolic ratio between different light colour temperatures. Initial exposure by “warm” light.

As before, the times recorded during the visual search task are presented in Figure 7.9. This time, “warm” exposure preceded “cold” exposure.



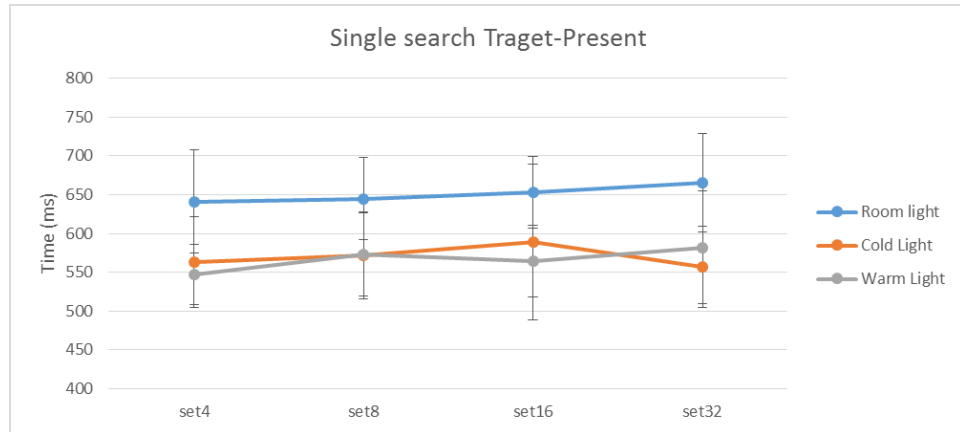
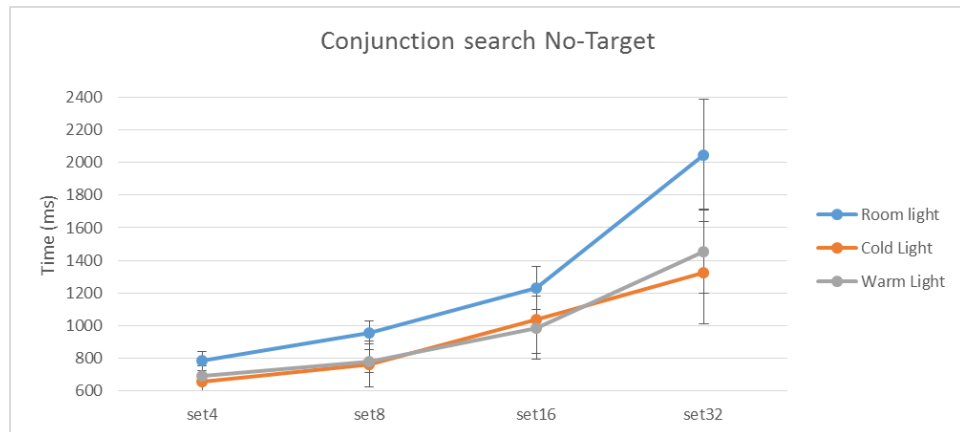
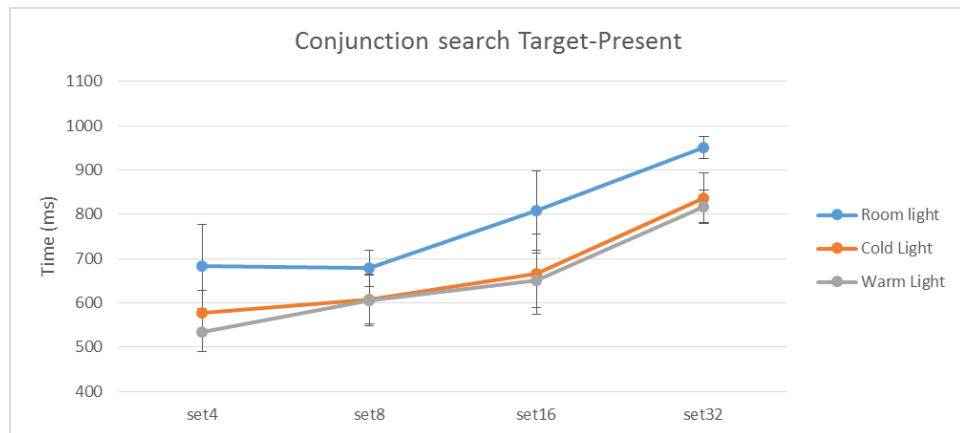
B**C****D**

Figure 7.9 Results of the reaction time task. Initial room light followed by “warm” then “cold” lights. (A) and (B): Field containing distractors of same colour as target shape, no target present and target present respectively. (C) and (D): Field containing distractors of same as well as different colour, no target present and target present respectively.

7.1.4 Discussion

Looking at the physiological data of the volunteer group initially exposed to “cold” light (Figures 7.4 and 7.5), it is evident that there is not a lot of variation in the parameters as a response to around half an hour of exposure to varying light colour temperatures. While 30 minutes of light

exposure was indicated to be the minimum required time to witness effects on people, the group of volunteers did not present any visible changes, despite the high sensitivity of the LAKK-M to physiological changes. The most likely reason for this could be the low exposure time. Further analysis with longer exposure times would be necessary to develop a more accurate understanding of light on physiological functions. It should also be noted that a volunteer group of six (with the removed outlier) is too low, especially considering the calculated required sample size of 28. Increasing the group to the required numbers could help reduce the relatively large recorded errors. Similarly, the data of the second group initially exposed to “warm” light (Figures 7.7 and 7.8) also displayed no significant alterations within their physiological conditions as well as a high level of error. The latter point is most likely the result of a very low number of volunteers within the second group. The issues with the volunteer numbers were not able to be resolved at the time of experimentation, however, due to the severe time constraints facing the work. In light of the limited availability of the light panel, only small groups of volunteers were measured.

The cognitive assessment results for the initially applied “cold” group are presented in Figure 7.6. It is important to take into account that the more distractors and the larger their variation, the longer the expected reaction time. Additionally, the absence of the target shape is also expected to increase reaction time. As such, reaction times with a field of four distractors are expected to be lower than those with a field of 32 distractors. Similarly, the reaction times on fields with no target shape are expected to be much higher compared to those with the target shape. This means that a field with 32 distractors of different varieties and no target will have a long reaction time, while a field of four distractors of one variety and the target present will have a very fast reaction time.

As is clear to see, all the reaction times increase in an expected manner, with the exception of Figures 7.6A and 7.6B. This, however, seems to fall within the error margins and, most likely being the result of low volunteer numbers. More interestingly, the reaction times for both “cold” light and “warm” light are reduced as compared to normal room light. Furthermore, “warm” light seems to display the fastest reaction times, though the high error makes this difficult to assess accurately.

In light of the potential influence of light on the psychological factors in the volunteers, it was important to ensure that the improved reaction times resulting from “warm” light were not, in fact, due to the practice effects, where volunteers improve their skill level from repeated sittings of the computer-based task. As such, the second group of volunteers were exposed to lights in reverse order. If the improved reaction times were truly related to an increasing skill level, a faster “cold” light (in relation to “warm” light) reaction time would be expected to develop. The results of these volunteers are presented in Figure 7.9.

The data presented in Figure 7.9, unfortunately, does not provide a defined difference between the “warm” and “cold” light effects upon the reaction times of participating volunteers nor does any statistical significance arise after t-test analysis. The most likely reason for this is the low number of volunteers (needing a calculated 64 volunteers per light-colour order group), resulting in

a high error. While a tendency may be observed for “warm” and “cold” light improving reaction times in the computer-based task, the volunteer base within this study was not large enough to determine any significant alterations in psychological effects of light exposure. Unfortunately, however, the earlier mentioned time constraint related volunteer numbers also affected this part of the study.

It is further important to take into account the nature of the task and its suitability for the experiment. An originally unaccounted-for element to consider is the ease at which blue objects such as the target of the visual search task and red objects such as the distractors, can be observed in “cold” and “warm” lights (which tend to appear blue or amber). Such an element could complicate or ease the search process of the target shape and thus alter the results. Similar tests exist, however, which provide an alternative approach requiring the target to be distinguished by shape, boldness or rotation direction (Wolfe 1998). Finding, for example, a vertical black line in a field of distractors including horizontal black and white distractors and vertical white lines, or a thick line rotating left in a field of distractors including thick and thin lines rotating right and thin lines rotating left would remove the alteration of data potentially due to light colour related factors.

Thus, the study could be substantially improved by taking into account the above test alterations. Furthermore, longer exposure times to lights of varying wavelength and temperature as well as a pool of volunteers sufficient for statistically significant outcomes would advance this study from a proof of concept and present much clearer effects of light on human physiological and psychological parameters. Given these improvements, data that are more diverse could be sought. Sex-dependent changes or age dependent changes may act as the following step for investigation.

7.1.5 Conclusion

This preliminary experiment has indicated a fascinating potential direction of investigating the effects of light on the human body. While the experiment did not show any significant differences in short term “warm” and “cold” light exposure on volunteers, certain tendencies towards improved reaction performances were observed as compared to room light. At the current stage, various time constraints and access to specific apparatus resulted in a premature completion of the investigation. A further investigation employing longer exposure times and a larger volunteer pool, as well as certain adaptations to the visual search task and potential introduction of other cognitive tasks, could greatly increase our understanding of light temperature and wavelength effects on various human systems.

7.2 Objective analysis of anterior eye health

7.2.1 Introduction

Ophthalmological clinical practice relies heavily on accurate and repeatable methods to observe, distinguish and diagnose potential pathological changes within the anterior eye from regular physiological variation. Due to the professional nature of clinicians, this must also be successfully achieved by more than one clinician on the same patient. To this effect, in addition to written record keeping and sketches, efforts were made in the 1990s to standardise observable anterior eye health. These came in the form of subjective grading scales (Efron et al. 2011).

The use of such grading scales, along with written descriptions and sketches or photographs obtained from slit lamp examination, currently serve as the gold standard for detailing anterior eye health. Unfortunately, these methods are highly subjective. Sketching requires a level of artistic skill that some clinicians may not possess, while subjective grading still leaves a lot of potential variability. As presented by Wolffsohn et al. (2015), only a third of optometrists indicated use of sketches, with even less relying on photographs (2%). Moreover, while offering a level of standardisation, various grading systems are not compatible and therefore mutually exclusive. Additionally, implementation of grading scales was highly variable depending on anterior eye features. Thus, together with the fact that there is still a level of observer-based variability even with a grading system, there exists a need for more objective markers of anterior eye health.

The development of low power photonics-based diagnostics devices provides a potential avenue for non-invasively and harmlessly recording objective measures of anterior eye health. Certain technologies have already been employed in order to measure features of the eye such as the retina and choroid (Kimura et al. 2003) or even act as marker for conditions such as cataracts (Schweitzer et al. 2007). As such, this study was conducted on volunteer participants both with and without a history of contact lens wear with the ultimate goal of establishing a set of objective physiological markers capable of aiding clinicians' ability to predict positive or negative outcomes, which may arise from prescription contact lenses.

7.2.2 Methods and materials

7.2.2.1 *Ethical approval*

This study was reviewed and given favourable opinion by the Aston University's Ethics Committee. Due to the nature of the study, no higher ethical approval was necessary.

7.2.2.2 Experimental equipment setup

The experiment was conducted in a laboratory with enough space to easily enable at least one volunteer and two research staff to work the equipment. Prior to the experiment, blinds on the laboratory windows were closed to ensure minimal external light. The LAKK-M device was set up in accordance to procedure described in chapter 4. Both microcirculatory and fluorescence spectroscopy channels were employed in this experiment. It should be noted, only the UV (365 nm), blue (450 nm) and green (532 nm) sources were required during the fluorescence spectroscopy in this experiment.

A specialised headrest commonly employed for ophthalmological slit lamp use was utilised for the experiment (Figure 7.10). The key feature of the headstand for this specific experiment was the clasp capable of holding the fibre probe of the LAKK-M at a steady position and provide smooth, accurate and small scale movement along the x, y and z axis.



Figure 7.10 Standard headrest for ophthalmological slit lamp use.

The setup was positioned in a location where volunteers could comfortably sit with their head in the headrest, while research staff positioned the fibre probe to the desired location without coming into direct contact with the volunteers.

7.2.2.3 Participants

A total of 16 participants between the ages of 25 – 45 were involved in this experiment. Selection was done through internal Aston University advertisement in collaboration with members from the Aston University Ophthalmology department. The volunteer participants comprised of 8 males and 8 females. Furthermore, the individuals further broke down into those who wore contact lenses in their daily life and those who did not use contact lenses at all (4 of each per sex group). All volunteers confirmed that they were healthy and had no prior ocular conditions of any kind.

The volunteers were provided information about the study and were asked to complete a simple consent form (appendix 2a and 2b respectively). They were also informed that they could terminate participation at any time without any consequences or reasons. No data already gathered on the participant would be stored in the event of such termination.

7.2.2.4 Experimental protocol

After the participants signed the consent form and confirmed they understood what is involved in the experiment, their left anterior eye was subjectively graded using a portable slit lamp and the clinical grading scale. Bulbar and limbal hyperaemia were assessed and recorded to one decimal point using the Efron scale. Additionally, patients were asked to indicate the comfort of their eye on a scale of 1 to 10 (1 being lowest comfort, 10 being highest comfort).

Upon completion of grading, participants were asked to comfortably place their heads on the chin pad of the headrest and focus on an object to their right to ensure their eyes were fixated allowing maximal access to the temporal conjunctiva of the left eye (area of interest). During this time, the probe of the LAKK-M, fixated on the headrest clip was moved into a position 5 mm away from the eye. It should be noted here that the LAKK-M was not turned on at this point to ensure no excess laser radiation entered the participants' eyes. Upon placing the probe in the desired position, the movable base of the headrest was locked in place and the LAKK-M fibre probe slid out of the clip.

With the probe unclipped, the LAKK-M device was calibrated to measure microcirculatory parameters as described in chapter 4. The only major difference in approach was the removal of the probe cap to reduce the diameter of the probe. Once calibrated, the fibre was replaced in the headrest clip and a 10-second recording was taken to obtain perfusion, saturation and blood velocity parameters. An image of the setup is displayed in Figure 7.11. It is important to note that participants were constantly reminded to focus on an object to their right to avoid looking into the laser beam path. The research staff made sure that the laser beam did not reach the pupil. Upon completion of the measurements, the LAKK-M channel was turned off and fibre moved away from volunteers' eyes. The volunteer was given time to rest their eyes. This was particularly important as volunteers were asked not to blink during measurement to preserve data viability.

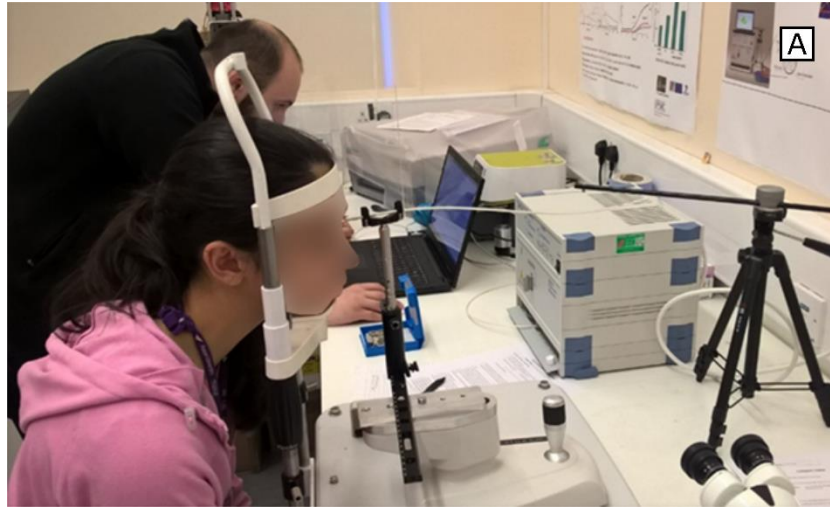


Figure 7.11 Figures depict experimental setup in use. A) Measurement of microcirculatory parameters and the connection of the LAKK-M device to the headstand. B) Measurement of fluorescence. The room is visibly darker during fluorescence measurements. Both images have had participants face blurred for privacy.

Following microcirculatory measurements, the fibre was replaced into the clip and returned to the previous position, 5 mm away from the participant's eye. In the same setup as described above, the fluorescence channel was initiated, calibrated and utilised as detailed in chapter 4. UV (365 nm), blue (450 nm) and green (532 nm) excitation wavelengths were used. No more than 5 seconds was spent per measurement.

Upon completion of measurements, participants were asked to insert a contact lens into their left eye. A +7.00 DS, 8.8 mm base curve and 14.0 mm diameter soft contact lens was inserted for a duration of 15 minutes. This form of lens was chosen due to its thick design, likely to cause most irritation and induce changes within the ocular physiology at a level high enough to observe easily. The experimental measurements were repeated as stated above after the allocated time.

7.2.2.5 Data analysis

Data was obtained and organised into multiple forms. By comfort level, by assigned condition and according to participants history of lens-wear. The former condition was based on the subjective criteria provided by the volunteers. These criteria were labelled as normal (unchanged), small drop in comfort (drop by one arbitrary unit) and large drop in comfort (drop by two or more arbitrary units). The assigned condition was delivered on the basis of increased, unchanged or decreased perfusion observed in the eye (labelled as improvement – Imp, normal – Norm and deterioration – Det, respectively). The final condition was split the participants into individuals who already use contact lenses against those who do not/have not used them. It should be noted that experimenters were kept blinded to the volunteers who were lens wearers. This parameter was revealed after data had been analysed.

Furthermore, microcirculatory and metabolic parameters were also calculated in accordance to procedure described in 6.2.2.4. Overall, many parameters were compared in accordance to the criteria described above. These parameters were: k values of collagen, elastin, NADH, FAD, lipofuscin and crosslinked collagen/elastin (as noted by a slightly blue-shifted fluorescence peak around 400-410 nm), as well as the perfusion (I_m), saturation (S_tO_2), blood velocity (V_b), index of oxygen saturation to perfusion of microvascular blood flow (S_m), redox ratio (RR) and metabolic ratio (MR). A parametric t-test was employed to find significant differences for the above parameters. Significance was assumed with a $p < 0.05$.

7.2.3 Results

7.2.3.1 Subjective grading of eyes

The subjective grades following the Efron scale for bulbar and limbal eye redness are presented in Figures 7.12 and 7.13 respectively. The Figures compare eye redness before and after lens use for each participant.

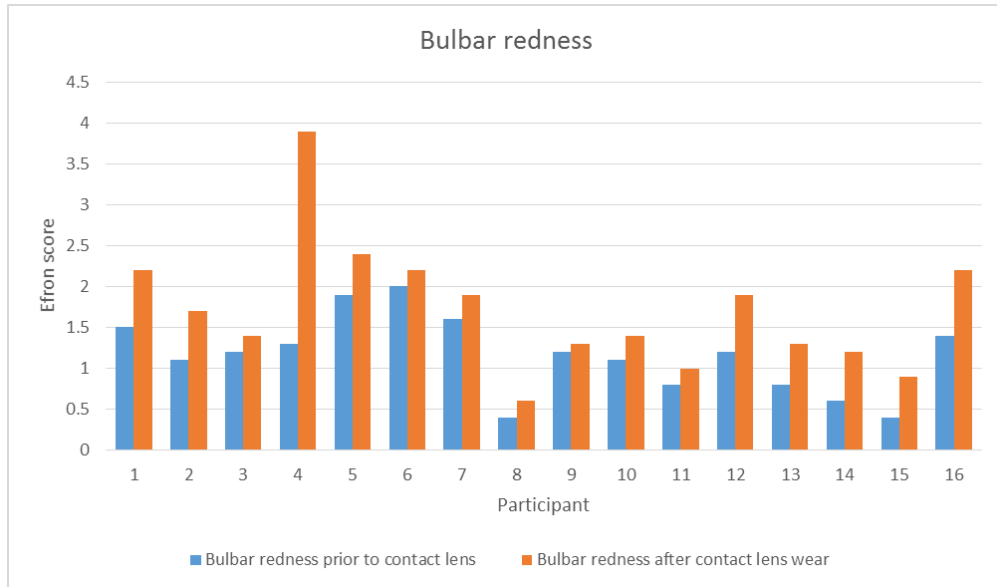


Figure 7.12 Bulbar redness obtained by subjective grading following Efron scale.

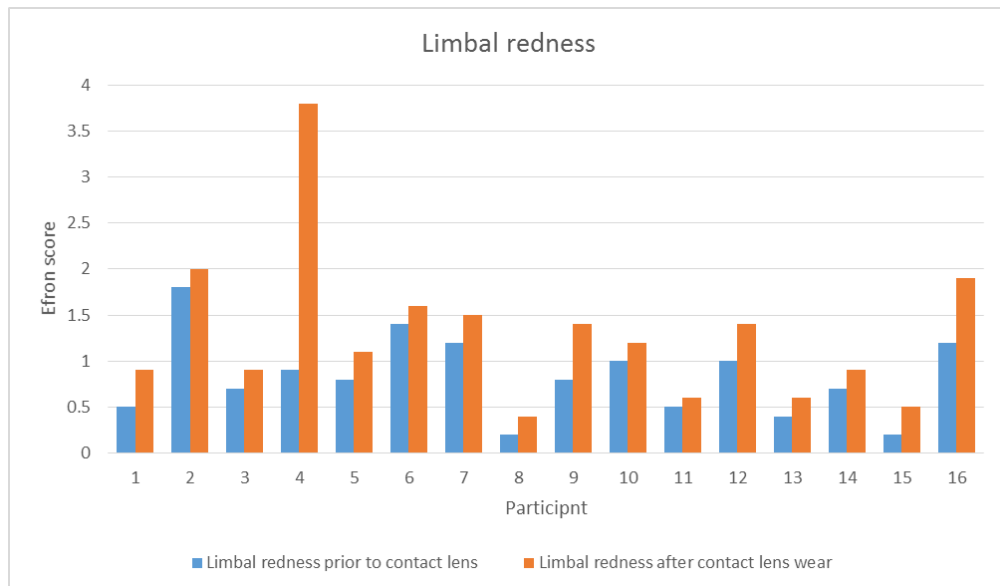


Figure 7.13 Limbal redness obtained by subjective grading following Efron scale.

Furthermore, following the subjective comfort level assessment, normal criteria displayed an $n = 8$, small drop an $n = 4$ and large drop also an $n = 4$.

7.2.3.2 Comparisons by comfort level

Out of the measured parameters, only the FAD, I_m , RR and MR displayed significant differences. This is displayed in the following Figures (non-significant data not presented).

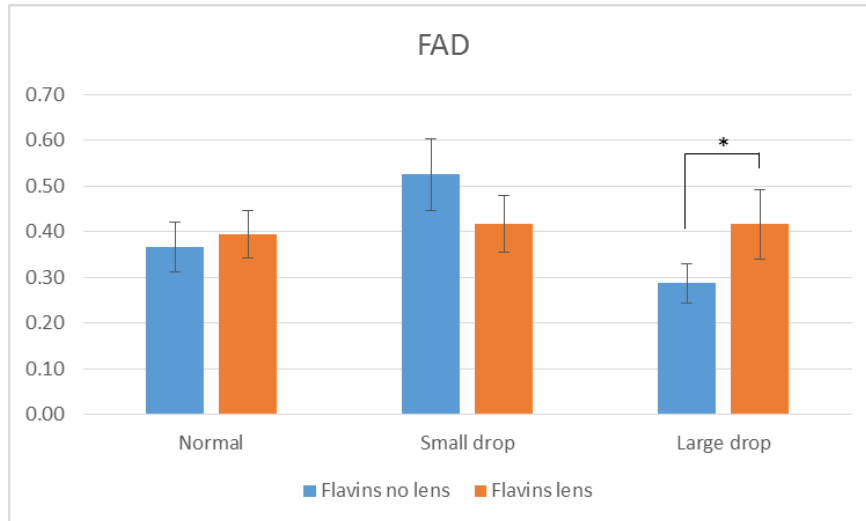


Figure 7.14 Measurement of FAD and comparison by comfort level change. Large drop in subjective comfort rating after lens use was accompanied by a significant difference in FAD (* represents $p < 0.05$).

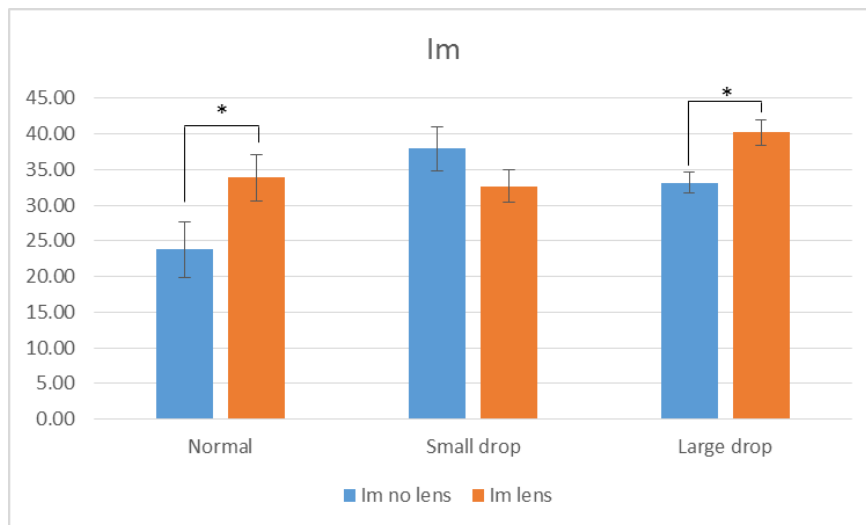


Figure 7.15 Measurement of Im and comparison by comfort level change. Large drop in subjective comfort rating after lens use was accompanied by a significant difference in perfusion, however a similar difference was observed in the group with no subjective comfort change (* represents $p < 0.05$).

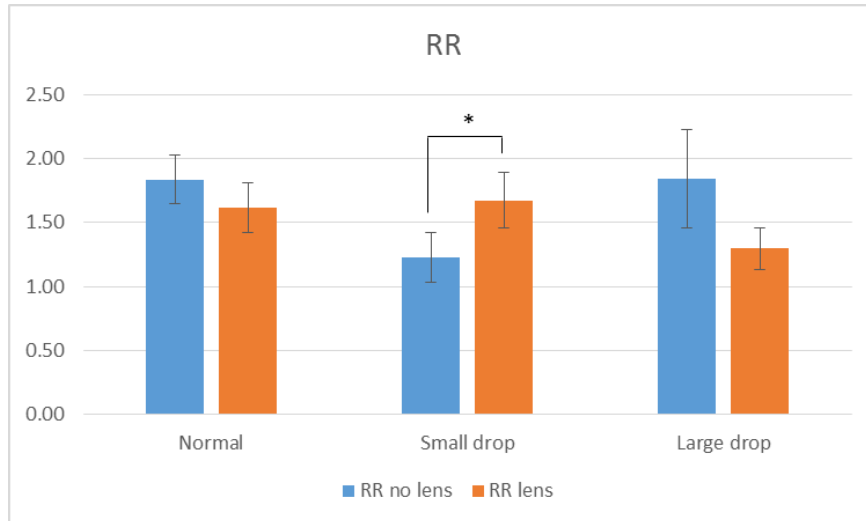


Figure 7.16 Measurement of RR and comparison by comfort level change. Small drop in subjective comfort rating after lens use was accompanied by a significant difference in RR (* represents $p < 0.05$).

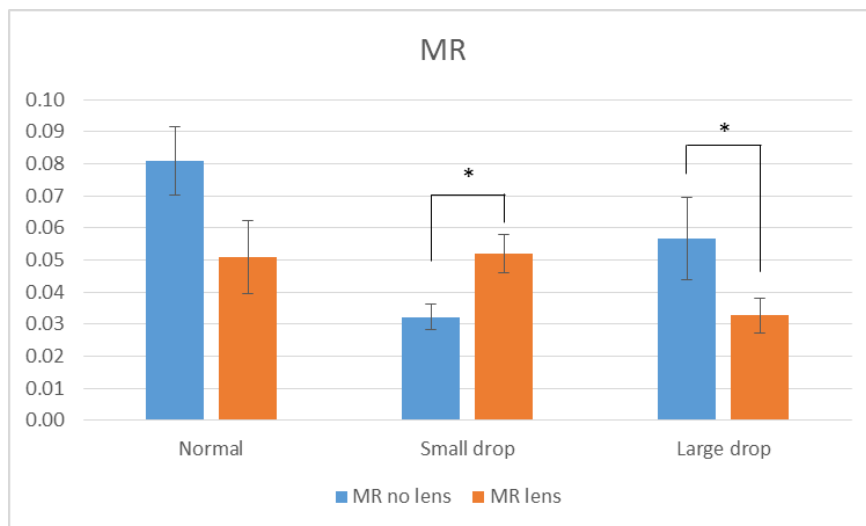


Figure 7.17 Measurement of MR and comparison by comfort level change. Large drop and small drop in subjective comfort ratings after lens use were accompanied by significant difference in MR (* represents $p < 0.05$).

7.2.3.3 Comparisons by assigned condition

Assigning a condition to the volunteer data resulted in the formation of three groups. An unchanged group with $n = 7$, an “improved” group with $n = 4$ and a “deteriorated” group with $n = 5$. The graphs below display parameters by which each of the assigned condition groups displayed significant difference in after a period of contact lens wear (non-significant parameters are not presented).

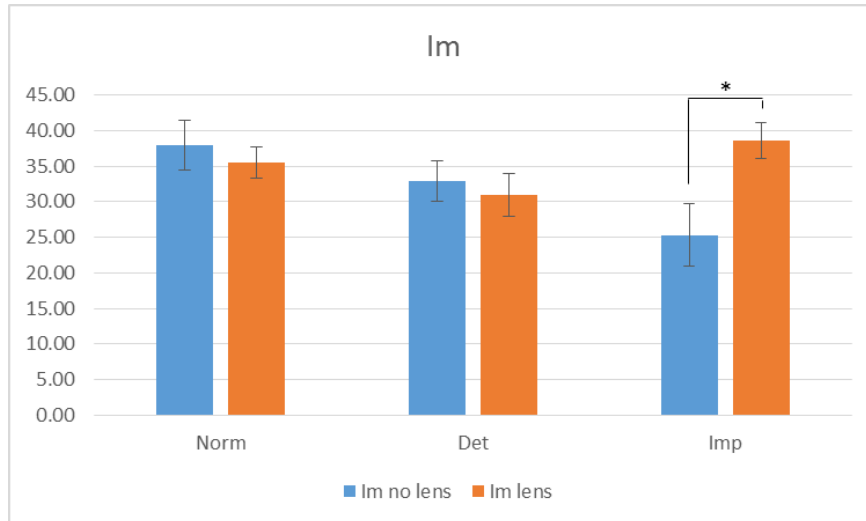


Figure 7.18 Measurement of Im and comparison by assigned condition differences. As expected, individuals with improved perfusion in the eye display a significant difference pre and post lens wear (* represents $p < 0.05$).

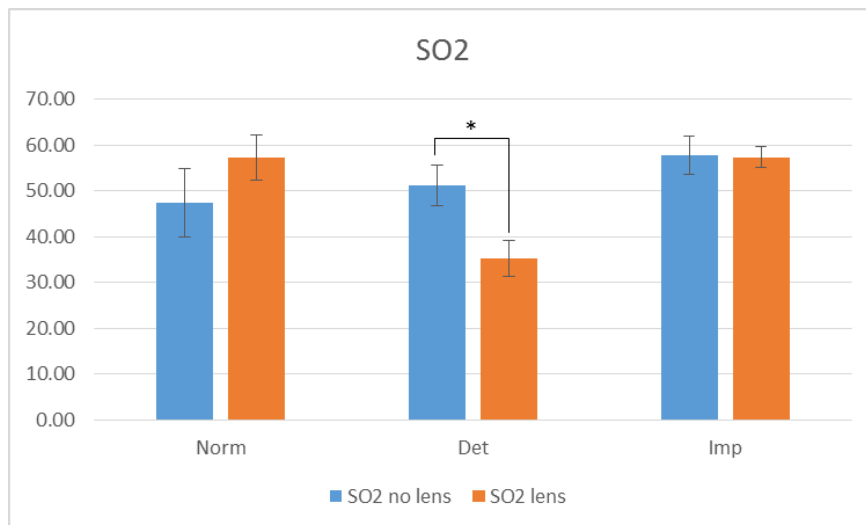


Figure 7.19 Measurement of StO2 and comparison by assigned condition differences. Significant difference pre and post lens wear was only observed in individuals with a deteriorated condition (* represents $p < 0.05$).

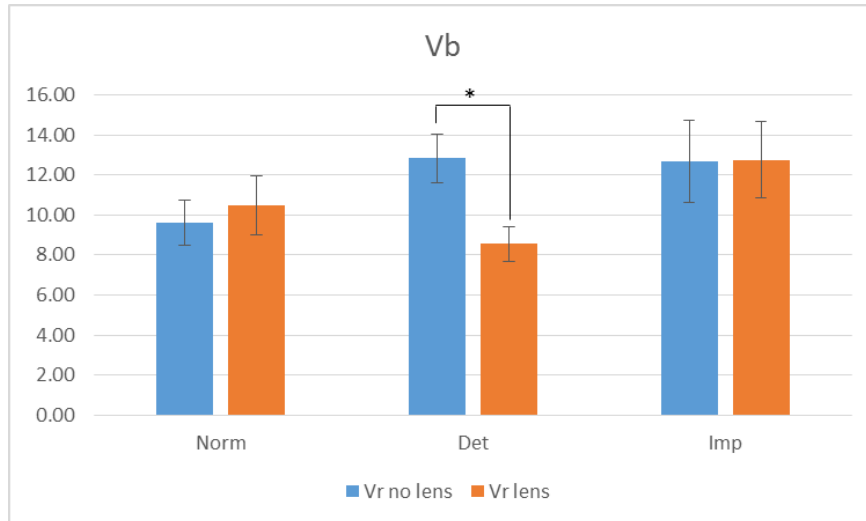


Figure 7.20 Measurement of Vb and comparison by assigned condition differences. Significant difference pre and post lens wear was only observed in individuals with a deteriorated condition (* represents $p < 0.05$).

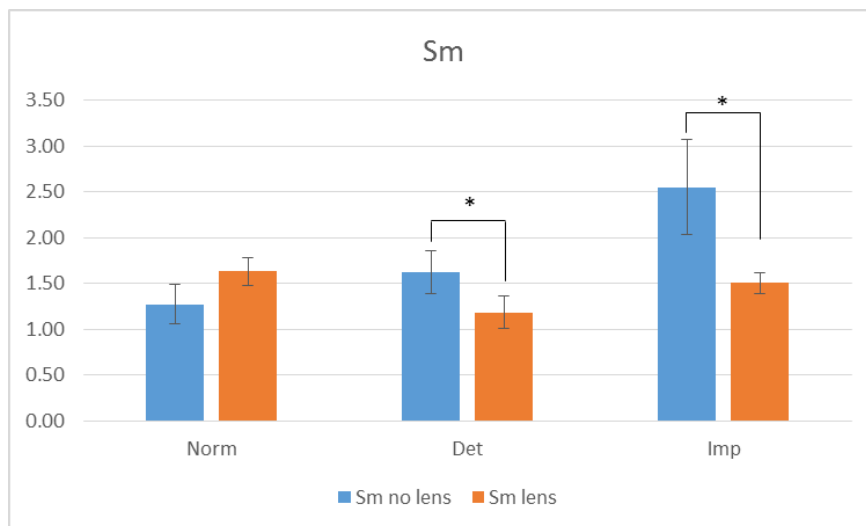


Figure 7.21 Measurement of Sm and comparison by assigned condition differences. Significant difference pre and post lens wear was observed in individuals both with a deteriorated and an improved condition (* represents $p < 0.05$).

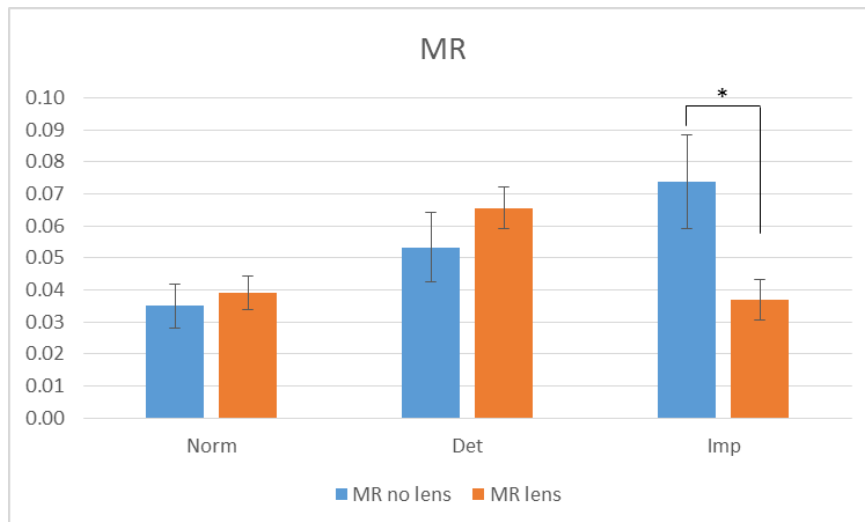


Figure 7.22 Measurement of MR and comparison by assigned condition differences. Significant difference pre and post lens wear was observed in individuals with an improved condition (* represents $p < 0.05$). A tendency towards an opposite difference was also noted in the deteriorated group.

Comparison of assigned criteria with individuals who wear lenses in their daily life displayed that three out of four “improved”, three out of seven “normal” and two out of five “deteriorated” volunteers were lens wearers.

7.2.3.4 Comparisons by history of lens wear

Half of the volunteers had prior history of wearing contact lenses. However, no statistical differences were observed when comparing measured parameters before and after lens wear. Non-significant data is not presented.

7.2.4 Discussion

The use of novel photonics based technologies and methodologies opens many possible avenues for determining how well a particular individual will take to forms of medical intervention. In addition to this, comfort and quality of life in individuals is also of great importance and thus, must be investigated. In the case of this study, intervention comes in the form of relatively common and benign lens wear. In light of this, the first part of this investigation looks at the comfort level before and after lens wear. It is portrayed in Figure 7.14 that volunteers indicating a large drop in comfort also displayed a notable increase in FAD fluorescence. As shown in Figure 7.16 however, a redox ratio change was only significantly observed in participants indicating a small level of discomfort. When taken together with measurements of perfusion (Figure 7.15) we can observe the changes in metabolic rate on Figure 7.17. This portrays an increase of metabolic rate after lens wear

in participants claiming a small drop in comfort and the opposite outcome for individuals claiming a large drop in comfort. Interestingly, the group of participants that claimed no change in comfort level also displayed an increased level of perfusion after 15 minutes of lens wear. It should be noted that, while not all lens wearers participating in this study displayed unchanged comfort levels, all participants who claimed no change in comfort level were already lens wearers.

Assessing the above parameters, metabolic changes seem to have an impact on the comfort level of individuals wearing contact lenses. However, a larger group of participating volunteers would be required for clarification of the exact metabolic causes of the comfort changes. Further study on contact lens wearers and individuals who do not use contact lenses should also be conducted. Considering that wearers of contact lenses were also found in the small and large discomfort groups, there is currently no established method to know whether use of contact lenses results in physiological adaptation and improved comfort levels, or if certain individuals will result in continued discomfort regardless of lens use duration. It should also be noted that redness within the eye of participants did not necessarily correspond to a drop in comfort level.

Ultimately, investigations as described above will always suffer from the arbitrary nature of “comfort”, which will differ between each individual participant. Thus, the study conducted here additionally analysed participants based on whether contact lenses resulted in perfusion differences in the eyes of wearers. Contact lenses that did not restrict perfusion, or improved the parameter were considered “normal” and “improved”, while those which restricted perfusion were thought of as “deteriorating”. Portrayed in Figure 7.18, the largest perfusion increase was, as expected, in the “improved” group. However, both S_tO_2 and V_b parameters were observed to drop only for the “deteriorated” group (Figures 7.19 and 7.20). This establishes the saturation and blood velocity parameters as potential markers for predicting issues in anterior eye health in contact lens wearing individuals. Interestingly, a drop was also observed in the S_m parameter for both “improved” and “deteriorated” groups (Figure 7.21). However, the metabolic rate parameter does decrease in the individuals of the “improved” group after lens wear. It is also useful to note that there seems to be a tendency towards an increase in MR for the “deteriorated” group (Figure 7.22). Such opposite reactions would make MR the best criteria to predict outcomes of lens use in individuals. It should also be noted again, that outcomes of measurements did not specifically correspond to eye redness.

Finally, it bears mentioning that comparison of metabolic and microcirculatory parameters between the group of individuals with a history of lens wear and those without did not yield any tangible differences (thus no graphs were presented in the results section). While this could be the result of the two compared groups not having physiological differences in response to contact lens based eye irritation, it is more likely a side effect of the sample size. A post hoc power analysis on the volunteer groups established that the experimental power was 0.15. Due to such a low power, there is a likelihood that an important difference was simply missed. Unfortunately, while the number

would have to be eight times what was measured (as calculated in retrospect), the study was limited to the available volunteers.

This study establishes a number of parameters by which the condition of eyes in individuals wearing or planning to wear lenses can be assessed and potential negative outcomes predicted. However, there is a large spread in criteria by which to judge such outcomes. One major improvement to this study should come in the form of increased participant numbers (especially with a history of wearing contact lenses and with no such history). From only these preliminary results, it is difficult to predict beneficial or negative outcomes of lens wear using the majority of parameters studied, but S_tO_2 , V_b and MR have shown themselves as the most effective.

7.2.5 Conclusion

Contact lens use is very common and affects many people worldwide. The use of contact lenses, however, does come with a level of irritation to the eyes. Thus, an approach to predicting which individuals will have a greater negative reaction to first time and continued use of contact lenses could be of great interest for ophthalmologists. The above preliminary study was able to determine that photonics based measurements of S_tO_2 , V_b and MR could act as effective markers for predicting positive or negative contact lens effects on eye health and comfort level. The study also demonstrated that potential other markers could be used in this manner.

The methodology described above, conducted through devices such as the LAKK-M or other available photonics based diagnostics devices, could be conducted as a rapid and routine test by optometrists prior to potential contact lens prescriptions. The fast, relatively low cost and easy to use approach can further improve prescriptive and diagnostic capacity in areas of the world that currently do not have easy access to standardised and effective ocular healthcare. However, before the above technology reaches clinical practice, extensive further investigation is required on a larger, more diverse volunteer base.

References

- An, M. et al., 2009. Time-of-day-dependent effects of monochromatic light exposure on human cognitive function. *Journal of physiological anthropology*, 28(5), pp.217–223.
- Efron, N. et al., 2011. How optometrists record corneal staining. *Clinical and Experimental Optometry*, 94(1), pp.82–86.
- GoCognitive - Educational tools for cognitive neuroscience, 2017. Visual Search demo. Available at: <http://www.gocognitive.net/demo/visual-search> [Accessed April 19, 2017].
- Kimura, I. et al., 2003. Scanning laser Doppler flowmeter study of retinal blood flow in macular area of healthy volunteers. *The British journal of ophthalmology*, 87(12), pp.1469–73. Available at: <http://www.ncbi.nlm.nih.gov/pubmed/14660455>.
- Litvinova, K.S. et al., 2016. A pilot study using laser-based technique for non-invasive diagnostics of hypertensive conditions in mice. *SPIE proceedings*, 9689(0), p.96893H. Available at: <http://proceedings.spiedigitallibrary.org/proceeding.aspx?doi=10.1117/12.2213026>.
- Schweitzer, D. et al., 2007. Towards metabolic mapping of the human retina. *Microscopy research and technique*, 70(5), pp.410–9. Available at: <http://doi.wiley.com/10.1002/jemt.20427>.
- Trick, L.M. & Enns, J.T., 1998. Lifespan changes in attention: The visual search task. *Cognitive Development*, 13(3), pp.369–386.
- Turner, P.L., Van Someren, E.J.W. & Mainster, M.A., 2010. The role of environmental light in sleep and health: Effects of ocular aging and cataract surgery. *Sleep Medicine Reviews*, 14(4), pp.269–280. Available at: <http://dx.doi.org/10.1016/j.smrv.2009.11.002>.
- Vandewalle, G., Maquet, P. & Dijk, D.J., 2009. Light as a modulator of cognitive brain function. *Trends in Cognitive Sciences*, 13(10), pp.429–438.
- Weitbrecht, W.U. et al., 2015. Wirkung der Farbtemperatur des Lichts auf Konzentration und Kreativität Effect of Light Color Temperature on Human Concentration and Creativity. *Fortschr Neurol Psychiatr*, 83, pp.344–348.
- Wolfe, J.M., 1998. Visual Search. *Attention, Perception, & Psychophysics*, 20(8), pp.13–73. Available at: <http://psycnet.apa.org/journals/rev/96/3/433/>.
- Wolffsohn, J.S. et al., 2015. Anterior eye health recording. *Contact Lens and Anterior Eye*, 38(4), pp.266–271. Available at: <http://dx.doi.org/10.1016/j.clae.2015.03.001>.

Thesis conclusions

Currently, the research and clinical fields are undergoing great advancement in terms of diagnostics technology. The field has become very popular and much time and effort around the world is dedicated to its advancement. However, it is also relatively young and highly cross-disciplinary in nature, demanding that a strong foundation of science and research is established. This thesis has attempted to introduce and elaborate upon the various developed and developing technologies employed for research and clinical diagnostics of organic materials and tissues. Furthermore, this thesis also outlined work carried out in order to form a basis on which further research could advance. Utilising a number of the described technologies simultaneously, the work summarises preliminary trials in a number of differing diseases and health monitoring modalities to validate and create viable metrological support for numerous non-invasive approaches.

Photonics based technology has been steadily advancing over the last few decades, finding application in many fields, from telecommunications to biomedicine. Particularly in healthcare and clinical practice, application of photonics based diagnostics can revolutionise the field, improving the stage of disease diagnosis and reducing the need for invasive procedures. The various techniques available present a large potential for many clinical and health monitoring applications. Importantly, the thesis combined the investigations in such a wide range of subjects, as the potentials of photonics based diagnostics are vast, but have still not been fully realised. With this thesis, the capabilities of various techniques were demonstrated to be effective in largely differing applications. Thus, the methods describe a validation for the application of novel photonics based techniques as well as form a vital foundation for future research. Whether the intention is to improve early detection of cancer (various forms) or to assess the physiological and psychological responses to unnatural light, the work described in this thesis forms a stepping-stone into more extensive photonics based research.

Ultimately, the author of this thesis presented evidence for the effectiveness of novel non- and minimally- invasive photonics based diagnostics in monitoring and aiding diagnosis of various diseases and conditions, including urinary bladder cancer, pre-eclampsia, contact lens induced eye irritation and artificial light induced physiological changes. While the applicable fields for the presented technologies and methodologies are diverse, the approaches presented are not limited by those specific niches. The photonics based technology and methodology applied to bladder cancer, for example, can be easily modified towards detecting other forms of cancer. The monitoring of physiological conditions in pre-eclampsia murine models is but a single example of the technological potential. Other CVD models can be similarly monitored. Furthermore, the same form of monitoring and detection could be transferred to humans. Similar forms of expansion of the technology are possible with both ocular health monitoring and diagnostics as well as assessments of the physiological conditions in association with psychological health.

It is also important to note that the non- and minimally invasive technologies and methodologies presented in this thesis can be expanded into fields that are not covered by the work presented. As this thesis has established, the applicability of photonics diagnostics has great potential in many medical and healthcare fields. While not described above, research directed towards other major diseases such as diabetes or stroke may yield a wealth of results.

Appendix 1a: Lighting effects on biological function information sheet



Date: 6/09/16

Version Number: 4

Information Sheet

Title of Project: **Assessment of light colour panel on physiological and psychological parameters in healthy volunteers**

Name of Chief Researcher: Prof Rafailov

You are invited to participate in a study aimed at determining the effects of light colour temperature on the physiological and psychological effects in humans. Below is a brief description of the research study, to help you make an informed decision regarding participation.

The research conducted is aimed at finding beneficial effects of varying light colour temperatures on people. An example of this would be potentially improved performance during studying or problem solving tasks under light of either warm or cold colours as compared to natural light. Additionally the study looks at any possible physiological alterations that result from exposure to such light.

This experiment requires enough volunteers to run accurate statistical analysis on their data. These volunteers must be healthy with no longstanding diagnosed medical conditions. Such conditions include heart disease/angina, diabetes, circulatory conditions/diseases and epilepsy/seizures. Please also note that visual impairment may hinder ability to carry out the computer based visual trial section of the experiment, which relies on differentiating and locating a small coloured shape in a field of distractors (similar looking coloured shapes). If you feel you meet the required criteria, we encourage you to participate.

Should you choose to go ahead with the experiment, we ask that you do not ingest any caffeine or alcohol containing drinks at least 3 hours prior to your allocated session or during the one-hour break between the two parts of the experiment (please also avoid eating food for the duration of the break). Please also avoid altering your daily routine on the day of the experiment (for example, do not cycle in to work if you usually drive in). Upon arrival at the experiment, you will be asked to complete a short questionnaire regarding your current health status. You will then be subjected to an environment illuminated by “cold” light, followed by a measurement of your physiological condition using a non-invasive multi-functional diagnostics device (LAKK-M). A measurement of your reaction times will also be taken using a computer-based test. This entire procedure will take around one hour, with

no less than 30 minutes of that being spent in illumination by the “cold” light. During the illumination portion of the experiment, we encourage you to partake in an activity like reading (if you wish to bring your own reading material, you are welcome to do so). At this point, you will be given an hour break, during which we kindly ask you not to drink any caffeinated or alcoholic drinks. The experiment is then repeated with “warm” light. Around two hours total will be spent on experimental procedure, with an extra hour provided for the break.

We would like to stress that none of the procedures in this experiment are harmful. Due to the experiment, however, you will spend no less than half an hour in environments illuminated by “cold” or “warm” coloured light. This may potentially bring mild discomfort. We expect no negative effects on the short- or long-term health of participants, nor any following side effects of the experiment. If, however, you feel you do not wish to continue, you may opt out of participation at any time and without given reason. This will terminate your participation in the study without affecting you in any further way. Any of your data received to the point of withdrawal will be terminated.

We would also like to note that your personal details will not be stored on our databases. Your data will be stored in a numbered, unnamed, anonymous format. The results of this work will be analysed at the end of the experimental procedures and, given viable outcomes, be written up for publication in peer-reviewed journals. Should the results be published, you will be notified by the contact email you provide at the bottom of this form.

This study has been reviewed and given favourable opinion by the Aston University's Ethics Committee.

If you wish to ask a question, one of the researchers in charge of the experiment will be present for the duration of your participation in the experiment. Any questions outside of the experiment should be sent to Mr Rafailov at rafailoi@aston.ac.uk.

If you have any concerns about the way in which the study has been conducted, you should contact Mr John Walter, the Director of Governance by email at j.g.walter@aston.ac.uk or telephone 0121 204 4869.

This study has been organised by the Optoelectronics and Biomedical Photonics Group, Aston University. It is partially funded by M-Squared Lasers Ltd.

Appendix 1b: Lighting effects on biological function consent form



Date: 6/09/16

Version Number: 3

PARTICIPANT CONSENT FORM

Title of Project: **Assessment of light colour panel on physiological and psychological parameters in healthy volunteers**

Name of Chief Researcher: Prof Rafailov

		Initial here
1	I confirm that I have read and understand the information sheet (Version 4 dated 6/09/2016) for the above study.	
2	I have had the opportunity to consider the information, ask questions and have had these answered satisfactorily.	
3	I understand that my participation is voluntary and that I am free to withdraw at any time without giving any reason, without my legal rights being affected.	
4	I give permission for my anonymised data to be used in any future scientific publication that may result from this work.	

Name of participant

Date

Signature

Name of Person taking consent

Date

Signature

Appendix 2a: Objective analysis of anterior eye health information sheet

PATIENT INFORMATION SHEET



Aston University Investigators: James Wolffsohn PhD PgDipAdvClinOptom PgCHE MBA
Danielle Edwards

Project Title: Investigations into conjunctival physiology

Invitation:

You are being invited to take part in a research study. Before you decide, it is important for you to understand why the research is being done and what it will involve. Please take time to read the following information carefully.

What is the purpose of the study?

The purpose of this study is to use the latest technology to measure the health of the conjunctiva by assessing the conjunctival blood vessels, and to investigate whether conjunctival health is impacted by factors such as dry eyes, allergy and contact lens wear. While contact lens wear is considered generally very safe, some patients do eventually have complications and the ability to identify who is likely to have problems and when would be of great clinical benefit.

Why have I been chosen?

You have been chosen as you have healthy eyes.

What will happen to me if I take part?

After the study has been explained to you and consent given, you will be invited to attend two appointments for your eye's physiology to be measured with a new light probe placed near your eye. This measurement will involve you placing your head against a chin rest and forehead bar and looking away from the probe. The probe will be positioned 5mm away from your eye for a period of about 10 seconds.

The duration of the appointments will be 10-15 minutes each. By volunteering to participate, you will be giving anybody in the research team consent to analyse your results.

Are there any potential risks in taking part in the study?

The tests do not make contact with your eyes and have been tested to ensure they are safe. The laser will not be directed into your eye although has been confirmed as 'eye safe'. Even so, you should not look into the laser. Your data will be anonymised before storage.

Do I have to take part?

No, you do not have to participate if you do not wish to do so. This information sheet is yours to keep. If you would like to participate, you will be required to sign the enclosed consent form. You are free to withdraw at any time from the project. No sanctions will be taken against any patient who refuses to participate in or withdraws from this project. A decision to withdraw at any time, or a decision not to take part, will not affect the standard of care you receive.

Expenses and payments:

No payment is available for participation in this study. Ocular examination does not replace your need for regular eye health checks.

Will my taking part in this study be kept confidential?

Yes, your participation in the study will be fully confidential. There will be no way to link any research data to any individual participant. Aston University will review the anonymised data for monitoring purposes.

What will happen to the results of the research study?

We aim to publish the results of this project. However, there will be no reference to any individual's performance in any publication. You may request your own results and a summary of the study results.

Who is organising and funding the research?

The study is organised by the Ophthalmic Research Group at Aston University and has not been externally funded.

Who has reviewed the study?

The research has been reviewed by Aston University's Ethics Committee.

Who do I contact if something goes wrong or I need further information?

Please feel to contact Prof James Wolffsohn (j.s.w.wolffsohn@aston.ac.uk, 01212044140).

Who do I contact if I wish to make a complaint about the way in which the research is conducted?

If you have any concerns about the way in which the study has been conducted, then you should contact Secretary of the University Research Ethics Committee: j.g.walter@aston.ac.uk or telephone 0121 204 4665.

Appendix 2b: Objective analysis of anterior eye health consent form

Personal Identification Number for this study: _____
--



CONSENT FORM

Title of Project: Investigations into Conjunctival Physiology

Research Venue: Ophthalmic Research Group Labs, Aston University

Aston University Investigators: James Wolffsohn PhD PgDipAdvClinOptom PgCHE MBA
Danielle Edwards

initial box

Please

1. I confirm that I have read and understand the information sheet dated
for the above study and have had the opportunity to ask questions.
2. I understand that my participation is voluntary, the study tests are not part of any
medical treatment or negate the need for regular eye examination.
3. I understand that I am free to withdraw at any time, without giving any reason, without
my legal rights being affected.
4. I agree to take part in the above study.

Name of Research Participant

Date

Signature

Name of Person taking Consent

Date

Signature

1 copy for research participant; 1 copy for Aston University

Appendix 3: Publications

Journal publications

1) Dremine, Victor V., Zherebtsov, Evgeny. A., Sidorov, Victor. V., Krupatkin, Alexander I., Makovik, Irina N., Zherebtsova, Angelina I., Zharkikh, E.V., Potapova, E.V., Dunaev, Andrey V., Doronin, A., Bykov, A.V., **Rafailov Ilya E.**, Litvinova, Karina S., Sokolovski, Sergei G., Rafailov, Edik U. 2017. Multimodal optical measurement for study of lower limb tissue viability in patients with diabetes mellitus. *Journal of Biomedical Optics*, 22(8), p.1.

2) Makovik, Irina N., Dunaev, Andrey V., Dremine, Viktor V., Krupatkin, Alexander I., Sidorov, Victor V., Khakhicheva, Lyudmila S., Muradyan, Vadim F., Pilipenko, Olga V., **Rafailov, Ilya E.**, Litvinova, Karina S. 2017. Detection of angiospastic disorders in the microcirculatory bed using laser diagnostics technologies. *Journal of Innovative Optical Health Sciences*, 11(1), p.S179354581750016X.

3) **Rafailov, Ilya E.**, Dremine, Victor V., Litvinova, Karina S., Dunaev, Andrey V., Sokolovski, Sergei G., Rafailov, Edik U. 2016. Computational model of bladder tissue based on its measured optical properties. *Journal of Biomedical Optics*, 21(2), p.25006.

4) Dunaev, Andrey V., Dremine, Victor V., Zherebtsov, Evgeny A., **Rafailov, Ilya E.**, Litvinova, Karina S., Palmer, Scott G., Stewart, Neil A., Sokolovski, Sergei G., Rafailov, Edik U. 2015. Individual variability analysis of fluorescence parameters measured in skin with different levels of nutritive blood flow. *Medical engineering & physics*, 37(6), pp.574–583.

5) Dunaev, Andrey V., Sidorov, Victor V., Krupatkin, Alexander I., **Rafailov, Ilya E.**, Palmer, Scott G., Stewart, Neil A., Sokolovski, Sergei G., Rafailov, Edik U. 2014. Investigating tissue respiration and skin microhaemocirculation under adaptive changes and the synchronization of blood flow and oxygen saturation rhythms. *Physiological Measurement*, 35, pp.607–621.

6) Litvinova, Karina S., **Rafailov Ilya E.**, Sokolovski, Sergei G., Rafailov, Edik U. 2017. Compact lasers for innovative non-invasive biomedical research and diagnostics. *Progress of Quantum Electronics* (accepted).

Conference proceedings

1) Dremine, Victor V., Zherebtsov, Evgeny A., Makovik, Irina N., Kozlov, Igor O., Sidorov, Viktor V., Krupatkin, Alexander I., Dunaev, Andrey V., **Rafailov, Ilya E.**, Litvinova, Karina S., Sokolovski, Sergei G., Rafailov, Edik U. 2017. Laser Doppler flowmetry in blood and lymph monitoring, technical aspects and analysis. *SPIE proceedings*, 10063, p.1006303.

2) Dremine, Victor V., Zherebtsov, Evgeny A., **Rafailov, Ilya E.**, Vinokurov, Andrey Y., Novikova, Irina N., Zherebtsova, Angelina I., Litvinova, Karina S., Dunaev, Andrey V. 2016. The development of attenuation compensation models of fluorescence spectroscopy signals. *SPIE proceedings*, 9917(0), p.99170Y–99170Y–6.

3) Litvinova, Karina S., Ahmad, Shakil, Wang, Keqing, **Rafailov, Ilya E.**, Sokolovski, Sergei G., Zhang, Lin, Rafailov, Edik U., Ahmed, Asif. 2016. A pilot study using laser-based technique for non-invasive diagnostics of hypertensive conditions in mice. *SPIE proceedings*, 9689(0), p.96893H.

4) Dremine, Victor V., Sidorov, Viktor V., Krupatkin, Alexander I., Galstyan, Gagik R., Novikova, Irina N., Zherebtsova, Angelina I., Zherebtsov, Evgeny A., Dunaev, Andrey V., Abdulvapova, Zera, N., Litvinova, Karina S., **Rafailov, Ilya E.**, Sokolovski, Sergei G., Rafailov,

Edik U. 2016. The blood perfusion and NADH / FAD content combined analysis in patients with diabetes foot. SPIE proceedings, 9698(0), p.969810.

5) Litvinova, Karina S., **Rafailov, Ilya E.**, Dremin, Victor V., Dunaev, Andrey V., Sokolovski, Sergei G., Rafailov, Edik U. 2015. 3D model of bladder cross-section tissue for visualisation of optical properties. In PHOTONICA2015. p. 134.

6) Dremin, Victor V., Zherebtsova, Angelina I, Novikova, Irina N., Zharkikh, E., Zherebtsov, Evgeny A., Dunaev, Andrey V., Litvinova, Karina S., **Rafailov, Ilya E.**, Krupatkin, Alexander I., Sidorov, Viktor V. 2015. Experimental study of the influence of blood flow on the fluorescence signal of biological tissue Apoptotic changes visualization in cisplatin-treated leukemic cells using second-harmonic generation imaging. In PHOTONICA2015. pp. 139–140.

7) **Rafailov, Ilya E.**, Palmer, Scott G., Litvinova, Karina S., Dremin, Victor V., Dunaev, Andrey V., Nabi, Ghulam. 2015. A novel excitation-emission wavelength model to facilitate the diagnosis of urinary bladder diseases B. Choi et al., eds. SPIE proceedings, 9303(0), p.93030W.

8) Dunaev, Andrey V., Sidorov, Viktor V., Krupatkin, Alexander I., Palmer, Scott G., **Rafailov, Ilya E.**, Stewart, Neil A., Sokolovski, Sergei G., Rafailov, Edik U. 2014. The study of synchronization of rhythms of microvascular blood flow and oxygen saturation during adaptive changes. SPIE proceedings, 8935, p.89350A.

Other presented work

1) **Rafailov, Ilya E.**, Dremin, Victor V, Litvinova, Karina S., Dunaev, Andrey V., Sokolovski, Sergei G., Zhang, Lin, Rafailov, Edik U. 2015. Cross-sectional model to simulate and visualise the optical properties in urinary bladder. Optical Technologies for Society, Madrid, Spain.

2) **Rafailov, Ilya E.**, Dremin, Victor V, Litvinova, Karina S., Dunaev, Andrey V., Sokolovski, Sergei G., Zhang, Lin, Rafailov, Edik U. 2015. Improved cross-sectional model for simulating and visualising optical properties of bladder tissue. Aston Year of Light, Birmingham, UK.